Computational Intelligence Techniques for Energy Storage Management

Teo Tiong Teck

School of Engineering
Newcastle University

A thesis submitted to the Newcastle University for the degree of
Doctor of Philosophy

August 2019

Abstract

The proliferation of stochastic renewable energy sources (RES) such as photovoltaic and wind power in the power system has made the balancing of generation and demand challenging for the grid operators. This is further compounded with the liberalization of electricity market and the introduction of real-time electricity pricing (RTP) to reflect the dynamics in generation and demand. Energy storage sources (ESS) are widely seen as one of the keys enabling technology to mitigate this problem. Since ESS is a costly and energy-limited resource, it is economical to provide multiple services using a single ESS. This thesis aims to investigate the operation of a single ESS in a grid-connected microgrid with RES under RTP to provide multiple services.

First, artificial neural network is proposed for day-ahead forecasting of the RES, demand and RTP. After the day-ahead forecast is obtained, the day-ahead schedule of energy storage is formulated into a mixed-integer linear programming and implemented in AMPL and solved using CPLEX. This method considers the impact of forecasting errors in the day-ahead scheduling. Empirical evidence shows that the proposed near-optimal day-ahead scheduling of ESS can achieve a lower operating cost and peak demand.

Second, a fuzzy logic-based energy management system (FEMS) for a grid-connected microgrid with RES and ESS is proposed. The objectives of the FEMS are energy arbitrage and peak shaving for the microgrid. These objectives are achieved by controlling the charge and discharge rate of the ESS based on the state-of-charge (SoC) of ESS, the power difference between RES and demand, and RTP. Instead of using a forecasting-based approach, the proposed FEMS is designed with the historical data of the microgrid. It determines the charge and discharge rate of the ESS in a rolling horizon. A comparison with other controllers with the same objectives shows that the proposed controller can operate at a lower cost and reduce the peak demand of the microgrid.

Finally, the effectiveness of the FEMS greatly depends on the membership functions. The fuzzy membership functions of the FEMS are optimized offline using a Pareto

based multi-objective evolutionary algorithm, nondominated sorting genetic algorithm-II (NSGA-II). The best compromise solution is selected as the final solution and implemented in the fuzzy logic controller. A comparison was made against other control strategies with similar objectives are carried out at a simulation level. Empirical evidence shows that the proposed methodology can find more solutions on the Pareto front in a single run. The proposed FEMS is experimentally validated on a real microgrid in the energy storage test bed at Newcastle University, UK. Furthermore, reserve service is added on top of energy arbitrage and peak shaving to the energy management system (EMS). As such multi-service of a single ESS which benefit the grid operator and consumer is achieved.

I would like to dedicate this thesis to my loving family...

Acknowledgements

I am extremely fortunate to have met people who believe in me and immensely grateful for the opportunities they had given me.

I would like to express my sincere gratitude to my thesis supervisors, Dr. Thillainathan Logenthiran, for his guidance and encouragement throughout this journey. He had provided me with numerous opportunities to showcase and exchange ideas with both internal and external partners. Dr. Wai Lok Woo, for igniting my interest in research and not settling for mediocre work. He encouraged me to persist a little more in the face of difficulties and for the hard questions which widen my research from different perspectives. Dr. Khalid Abidi, who gives me the freedom of research and proofreading this thesis.

I am also grateful to the people I have met at Newcastle University over the Summer of 2018, Professor Phi Taylor, Dr. Neal Wade, Dr. David Greenwood, Dr. Haris Patsios, and Mr. Martin Feeney, who provided me the great opportunity and support to work on my research in your facilities.

I would like to thank my friends, Low See Rong and Tang Litian for the thought-provoking discussions and rage inducing game sessions. Wong Yaozu, for his efforts in proofreading this thesis and Billy Fok, for constantly checking on my well-being when things get too much to handle. I would also like to thank Muhammad Ramadan, Tan Szepei and Lee Yuzhen, for the late-night coffee and endless laughter.

Liu Miaohui, for giving me a "peace of mind" and your thoughtfulness throughout this trying period of thesis writing. Thank you for making the tough days more bearable and giving me a place to rest my weary head.

Finally, my deep and sincere gratitude to my family, for their continuous and unparalleled emotional and financial support throughout this fulfilling and trying time. I am forever indebted to my parents, Foo Pui Jee and Teo Keng Guan, who bore and raise me.

Publications, Awards and Seminars

Journal Papers

1. **T. T. Teo**, T. Logenthiran, W. L. Woo and K. Abidi, "Intelligent Controller for Energy Storage System in Grid-Connected Microgrid," in IEEE Transactions on Systems, Man, and Cybernetics: Systems. doi: 10.1109/TSMC.2018.2881458

2. **T. T. Teo**, T. Logenthiran, W. L. Woo and K. Abidi, 'Advanced control strategy for an energy storage system in a grid-connected microgrid with renewable energy generation', IET Smart Grid, 2018, 1, (3), p. 96-103, DOI: 10.1049/iet-stg.2018.0024

3. **T. T. Teo**, T. Logenthiran, W. L. Woo, K. Abidi, N. Wade, D. Greenwood, C. Patsios, T. John, P.C. Taylor, "Optimization of Fuzzy Energy Management System for Grid-Connected Microgrid Using NSGA-II," IEEE Transactions on Cybernetics (Submitted and under review)

Conference Proceedings

1. **T. T. Teo**, T. Logenthiran and W. L. Woo, "Forecasting of photovoltaic power using extreme learning machine," 2015 IEEE Innovative Smart Grid Technologies - Asia (ISGT ASIA), Bangkok, 2015, pp. 1-6. doi: 10.1109/ISGT-Asia.2015.7387113

2. **T. T. Teo**, T. Logenthiran, W. L. Woo and K. Abidi, "Forecasting of photovoltaic power using regularized ensemble Extreme Learning Machine," 2016 IEEE Region 10 Conference (TENCON), Singapore, 2016, pp. 455-458. doi: 10.1109/TENCON.2016.7848040

3. **T. T. Teo**, T. Logenthiran, W. L. Woo and K. Abidi, "Fuzzy logic control of energy storage system in microgrid operation," 2016 IEEE Innovative Smart Grid Technologies - Asia (ISGT-Asia), Melbourne, VIC, 2016, pp. 65-70. doi: 10.1109/ISGT-Asia.2016.7796362

4. A. W. L. Lim, **T. T. Teo**, M. Ramadan, T. Logenthiran and V. T. Phan, "Optimum long-term planning for microgrid," TENCON 2017 - 2017 IEEE Region 10 Conference, Penang, 2017, pp. 1457-1462. doi: 10.1109/TENCON.2017.8228087

5. J. E. C. Tee, **T. T. Teo**, T. Logenthiran, W. L. Woo and K. Abidi, "Day-ahead forecasting of wholesale electricity pricing using extreme learning machine," TENCON 2017 - 2017 IEEE Region 10 Conference, Penang, 2017, pp. 2973-2977. doi: 10.1109/TENCON.2017.8228371

6. Y. Q. Neo, **T. T. Teo**, W. L. Woo, T. Logenthiran and A. Sharma, "Forecasting of photovoltaic power using deep belief network," TENCON 2017 - 2017 IEEE Region 10 Conference, Penang, 2017, pp. 1189-1194. doi: 10.1109/TENCON.2017.8228038

7. V. De, **T. T. Teo**, W. L. Woo and T. Logenthiran, "Photovoltaic Power Forecasting using LSTM on Limited Dataset," 2018 IEEE Innovative Smart Grid Technologies - Asia (ISGT Asia), Singapore, 2018, pp. 710-715. doi: 10.1109/ISGT-Asia.2018.8467934

8. **T. T. Teo**, T. Logenthiran, W. L. Woo and K. Abidi, "Near-Optimal Day-Ahead Scheduling of Energy Storage System in Grid-Connected Microgrid," 2018 IEEE Innovative Smart Grid Technologies - Asia (ISGT Asia), Singapore, 2018, pp. 1257-1261. doi: 10.1109/ISGT-Asia.2018.8467921

Awards and Grants

1. A winner of poster competition of IEEE Symposium on Emerging Topics in Smart and Sustainable Grids, Singapore 2016

2. IEEE PES Student Travel Grant Award from IEEE ISGT - Asia, Singapore, 2018

3. IEEE PES Student Travel Grant Award from IEEE ISGT - Asia, Melbourne, Australia, 2016

4. IEEE PES Student Travel Grant Award from IEEE ISGT - Asia, Bangkok, Thailand, 2015

5. Conference Support Grant Award from IEEE PES Singapore Chapter, 2015

Seminars

1. One-day workshop exchange with University of Strathclyde, National University of Singapore, Newcastle University in Singapore, organized by School of Electrical and Electronic Engineering, Nanyang Technological University 2018

2. Poster presentation at IEEE Symposium on Emerging Topics in Smart and Sustainable Grids, Singapore, 2016

3. Poster presentation at Singapore International Energy Week, Singapore, 2016

4. Technical Talk @ Newcastle University jointly organized by School of Electrical and Electronic Engineering, Newcastle University and Power & Energy Chapter -IEEE Singapore Section, 2015

Table of contents

List of figures

List of tables

Nomenclature

Acronyms / Abbreviations

AC Alternating Current

AEMO Australia Energy Market Operator

AGC Automatic Generation Control

Ah Ampere hour

AMPL A Mathematical Programming Language

ANN Artificial Neural Network

APL Average Peak Load

ARIMA Autoregressive Integrated Moving Average

DBN Deep Belief Network

DC Direct Current

DISCO Distribution Companies

ELM Extreme Learning Machine

EMCSG Energy Market Company Singapore

EMS Energy Management System

ESS Energy Storage System

ESTB Energy Storage Test Bed

FEMS Fuzzy logic-based Energy Management System

FIS Fuzzy Inference System

FLC Fuzzy Logic Controller

GA Genetic Algorithm

GENCO Generating Companies

ISO Independent System Operator

KNN k-Nearest Neighbor

LP Linear Programming

MAPE Mean Absolute Percentage Error

MAS Multi Agent System

MF Membership Function

MILP Mixed Integer Linear Programming

MO Mathematical Optimization

MOEA Multi-Objective Evolutionary Algorithm

MOGA Multi-Objective Genetic Algorithm

MOO Multi-Objective Optimization

N Negative

NB Negative Big

NPGA Niched Pareto Genetic Algorithm

NREL National Renewable Energy Laboratory

NS Negative Small

NSGA-II Nondominating Sorting Genetic Algorithm II

PB Positive Big

PBB Positive Big Big

PHES Pumped Hydroelectric Energy Storage

PS Positive Small

PSO Power System Operator

PV Photovoltaic

RBM Restricted Boltzmann Machine

RES Renewable Energy Sources

RMSE Root Mean Square Error

RS Reserve Service

RTP Real-Time Pricing

RTT Real-Time Target

SAEC Self-Adaptive ESS Control

SC Supercapacitor

SoC State-of-Charge

SPEA Strength Pareto Genetic Algorithm

TOU Time-of-Use

TRANSCO Transmission Companies

TTS Time to Service

VEGA Vector Evaluated Genetic Algorithm

ZE Zero

Chapter 1

Introduction

1.1 Motivation

The motivation of this research is to investigate the feasibility of providing multiple services using a single energy storage system (ESS) through computational intelligence techniques.

The stability of the power system is maintained through the real-time balancing of the generation and demand. With the increasing mix of stochastic renewable energy sources (RES) such as photovoltaic and wind power in the power system, it posses a serious challenge to the power system operator such as voltage and frequency deviation, low-inertia and power quality issues due to the stochastic nature of RES [1, 2].

ESS is seen as one of the key enabling technology for integration of RES into existing grid as it can provide instantaneous power [3, 4]. ESS also provides many services to the power system operator such as: (i) ensuring reliable operation for critical infrastructure during outages [5, 6], (ii) balancing supply and demand [6], (iii) reducing transmission congestion [7], (iv) providing ancillary services [8], (v) local frequency and voltage regulation [9, 10], (vi) shifting peak demand [11–13], (vii) operation of ESS based on different electricity pricing strategies [14–17].

ESS is a costly and energy-limited resource. It is economical to provide multiple services using a single ESS [18]. The energy storage management system must be designed to consider multiple services. This can formulated as a finite-resource optimization problem. This problem can be solved using two approaches.

1. Mathematical optimization
2. Computational intelligence techniques

In the first approach, it can be further broken down into *deterministic* and *nondeterministic* mathematical optimization. The former requires all the decision variables and constraints to be known at the time of solving. In this finite-resource optimization problem under stochastic environment, additional forecasting techniques are required. The latter considers a set of possible scenarios during the optimization. While reasonably good results can be obtained, it is computational expensive to store all the possible scenarios as it does not scale well to larger models [17]. Furthermore, having multiple services means formulating a multi-objective optimization. This requires additional steps such as formulating the other objective functions as constraints or using a weighted sum approach.

In the second approach, fuzzy logic controller (FLC) are well-suited to operate under stochastic environment and multiple services can be included in the design of the FLC. Furthermore, multi-objective evolutionary algorithm (MOEA) such as nondominated sorting genetic algorithm II (NSGA-II) can be used to tune the FLC parameters.

1.2 Research Aim and Objectives

The aim of this thesis is to develop an energy management system (EMS) for storage management using computational intelligence techniques. The EMS provides multiple stream of benefits to the storage owner and grid operator. The services of the EMS considered in this thesis are energy arbitrage, peak shaving and reserve services. When providing these services, the energy storage management systems does not rely on any demand side management techniques and solely rely on the operation of a single ESS.

This research proposes the use of computational intelligence techniques for energy storage management system. This research aims to propose and validate the feasibility of

- an EMS using computational intelligence
- a FLC for decision making in EMS
- the proposed EMS on a laboratory scale test bed

The objectives are

- Forecasting of uncertain variables of the microgrid using computational intelligence techniques
- Optimum operation of ESS through day-ahead scheduling
- Design a fuzzy logic-based energy management system (FEMS) to handle the uncertainties and provide multi-service using a single ESS in real-time
- Enhanced the performance of the proposed EMS using computational intelligence techniques

1.3 Main Research Contributions

The main contribution of this research is the conceptualization, development and application of computational intelligence techniques for multi-objective optimization of energy storage system in a grid-connected microgrid. The significant contributions of this thesis are as follows.

- The development of a mathematical model for grid-connected microgrid with renewable energies and energy storage system in MATLAB/Simulink environment.
- The uncertainty of RES, demand and real-time pricing (RTP) of electricity makes the optimization of energy storage nondeterministic. This nondeterministic problem is transform into a deterministic problem using day-ahead forecasting of the uncertain variables. Artificial neural network (ANN) techniques are used for day-ahead forecasting of the uncertain variables. A near-optimal day-ahead scheduling of ESS is obtained using mixed-integer linear programming (MILP) to minimize the operating cost and reduce the peak demand of the microgrid.
- A fuzzy logic-based energy management system (FEMS) was designed with historical data of the microgrid hence omitting the need for forecasting. The FLC parameters are designed to reduce the operating cost and peak demand of the microgrid. Several performance evaluation indices are proposed in this thesis to measure the effectiveness of the FLC. Since the effectiveness of the FLC greatly depends on the fuzzy membership function. A uniformly distributed triangle is usually chosen for simplicity purpose. However, it may not yield satisfactory

performance when the standard deviation of the variable is high. In this thesis, a median-σ method is proposed to design the membership function for the real-time electricity market price as it is volatile and non-stationary due to the dynamic market environment.

- The proposed FEMS are enhanced using MOEA, NSGA-II. The NSGA-II is used to optimize the membership functions of the FLC. The objectives are minimizing the operating cost and peak demand of the microgrid. Expert knowledge is integrated into the design process of optimizing FEMS. Pareto optimal solutions are found using NSGA-II, and the best compromise solution is selected without the imprecise nature of the decision maker's judgment. The proposed FEMS is experimentally validated in the energy storage test bed (ESTB) in Newcastle University, UK.

1.4 Outline of Thesis

The rest of this thesis is organized as follows.

- Chapter 2 provides a literature review of mathematical optimization and computational intelligence techniques and the background information of energy storage control and management.
- Chapter 3 proposes a mathematical model of the grid-connected microgrid and ESS. It also proposes the use of ANN for day-ahead forecasting, and mathematical formulation of MILP for day-ahead energy storage scheduling. Furthermore, a FEMS designed with expert knowledge is also proposed. On top of that, this FEMS is enhanced using NSGA-II.
- Chapter 4 provides the simulation results and discussion for hyperparameters tuning of the ANN for day-ahead energy forecast and MILP optimization of the ESS for day-ahead scheduling.
- Chapter 5 provides the simulation results and discussion for the proposed FEMS and enhanced FEMS. The enhanced FEMS is experimentally validated on the ESTB in Newcastle University, UK.
- Chapter 6 concludes this thesis and future research directions for the field of this thesis are discussed.

Chapter 2

Literature Review and Background Information

2.1 Overview

This chapter presents the current state of knowledge in the domain of energy storage control and management, energy forecasting, mathematical optimization and computational intelligence techniques. It also provides critical analysis, shortcoming and gaps in the literature.

2.2 Control of Energy Storage Systems

The control of energy storage system (ESS) are broadly categorized into three control levels. Hierarchical control strategy consists of three levels of control. They are primary, secondary and tertiary. Primary control automatically maintains the voltage and frequency at a preset level. Secondary control corrects the voltage and frequency deviations caused by change in operation state. Tertiary control manages the power flow between the main and microgrid. These levels of control are explained in the subsections.

2.2.1 Primary Control

Primary controls are designed to operate and react to local event independently and instantaneously in a predefined way without external sources or communication between different controllers. It uses locally measured parameters to maintain strict voltage and

frequency level as determine by grid operators. For instance, the Australian Energy Market Operator (AEMO) specifies a maximum long-term frequency between 49.5 Hz to 50.5 Hz [19] and voltage magnitude of -6% to +10% [20]. Power sharing between multiple generation units [21] and frequency control [22] are also part of the primary control due to their fast response time.

To maintain a balance between supply and demand at all times, the active and reactive power must always be equal to the demand. A droop controller can passively adjust and follow these changes.

$$f = f_0 + k_p(P_0 - P) \tag{2.1}$$

$$V = V_0 + k_q(Q_0 - Q) \tag{2.2}$$

where subscripted variables are the reference value, non-subscripted variables are the current value and k_p, k_q are the droop coefficient of the respective droop controller.

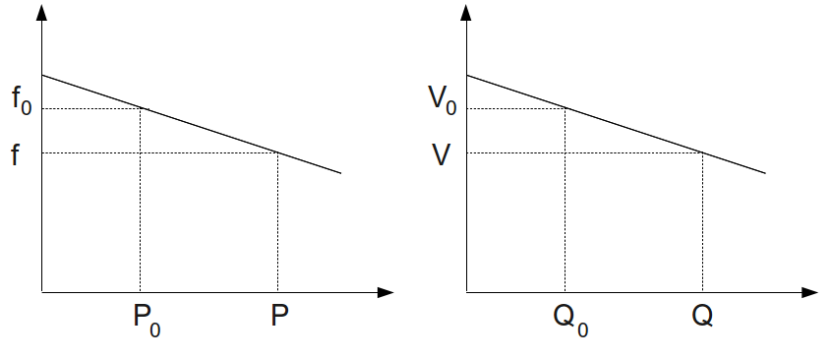

(a) Frequency Droop (b) Voltage Droop

Fig. 2.1 Characteristics of frequency and voltage droop

Fig. 2.1a show the frequency can increase from the reference value to increase the active power and Fig. 2.1b shows the voltage can decrease from the reference value to increase the reactive and vice-versa for both droop controller.

Droop control has several limitations when used in power sharing between multiple ESS. The power shared is proportional to their power capacities rather than their current state-of-charge (SoC). The ESS with a lower initial SoC will be depleted first.

A modified droop controller weights the power shared against their SoC. As such, the ESS with a lower SoC will discharge at a lower rate and approach a balance state as they empties. It also incorporates a frequency control between ESS and restoring them to reference level while maintaining accurate power sharing [23]. This control

strategy requires a neighbor to neighbor communication and improves both frequency and voltage regulation when ESS begins with different energy levels.

For multiple storage with different characteristic, a dead-band droop controller is proposed in [24]. It uses the SoC to set the power references of the storage system.

The limitations of a primary control are the limited reserves from the storage systems and the deviation must be fairly equally distributed among the available resources to prevent overloading of a single ESS.

2.2.2 Secondary Control

The secondary control can coordinate multiple primary controllers within the microgrid for economical optimal operation. The objectives of the secondary control are to correct the voltage and frequency deviation from its nominal values. It changes the set-point of participating generating units or start non-participating generation units in primary control. The secondary control is usually performed by automatic generation control (AGC).

- If the frequency is *lower* than the nominal values, the generation unit set-point have to be *increase*
- If the frequency is *higher* than the nominal value, the generation unit set-point have to be *decrease*

Load shedding can be performed instead of changing the set-point of the generating unit. Load shedding is an action which the power system operator (PSO) deliberately takes to reduce the demand in an event when there is not enough generating units. It is done to prevent a cascading collapse of the power system [25].

2.2.3 Tertiary Control

The highest level of control in power system operation. It operates at a slower response time compared to secondary control. Tertiary control provides signal to secondary control and typically operates in the orders of minutes onwards. It can consist of multiple secondary controllers.

It can also be referred as Energy Management System (EMS). EMS is the process of monitoring, controlling and conserving energy in a building, organization or a power system [26]. It also determines and coordinates long term objective of the entire power

system such as expansion and maintenance of the power system. The response time in this level is slower than primary control due to several reasons such as (i) sampling and communication of measured parameters between Primary and Secondary controller and (ii) time taken for complex calculation. Remotely measured parameters are used for optimizing tasks such as generation scheduling [27] and demand side management [28].

Tertiary control enhances the system control accuracy by coordinating between primary and secondary controllers. The voltage and frequency deviation, and power sharing errors from primary level droop control are corrected in the secondary control through adjustment of control set-points or load shedding.

Multiple ESS with different characteristic can be efficiently controlled [29]. The cost-free power of renewable energy sources (RES) is capitalized by coordinating multilevel control strategy instead of the traditional primary control. The primary control is used to follow the schedule of the ESS while voltage deviations and power tracking errors are compensated in secondary control. Furthermore, tertiary control limits the SoC variation of ESS to extend its life cycle.

An example of tertiary control is proposed in [30]. A multi-agent system (MAS) based power system comprises of different types of intelligent agent with different tasks and objectives. A tertiary control strategy using MAS was proposed in [30]. It focuses on generation scheduling and demand side management. A two-stage scheduling was done in day-ahead and real-time. In addition to two-stage scheduling, a demand side management performs load-shifting before day-ahead scheduling and load curtailment in real-time. This multilevel control strategy maximizes the usage of distributed generators and minimizes the operation cost.

The rapid advancement in technology and adoption of RES in the existing power system urgently requires control strategy which is capable of multilevel coordination. Apart from providing ancillary services, control strategies should aim to increase the benefits for both grid operator and end-user. Such as reducing operating cost of end-user through arbitrage operation or peak demand shaving to relief transmission congestion for the grid operator.

2.2.4 Charge and Discharge Methods for Energy Storage Systems

The different levels of control determine when to charge and discharge the storage system. The command of charging or discharging is either in power, voltage or current set points. The objective of charging and discharging an energy storage is to store or release energy when required. Apart from charging and discharging, the control methods also impact the battery performance, charging time, and overall life-span of the storage system.

There are several methods of doing so and they are discussed in this subsection. To avoid excessive repetition of "charging and discharging", it is only referred as "charging" in this subsection.

2.2.4.1 Constant Current or Voltage Charging

Constant current or voltage charging is the simplest form of storing energy into the storage device. It works by supplying a constant current or voltage to the storage without considering other parameters of the storage such as temperature.

During constant current charging, it avoids high over-current of the initial charge [31]. As voltage is not monitored in this method, it can cause overcharging and increase in temperature which results in the degradation of battery life [32].

During constant voltage charging, its initial current is high. As the storage voltage reaches the voltage limit, the charge current decreases. This results in long charging time and increases the ESS temperature which can result in the degradation of the storage lifespan [32, 33].

2.2.4.2 Intelligent Controller for Energy Storage

An intelligent controller for energy storage generally consists of some processor that is capable of receive inputs, process and generate output. The inputs can be the storage current characteristics and conditions and the output can be the voltage, current or power set-point. For instance, the intelligent controller would monitor the current capacity and temperature of the storage system [34].

Several intelligent controllers are proposed in the literature [35, 36, 10]. A rule-based control strategy for dispatching ESS integrated with RES is proposed in [35]. It considers the operating constraints of ESS, such as SoC limits, charge and discharge rate, and total life-cycle.

A power dispatch scheduling algorithm for the operation of ESS in a wind farm is proposed in [36]. It considers the uncertainties in wind energy generation and energy price to schedule the ESS dispatch.

Static and dynamic rule-based voltage control strategies are proposed and assessed in [10]. Economic benefits are maximized when using dynamic control. Furthermore, dynamic rule-based also reduces the occurrence of voltage violation and energy curtailment.

2.2.5 Summary of Control of Energy Storage

This section presents an overview of the primary, secondary and tertiary control of ESS in the power system. Primary control is a passive approach of operation without external sources or communication between different primary controllers to maintain strict voltage and frequency levels. Secondary control corrects any deviation of voltage and frequency from the primary control. Tertiary control coordinates the primary and secondary control for long term objectives of the power system.

The charge and discharge methods of the storage system are also discussed in this section. Degradation to ESS occurs during constant high over-current or over-voltage charging. Intelligent controllers can provide additional benefits to the end-user and grid operator at a tertiary control level.

2.3 Overview of Electricity Market

The electricity market can be broadly categorized into three parts:

1. Independent system operator
2. Utility companies
3. Consumers

The role of an independent system operator (ISO) focuses on monitoring and coordinating the generation units of the utility companies and the consumers. The ISO is also responsible for the reliability of the supply, operation of the power system and ensure system security. To ensure long-term stability of the power system, the ISO also carry out maintenance and expansion planning for the current infrastructure through power system studies.

The utility companies generally consist of generating companies (GENCOs), distribution companies (DISCOs) and transmission companies (TRANSCOs). They may be operated by a single company or multiple companies.

The GENCOs are responsible for operating and maintaining the power generation plants. They can either sell power with other GENCOs or to the consumers through DISCOs. They can also provide services such as voltage and frequency regulations or spinning reserve.

The TRANSCOs transmits electricity in bulk from the GENCOs to DISCOs for delivery to the consumers. They also own and maintain the transmission assets such as overhead/underground cables, and transformers. They interconnect multiple generation companies to the distribution network and finally consumers. They are also responsible for expanding, maintaining and operating of the transmission infrastructure.

DISCOs distribute the electricity to the consumers in a certain geographical region. They are considered the "last-mile transport" for electricity where they connect the consumers to the transmission lines. They are responsible for billing metering infrastructure and responding to network outages and power quality issues.

The consumers are the end-user of the electricity. The energy consumption ranges from large scale users such as heavy industrial factories to small scale residential housing. These utility companies can be fully or partially owned and operated by the ISO.

2.3.1 Deregulation of Electricity Market

Deregulation is the process of reducing or eliminating the influence of government regulations in industries. In the past, the energy sector was monopolized and operated by government bodies with a top-down hierarchy. In recent years, the deregulation of electricity market allows more competition and offer consumers the options to choose from various electricity retailer to meet their energy needs [37].

Electricity is unlike any other commodity which can be produce and store in warehouse or shelfs like rice grains or electronic devices. It is not cost effective to solely produce and store electricity in bulk. As such electricity are produced on demand even in the deregulated energy market. They are being traded like any other commodity under spot or derivative contracts. As such the decision making of consumers heavily rely on the energy forecast. The cost of over or under contracting in the balancing market can incur huge financial disadvantage to the utility companies.

2.3.2 Pricing Strategies

Real-time operation of ESS in electricity market has gained popularity in the research community in recent years due to the different electricity pricing strategies offered by ISO. Instead of a flat tariff, grid operator can offer real-time pricing (RTP) of electricity or time-of-use (TOU) tariff. RTP strategy employs different pricing based on the time of the day and the demand. TOU tariff employs different fixed pricing based on different periods of the day. Both RTP and TOU pricing strategies can incentivize consumers and power system operator [38].

2.3.2.1 Fixed Tariff

Fixed tariff is a fixed rate for each kilowatt-hour used. This is the simplest form of payment which usually applies to small-scale consumers.

2.3.2.2 Time-of-Use Tariff

Time-of-use tariff is the cost of electricity is based on the time of the day it was used. These prices are set for a specific time period and are known to the consumers in advance. This encourages the shift of demand from peak period, where the price is higher, to off peak period, where the price is lower.

2.3.2.3 Real-Time Pricing

The reliability of the power system relies on the balancing between supply and demand of power in real-time. However, the planned generation scheduled can differ in real-time. Therefore, a real-time pricing market is established to meet this requirement.

The RTP accounts for real-time energy imbalances. These imbalances are met with the spinning, non-spinning and other reserves which are readily available within a short period of time for the ISO to dispatch.

2.4 Energy Storage Applications and Architectures

There are many applications for energy storage in the power system. The operating time-scale for different application ranges from real-time to years ahead and are shown in Table 2.1. Applications with similar time scales can be stacked and operated with a single energy storage system [39, 40]. Some of the applications of energy storage are discussed further in this section.

Table 2.1 Examples of energy storage applications and time scales

Applications	Time scales
Frequency regulation [41, 42]	Less than 1s
Voltage support [43, 44]	Less than 1s
Synthetic inertia [45]	Few seconds to minutes
Energy arbitrage [14]	Minutes to few hours
Renewable energy time shift [46]	Minutes to few hours
Customer demand charge [47]	Minutes to few hours
Reserve services [48]	Few hours to days
Transmission congestion reduction [49]	Few hours to days
Deferment of transmission and distribution infrastructure [7]	Days to years

2.4.1 Energy Arbitrage

The proliferation of weather-dependent renewable energy sources has started to have significant impact on the energy price in the wholesale electricity market [50]. As such, the consumers can take advantage of this through energy arbitrage.

Energy arbitrage with ESS is a technique to charge the storage when the electricity market price is low and discharge when the price is high, to take advantage of the different in pricing. In the RTP of the electricity market, the prices usually correspond to the demand of the consumers. High energy prices correspond to the high demand and vice-versa. Energy arbitrage is to charge the storage when RTP is low and discharge when RTP is high. In this manner the consumers can take advantage of the difference in prices and profit from it.

2.4.2 Renewable Energy Time Shift

The peak generation of renewable energy sources may not coincide with the peak demand of the consumers. This mismatch between the RES and demand must be met by the grid.

For instance, in a microgrid with photovoltaic (PV) and residential load, the peak of the consumers usually occurs between 0600 to 0800 hours, when majority of the consumer begins to prepare for work. Whereas the peak generation of a PV usually occurs between 1000 to late afternoon at 1700. The energy storage can charge during the peak generation of the PV and discharge during the peak demand of the consumer.

2.4.3 Peak Demand Shaving

Peak shaving or peak load reduction is a technique to reduce the instantaneous power during period where the maximum demand occurs.

Similar to renewable energy time shift, peak demand shaving charges the storage during non-peak period and discharge during peak period. Fig. 2.2 illustrates the reduction of peak load. The base load generator power set-point is increased to charge the storage system during off peak period and discharge during peak period. In this manner, the operation of the costliest peaking generator is reduced.

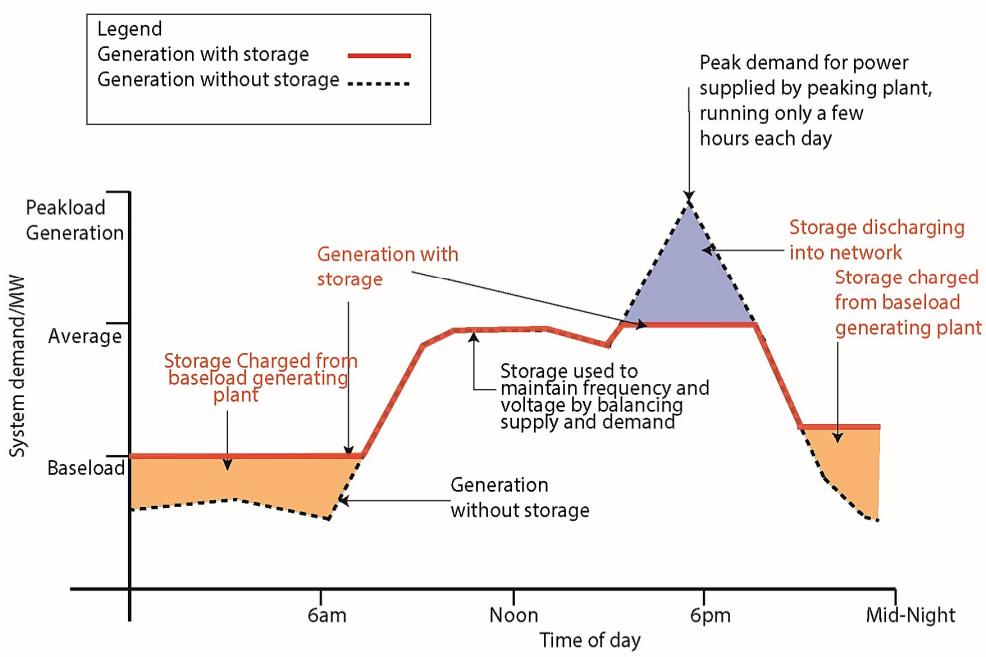

Fig. 2.2 Peak demand shaving using energy storage system. [1]

Furthermore, this can be useful to keep the transmission lines within its limits and reduce the use of peak load generators [51]. It helps the PSO to reduce or defer expensive infrastructure expansion and reduce the operating time of costly peaking generators.

[1]Special thanks to Mr. Lee Sheng Ming for creating this figure.

2.4.4 Reserve Service

Reserve service (RS) is traditionally being provided by the GENCOs to the ISO. However, with the increase in RES and ESS at the distribution side, the consumers can also participate in providing RS.

The exact requirements for RS differ in different markets. However, the contracts usually consist of the following:

1. Quantity of power to be delivered (kW)
2. Availability window
3. Paid based on availability window and utilization
4. Penalties if the committed power is not delivered

Firstly, the provider of the reserve service will commit an amount of power to be delivered. Secondly, the provider has to be on standby to provide the committed power during the availability window. Thirdly, the payment from ISO for being available during the availability window and the utilization of the commitment power. Finally, the provider will incur penalties when the committed power is not delivered during the availability window.

RS using ESS is based on forecasting and mathematical optimization to obtained an optimal schedule for ESS are proposed in [52, 53]. A two-stage stochastic unit commitment that considers energy arbitrage and RS for day-ahead market for ESS [54]. Day-ahead coordination between building loads and energy storage for energy arbitrage, primary and secondary reserve [55]. These methods are based on forecasting or mathematical optimization and does not operating in real-time.

2.4.5 Energy Storage Architectures

Power is traditionally generated from large centralized location. The voltage is stepped up and transmitted over a long distance and later stepped down to a lower voltage at a substation before reaching the consumer. As such the network topology can be separated into generation, transmission and distribution. ESS can be connected to different parts of this network. When it is connected to the generation side, it can be used for ancillary services, voltage/frequency regulation, spinning reserve or black start. On the transmission level, it can provide congestion management, infrastructure

deferment through reduction of peak demand and improving power quality. On the distribution level, it is used for renewable energy power smoothing [56].

2.4.6 Summary of Storage Applications and Architectures

The applications of energy storage are discussed in this section. Instead of having a single application for a single storage, multiple applications on a single storage is more economical to the owner. A single energy storage can provide multiple applications with similar operating time scales.

2.5 Energy Storage Model

ESS is capable of provide a wide spectrum of energy management solution through meticulously designed control ranging from large-scale generation, transmission applications to small-scale microgrid, residential applications.

The choice of storage technology depends on the type of application. Storage technologies can be classified according to their power and energy density. Power density is the amount of power per unit volume expressed as W/m^3. While energy density is the amount of energy per unit volume expressed as J/m^3. Since energy storage comes in multiple forms including chemical, gravitational potential, electrical potention or kinetic energy [57]. It can be difficult to quantify these properties into the storage model.

Storage model can be broadly classified into two types: technology specific model and generalized model. The former involves the modeling of the energy conversion from one form to another. The latter generalized the technical characteristics of the storage as follows:

1. Power/voltage/current rating
2. Energy capacity
3. Efficiency
4. Ramp rate
5. Self-discharge rate

There are several methods of modeling these technical characteristics of an energy storage. Each method has a similar aims of characterizing the energy storage in terms of power, energy rating, and efficiency [58]. Furthermore, parameters such as, self-discharge rate, storage aging and operating temperature of the storage can also be included in the model. However, these parameters are difficult to quantify accurately due to the nonlinear nature of energy storage, accurate mathematical models are overly complex [59]. As such, there is a trade-off between accuracy and complexity.

2.5.1 Technology Specific Models

An equivalent electric circuit model and pumped hydroelectric energy storage model are discussed in this subsection. The approach of modeling these two storage are briefly discussed. The purpose is to demonstrate that while technology specific model is more accurate, they are vastly different from another storage technology and non-interchangeable.

2.5.1.1 Equivalent Electric Circuit Model of Supercapacitor

A supercapacitor (SC) is a capacitor that has much higher energy density while having the same power density. Fig. 2.3 shows the equivalent electric circuit model. It is based on the galvanostatic approach which are widely used for parameterizing equivalent electric circuit model [57, 60].

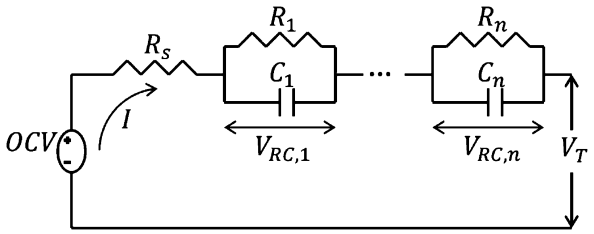

Fig. 2.3 Equivalent electric circuit model with "n" number of R-C branches [61]

The terminal voltage, V_T is calculated by appplying Kirchhoff's voltage law in (2.3). The first term, V_{OC} is the open circuit voltage of the supercapacitor. The second term, IR_s is the voltage drop across the series resistance. The third term, $V_{RC,j}$ is the total votage across n number of R-C branch.

$$V_T = V_{OC} + IR_s + \sum_{j=1}^{n} V_{RC,j} \tag{2.3}$$

The state-of-charge of the ideal capacitor is a linear function of the V_{OC} and can be estimated through coulomb counting in (2.4).

$$\frac{dSoC}{dt} = \frac{I}{CV_{max}} \tag{2.4}$$

where C and V_{max} is the total capacitance in farads and maximum voltage across the cell at full charge.

$$\frac{dV_{RC,j}}{dt} = -\frac{1}{R_j C_j} V_{RC,j} + \frac{I}{C_j} \tag{2.5}$$

where R_j and C_j are the resistance and capacitance of the j^{th} RC branch.

The total energy stored in the SC is estimated from the V_{OC} and V_{max}. The capacity of the SC is expressed as Ampere hours (Ah) and shown in (2.6) [61].

$$\text{SC capacity} = \frac{CV_{max}}{3600} \tag{2.6}$$

Instead of expressing the capacity in Ah, it can be expressed as SoC. SoC is a percentage between 0 and 100.

Where 0 and 100 are fully discharged and charged respectively. The SoC of the SC can be estimated from the V_{OC}, V_{max} and V_{min} as shown in (2.7) [62].

$$SoC = \frac{V_{OC} - V_{min}}{V_{max} - V_{min}} \tag{2.7}$$

The characteristic of a SC is nonlinear and challenging to model [63]. Apart from the parameters from (2.3) to (2.7), additional parameters such as frequency, temperature, internal and external resistance also effects the accuracy of the model [64, 65].

2.5.1.2 Pumped Hydroelectric Energy Storage

Pumped hydroelectric energy storage (PHES) stores the energy in the form of gravitational potential energy when the water is pumped from a lower elevation to a higher elevation.

The total energy stored by the PHES is calculated from (2.8).

$$\text{Total Energy} = \text{Potential Energy} + \text{Kinetic Energy} + \text{Pressure Energy} \tag{2.8}$$

The first term, mgh, is the potential energy.

$$\text{Potential Energy} = mgh \tag{2.9}$$

where m, g and h is the mass of water (kg), g is gravitational constant (9.81 m/s^2) and h is the height of elevation from the lower evaluation (m).

The second term, $\frac{1}{2}mv^2$, is the kinetic energy.

$$\text{Kinetic Energy} = \frac{1}{2}mv^2 \tag{2.10}$$

where v is the speed of the water (m/s).

The third term, $\frac{mP}{\rho}$, is the pressure energy.

$$\text{Pressure Energy} = \frac{mP}{\rho} \tag{2.11}$$

The total power of the PHES is calculated from (2.12).

where P and ρ is the pressure (N/m^2) and ρ is the density of water (1000 kg/m^3).

$$\text{Power} = H\rho gQ\eta \tag{2.12}$$

where Q is the flow rate (m^3/s) and η is the efficiency of the turbine ($0 < \eta < 1$).

This subsection presented two technology specific storage models. Even though the models are presented in different forms, these models can quantify the energy, power capacity and efficiency.

The drawback of technology specific model is that these models are specifically designed for a certain type of energy storage. These models are not interchangeable with another storage technology. Each storage technology must be modeled individually. From an operation point of view, a generalized storage model is favorable than a technology specific model. Furthermore, the generalized storage model parameters can be easily adjusted according to the storage technology during hardware implementation.

2.5.2 Generalized Storage Model

A generalized storage model is used in this thesis even though technology-specific model is more precise as it is based on experimental data of the specific storage [2]. This generalized storage model is applicable to most storage technology.

As the aim of the thesis is the operation of ESS rather than modeling of ESS. Modeling of specific ESS technology is beyond the scope of this thesis. Furthermore, the proposed methodologies would not be limited to any specific storage technology.

Even a highly detailed storage model requires some form of curve fitting or error correction through experimental findings [61, 62]. In this thesis, a generalized storage model with error correction lookup table strikes a balanced between a highly accurate model and a generalized model. A lookup table can be obtained experimentally by comparing between a generalized storage model and actual storage system. In this manner, the model will have a higher accuracy without the need to design an overly complex model and it can be easily applied to different storage technology.

2.5.3 Summary of Energy Storage Model

The technical characteristics of a storage model can be modeled using technology specific model or generalized model. For instance, the current capacity of a storage system can be quantify using ampere-hours, open circuit voltage or energy level of the system. There is a trade-off between accuracy and complexity depending on which type of storage model is used. The focus of this thesis is the operation of energy storage hence a generalized storage model is considered.

2.6 Energy Forecasting

The energy sector landscape has been reshaped with the proliferation of intermittent renewable energy sources and changing demand profiles. This phenomenon has made accurate energy forecasting a challenge. Energy forecasting refers to the forecasting in the energy sector. It includes but not limited to forecasting of demand, renewable energy sources and price of electricity.

Forecasting horizon is how far ahead into the future which the variables are forecast. They are loosely categorized into short-term, medium-term and long-term forecast. There is no consensus in the literature on what the threshold of these horizons should be. Stakeholders of the power system uses forecast of different horizons to ensure the short and long-term reliability and security of the power system are met.

1. Short-term forecast ranges from minutes to day-ahead forecast. They are usually used for real-time dispatch of generators or day to day market operation.

2. Medium-term forecast ranges from a few days to a few months ahead. They are usually used for generation scheduling and maintenance planning.

3. Long-term forecast ranges from months ahead to years ahead. They are usually used for infrastructure planning and expansion.

There are two main approaches in forecasting, qualitative and quantitative. In qualitative forecast, it is based on the expert knowledge in the variable of interest. While quantitative forecast is based on the available historical data in the variable of interest.

Qualitative forecasting is assuming that there is an underlying relationship or pattern in the data and are expected to stay the same in the future. There are many qualitative methods of forecasting such as weighted moving average, autoregressive integrated moving average (ARIMA), and artificial neural networks (ANN).

An accurate forecasting model should include all the prevailing factors which impact the variable of interest. For instance, in load forecasting, apart from load, other data such as temperature, time of the day and day of the week should be included in the model. However, these data are difficult to formulate into a mathematical model. ANN are capable of including multiple variable in the model for forecasting [27, 66–69]. Some of these models are discussed in subsection 2.8.3.

2.7 Mathematical Optimization

Mathematical optimization (MO) methods have been used in solving finite resources operation problems. For instance, facility layout planning, water pumps and timetable scheduling [70–73]. MO consists of maximizing or minimizing a set of objective functions within a set of equality and inequality constraints. It requires explicit modeling of the process or system, which can be difficult to obtained. The objective function and constraints must be mathematical formulated. If the problem is too complex, the number of variables and constraints can be quite large. The decision variables and constraints can either be predicted with certainty or cannot be predicted with certainty. The former is classified as deterministic problems while the latter is classified as nondeterministic problems.

MO can also be used to solve for multi-objective optimization by using a weighted sum approach or by changing the other objective functions into constraints. In the former approach, the selection of weight is difficult as it determines the importance of each objective function. In the latter approach, the value of the constraints for the objective functions must be selected as well. In both cases, only a single solution can be obtain and trade-offs between objective functions cannot be examined properly.

2.7.1 Deterministic Problem

Deterministic problem is where all constraints are known in advanced. It can be formulated and solved using linear programming (LP) or MILP. For instance, in a day-ahead generation scheduling problem, even though the day-ahead demand is uncertain, they can be forecasted and considered as a known coefficient. Hence this problem can be considered as a deterministic instead of nondeterministic since all the constraints are known.

2.7.1.1 Linear Programming

LP is a mathematical optimization method. It can either be a maximizing or minimizing linear function subject to linear constraints [74]. The cost function of LP is a linear objective function, subject to linear equality and inequality constraints. The canonical form of linear program is shown in (2.13).

$$\text{Minimize } cx \tag{2.13a}$$

$$\text{Subject to } Ax \leq b \tag{2.13b}$$

$$x \geq 0 \tag{2.13c}$$

where c and b are vectors of known coefficients, which represents the objective functions and constraints. x is a nonzero decision vector which must be determined. A is a matrix of known coefficients.

2.7.1.2 Mixed Integer Linear Programming

MILP, is similar to LP in terms of linear and inequality constraints. However, some or all of the decision variables are restricted to be integer as shown in (2.14d).

$$\text{Minimize } cx \tag{2.14a}$$

$$\text{Subject to } Ax \leq b \tag{2.14b}$$

$$x \geq 0 \tag{2.14c}$$

$$\text{and } x \in \mathbb{Z} \tag{2.14d}$$

MILP is useful when there are states associated with the model. For instance, an ESS can only charge or discharge at any one time and this can be represented by adding an

integer decision variable to the model. In power system or energy storage operation, LP and MILP are applied extensively for day ahead unit commitment problems for generator or energy storage dispatching.

2.7.2 Nondeterministic Problem

Nondeterministic problem is where some or all the constraints are uncertain can be solved with stochastic programming. An operation optimization problem is more practical when uncertainties are modeled into the problem formulation. For instance, in generation scheduling, the demand of the consumer is uncertain.

Stochastic programming an optimization problem where some of the decision variables or constraints is uncertain [75]. These uncertainties are characterized by a probability distribution. Stochastic programming is broken down into a two-stage decision making approach based on the data available at the time of the decision. The two-stage stochastic programming can be formulated as follows:

2.7.2.1 Stage 1: Linear Programming

The first stage of stochastic programming is similar to LP. However, the inequality constraint b is uncertain. The probability of the possible outcomes can be expressed as b.

$$\text{Minimize } cx \tag{2.15a}$$

$$\text{Subject to } Ax \leq b \tag{2.15b}$$

$$x \geq 0 \tag{2.15c}$$

2.7.2.2 Stage 2: Recourse Problem

Recourse problem refers to the modification of current solution, x, to adapt after a specific outcome of b is observed. From (2.16), after the value of b is known, a second set of decision, y, is made in the presence of uncertainty. This is done to adjust the first stage decision, x, to consider uncertainty.

$$\text{Minimize } qy \tag{2.16a}$$

$$\text{Subject to } My = b - Ax \tag{2.16b}$$

$$y \geq 0 \tag{2.16c}$$

where y is the stage 2 decision variable. M is a matrix which describes the difference between the stage 1 and stage 2 decision variables. q is the objective function.

While it is possible to consider many scenarios in stochastic programming, they are computational inefficient to solve [75]. The total number of possible solutions can be calculated using (2.17). Consider a problem with 10 discrete random variables with only 3 discrete outcomes, the total number of possible solutions would be $3^{10} = 59,049$.

$$\Omega = \omega^b \tag{2.17}$$

where Ω and ω represent the possible solutions and outcomes respectively.

2.7.3 Summary of Mathematical Optimization

Three mathematical optimization methods are presented in this section to solve deterministic and nondeterministic problems. Deterministic problems are solved using LP and MILP and nondeterministic problem are solved using stochastic programming. While there are many other methods in solving operations of finite resources problem other than LP, MILP and stochastic programming, they are beyond the scope of this thesis.

In the operation of energy storage under the uncertainty of renewable generation, energy price and demand, it is challenging to consider these in stochastic programming. As the problem would be computational expensive to obtain a solution using stochastic programming. As such, forecasting techniques are used to obtain the values of the uncertain variables and the solution is solved using LP or MILP as a deterministic problem in this thesis.

The MO methods mentioned in this section only deal with a single objective function. However, many practical problems have more than one objective. Apart from these methods, computational intelligence techniques such as fuzzy logic and genetic algorithms are well-suited to deal with multi-objective problems with vague and imprecise information [76–79]. These computational intelligence techniques are further discussed in the next section.

2.8 Computational Intelligence Techniques

Computational intelligence refers to the ability for the computer to learn from data to do a specific task without explicitly programming it to do so. They are effective in addressing real-world problems where the process is too complex for mathematical model or collecting data is easier than understanding the relationship between the input(s) and output(s).

There are five main paradigms of computational intelligence.

1. Fuzzy logic
2. Evolutionary computation
3. Artificial neural networks
4. Learning theory
5. Probabilistic methods

While the field of computational intelligence is wide and broad, this thesis only focuses on the following:

1. Fuzzy logic- Mandami type fuzzy inference system
2. Evolutionary computation- Genetic algorithm and nondominated sorting genetic algorithm-ii
3. Artificial neural networks- Extreme learning machine and deep belief network

Computational intelligence are discussed in the next subsections.

2.8.1 Fuzzy Logic

Fuzzy sets theory was first introduced by Zadeh [76]. It is based on the principle that people make decisions based on imprecise or vague information which is difficult to translate into a mathematical model. There are several advantages of using a fuzzy inference system (FIS). Firstly, it is based on natural language, the control objectives of a FIS can be implemented as If-Else statements. It can easily translate expert knowledge into the design of FIS without complicated mathematical model. Secondly, it is tolerant to imprecise information. All the input(s) and output(s) are given a degree

of membership to quantify how much it belongs to a specific linguistic term. Finally, it can be used as a real-time decision making controller under uncertain conditions as is well-suited to handle vague and imprecise information.

The general diagram of a FIS is shown in Fig. 2.4. A $Mamdani - type$ FIS is used in this thesis.

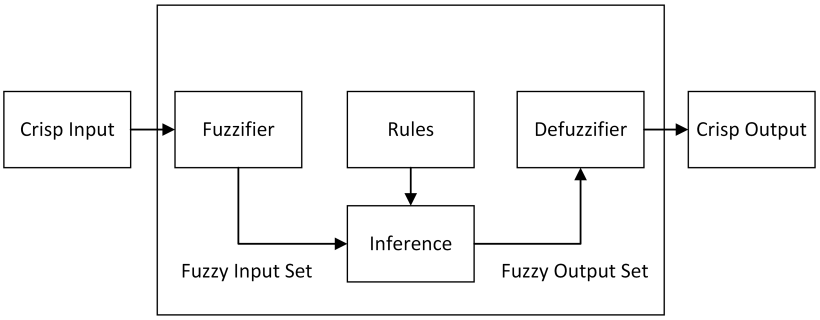

Fig. 2.4 General diagram of fuzzy inference system

Firstly, the crisp inputs are fuzzified using the fuzzy membership functions and are given a *degree of truth* or *truth values*. Secondly, these truth values evaluated simultaneously using the fuzzy rules. Thirdly, depending on which rules are activated, these values are applied to compute the output function. Finally, the output function is defuzzified to obtain the crisp output.

2.8.1.1 Crisp Input and Fuzzifier

The numerical values of the inputs are crisp inputs. Fuzzifier is the process where crisp or real input are mapped to linguistic term using $membership\ function$. Membership function (MF) introduces nonlinearity to the input(s). The system's designer chooses the membership function.

2.8.1.2 Fuzzy Rules and Inference

Fuzzy rules are a set of *linguistic statements* based on a collection of IF-THEN statement, which are typically based on human expert knowledge. It is easy to interpret these rules as they are highly similar to natural human language. The effectiveness of FIS is proportional to the knowledge of the designer.

IF *antecedent*, THEN *consequent*.

Inference is the process of using the IF-THEN rules to converts the fuzzy input to fuzzy output through an aggregator. This work uses a mamdani fuzzy inference.

2.8.1.3 Defuzzifier and Crisp Output

Defuzzifier converts the fuzzy output into a crisp output similar to how the crisp input are converted into fuzzy input. There are many defuzzifier proposed in the literature such as centroid of area, mean of maximum and largest of maximum. The defuzzifier used in this work is centroid of area.

2.8.2 Evolutionary Algorithm

Evolutionary algorithm is a population-based metaheuristic optimization algorithm. It is loosely inspired by the biological evolution. Generally, biological evolution consists of reproduction, mutation, recombination and selection.

The solutions obtained from evolutionary algorithm are sufficiently good to the optimization problem. It is suitable for problems where there is incomplete information such as stochastic optimization where the solution depends on a set of random variables.

2.8.2.1 Genetic Algorithm

Genetic algorithm (GA) is loosely inspired by Darwin's theory of evolution and the survival of the fittest and first proposed by Holland [80]. It theorized that the weak and unfit species within the population faces extinction by natural selection as the stronger ones have a greater chance of survival. The stronger species have a higher chance of reproducing and passing their genes to the next generation. Eventually, the species carrying the stronger genes become dominant in the population. During the passing of genes from one generation to another, random changes may occur and alter the genes. These changes are kept if it provides an advantage to the new species and eliminated if otherwise.

GA generates a population of possible solutions and searches through the solution space by evaluation each of the solution. The quality of the solutions is measured using a fitness function. The fitter solutions are selected for genetic operations, such as crossover and mutation, while less fit solutions are discarded.

GA encodes the possible solutions of the problem into a vector called chromosomes. Genes are contained in chromosomes. Each gene controls the traits of the chromosomes. The genes can be encoded into the chromosomes as a string of binary or real numbers [80, 81].

GA uses two genetic operators to generate new chromosomes from the existing population: crossover and mutation. Before undergoing these operations, the fitter

chromosomes must be selected first. The preference of selection is given to the fitter chromosomes from the population. This can be achieved through various selection techniques such as binary tournament selection, roulette wheel selection or rank selection [82].

Elitism ensures that the fittest solution of the current generation survive to the next generation. This can speed up the convergence of GA significantly and avoid the loss of good solutions once they are found in the previous generations [83, 84].

The crossover operator takes the solution of the parent chromosome and exchange parts of the solutions to create offspring chromosome. Typically, two chromosomes are selected for crossover. While there are many methods of crossover, ranging from simple one-point crossover to complicated simulated binary crossover. The goal of these crossover methods is the same; to create solutions similar to the parent chromosome.

The mutation operator randomly changes the gene of the chromosomes. This is typically done by having a probability of mutation, followed by replacing the gene of the chromosome. This is to introduce diversity back to the population of chromosome to promote diversity.

2.8.2.2 Multi-Objective Genetic Algorithms

Many complex real-life engineering problems involves multi-objective optimization (MOO). It involves one or more objective functions to be optimized simultaneously. The optimization process usually considers trade-off between two or more competing objectives [77, 85–87]. When there is a trade-off between two or more competing objectives, no single solution exists that simultaneously optimizes each objective. However, there exist a set of Pareto optimal solutions. A solution is part of the Pareto optimal set if none of the other objective functions can be improved without degrading the other objective functions. Without any additional information, all Pareto optimal solutions are considered equally good.

The classic approach to solve a multi-objective optimization problem using GA is assigning a weight to each of the normalized objective function. The objective functions are sum into a single figure of merit which yields a single solution. If multiple solutions are required, the problem must be solved multiple times with different weight. The assignment of weights itself is a difficult task as it affects the importance of each objectives. This approach is straightforward and require minimum changes to GA. However, to obtain a set of Pareto optimal solution requires many iterations of GA with different weight assignments [84].

Apart from the weighted sum approach, a Pareto front-based approach can be used. Multi-objective Genetic Algorithm (MOGA) have been widely used to obtain the Pareto optimal solutions in a single run [88]. There are many MOGAs proposed in the literature [88]. The typical objectives of these Pareto front-based approach are [89]:

- to preserve non-dominated solutions in the objective space
- to make progress towards the Pareto optimal front in the objective space
- to maintain diversity in the non-dominated on the Pareto optimal front
- to provide the decision maker with a set of Pareto optimal solutions

Vector Evaluated Genetic Algorithms (VEGA) is one of the first notable work in the attempt to find Pareto optimal solutions using MOGA [78]. Following the work of [78], several other MOGA are proposed in the literature including Niched Pareto genetic algorithm (NPGA) [90], Strength Pareto evolutionary algorithm (SPEA) [91] and non-dominant sorting algorithm II (NSGA-II) [79]. These methods have been used in induction machine design [92], generation and transmission expansion planning [93, 94] and electric power dispatch problem [95–97].

In VEGA, population P_t is equally divided into $p_1, p_2, ..., p_k$, where k is the k^{th} objective function. The solutions in sub-population p_k are assigned a fitness value based on objective function f_k. For instance, if there are two objective functions, f_1 and f_2, then the population is divided into two sub-population p_1 and p_2. After that, sub-population p_1 is evaluated with f_1 and p_2 with f_2. The implementation of VEGA is straightforward, however in essence, it is still evaluating the solutions against a single objective function. It tends to converge into the extreme points and does not maintain diversity in the solutions.

In NPGA, it attempts to address the drawback of VEGA by introducing Pareto domination tournaments during the selection process to promote diversity. The solutions are assignment with a domination count. After that two solutions are picked at random from the population. A comparison between the two candidates are done, if one candidate dominates the other, the former is chosen for reproduction. If neither candidate dominates the other, a new parameter, niche count is introduced. Niche count estimates how crowded is the solution space. Without going into the details, the user is required to select a sharing parameter, σ_{share}, to determine the niche count.

In NSGA-II, it can find a more diverse solution on the Pareto-optimal front when compared to other multi-objective evolutionary algorithms [79]. NSGA-II does not

require additional parameters such as niche count or sharing to promote diversity on the Pareto front. It is favorable as it does not require user intervention to determine the additional parameters.

2.8.3 Artificial Neural Network

The ANN is loosely inspired by the biological architectural of the brain [98]. It is made up of several layers of interconnected nodes. Fig. 2.5 shows a single layer feedforward network. It consists of an input layer, hidden layer and output layer. Each layer is interconnected through a weight.

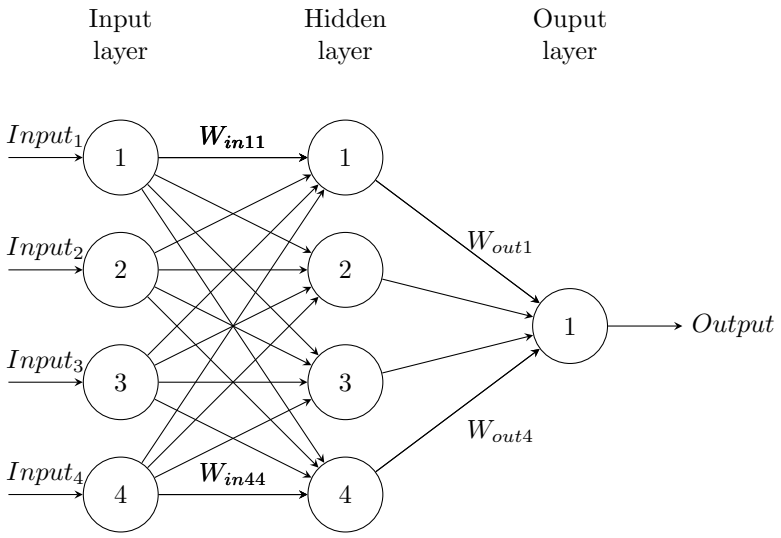

Fig. 2.5 General diagram of the artificial neural network

ANN can be used for various tasks, including forecasting, classification and natural language processing [99–101]. In order for ANN to "learn" these tasks, the process can be broadly split into three parts.

1. Data pre-processing
2. Training of ANN
3. Testing of ANN

Firstly, in data preprocessing, the dataset is split into two or more sets. The dataset is split into training, validating and testing set. In some cases, it is splitted into training and testing set. After the dataset is split into the different sets, the ANN is presented

with the input and expected output of the data. For instance, in forecasting, the input data can be the lagged observation of the data and the output data is the expected value for the current observation.

Secondly, in training of ANN, the model adjusts its weights using training algorithm. The main objective of training algorithm is to adjust the weights in a manner which minimizes the forecasting error. For instance, adjusting the weights to make the output equals to the expected output. The value of these weights affects the effectiveness of ANN. There are many methods of tuning of the weights such as back-propagation [102], Quasi-Newton [103], Levenberg-Marquardt [104]. These iterative based training algorithms are computationally intensive and does not guarantee a global minimal solution [105]. Three training algorithms are considered in this thesis.

Finally, to test the performance of ANN, the model is presented with a new set of data which are not used in training. In this manner the actual performance of the ANN can be evaluated accurately.

There are different architectural of ANN apart from the single layer feed-forward network in Fig. 2.5. The architectural of these ANN are different, but they contain similar hyperparameters such as size and division of dataset, number of hidden nodes and activation function. Two types of ANN are considered in this thesis. They are extreme learning machine (ELM) and deep belief network (DBN). These ANNs have been used in renewable energy forecast [27, 66–68].

2.8.3.1 Extreme Learning Machine

ELM is a fast and none iterative method to tune the weights of a single layer feed forward has been proposed in [106]. This learning algorithm can overcome the shortcoming of traditional gradient descent-based algorithm such as slow training speed, local minimal and tuning of hyperparameters. Furthermore, ELM is also compared with support vector machine and it has demonstrated that it can achieve a higher prediction accuracy and shorter training time. Empirical evidence has shown that ELM is capable of generalization and has universal approximation capability. ELM addressed the long-standing problem of long training time of iterative training algorithms while retaining its generalization and universal approximation capabilities.

2.8.3.2 Deep Belief Network

Deep belief network (DBN) is a variant of deep neural networks with multiple hidden layer in-between the input and output layer [107]. It is a fast and greedy learning algorithm that can be fine-tuned in deep neural networks with many hidden parameters and layers.

DBN consists of multiple layers of interconnected hidden nodes, but not within each layer. It is made up of multiple Restricted Boltzmann Machine (RBM), where the hidden layer is used as the visible input layer for the next hidden layer. Each layer of the RBM are tuned using gradient-descent contrastive divergence algorithm.

2.8.3.3 Hyperparameters of Artificial Neural Network

There are several hyperparameters that repeatedly appears in the literature which require user intervention before implementing any ANN.

- Size and division of dataset
- Number of hidden layer(s) and hidden nodes
- Activation functions
- Performance evaluators

The size and division of dataset are the ratio between training, validating and testing set can be 80:10:10 or 80:20 if there are only training and testing set. The optimal division of dataset remains an open question [108]. However, the literature offers some guidance on this. Several approaches are proposed in the literature such as trial-and-error and k-fold cross-validation [27, 109].

There is a trade-off between having more training set and testing set. A larger training set can contain more information than a smaller dataset, however it may also contain more noise. While a smaller training set would contain less information and less noise. It is important that the training set have sufficient information to uncover the underlying relationship between the input and output.

Regardless of the type of ANN, the size and division of dataset affect the performance of the model. The size of dataset would determine the time taken to train the model. The time taken to train a large dataset may not be feasible or provide a marginal improvement over smaller dataset.

The number of hidden layer and hidden nodes affects the performance of the ANN. A single layer feedforward network is use as a universal approximator. The optimal number of hidden nodes is difficult to determine. Too little hidden nodes and the model will under-fit, it will not be able to approximate the function. Too many hidden nodes and the model will memorize the function. There are many methods to determine the number of hidden nodes such as trial-and-error, genetic algorithm, formulas. However, this method also doesn't scale well with data. Also, the lower and upper limit of the number of hidden nodes remains a question as well.

For trial-and-error approach, some authors suggest incrementing the number of hidden nodes from one to an upper limit to and plot the performance of the model with each increment [66]. The main drawback of this method is it does not scale well with data. As the number of training sample increases, the computation time will also drastically increase.

Determining the number of hidden nodes using formula has been proposed in [110]. However, it does not guarantee an optimal number of hidden nodes and only serves as a guide. The number of hidden nodes can be calculated from (2.18).

$$L_h = \frac{1}{2}(L_i + L_o) + \sqrt{L_p} \tag{2.18}$$

where L_h, L_i and L_o are the hidden, input and output nodes. L_p is the total number of training samples.

Activation function introduced a degree of nonlinearity to the model. When an activation function is nonlinear, then a single layer feedforward network has a universal approximator capability [106]. It also has to be continuously differentiable for it to work with gradient descent-based training algorithms. Several activation functions are proposed in the literature. Most notably, logistic and hyperbolic tangent functions [111].

Performance evaluators are used to measure the predictive accuracy of the ANN models. Typical evaluators are root mean squared error or mean absolute percentage error. They are used to tune the hyperparameters of the model or as a comparison metric with other ANN models. The hyperparameters which requires user intervention depends on which ANN is being implemented. A summary of the different hyperparameters required by each ANN is shown in Table 2.2. For instance, ELM is a single layer feedforward neural network. However, for DBN, the number of hidden layers has to be determine experimentally.

Table 2.2 Hyperparameters of different ANN

Hyperparameters	ELM	DBN
Size and division of dataset	✓	✓
No. of hidden layers		✓
No. of hidden nodes	✓	✓
Performance evaluation	✓	✓

2.8.4 Summary of Computational Intelligence

This section provides an overview of the computational intelligence paradigm. Firstly, the procedure to design and implement a FIS are discussed. Fuzzy logic is well-suited for problem with imprecise or vague information. The effectiveness of the fuzzy logic controller is proportional to the knowledge of the system's designer.

Secondly, single and multi-objective genetic algorithms are discussed. While MOO can be solved using GA, it requires many iterations to obtain the Pareto optimal front solutions. As such, MOGA are proposed to obtain the Pareto optimal front in a single run. Notably, NSGA-II has a lower computational complexity, elitism is ensured and does not require additional parameters to ensure diversity in the population.

Finally, the architectural and three variants of ANN are discussed. The procedure to implement ANN is also discussed. ELM is able to generalize and have universal approximation capability without having additional hyperparameters when compared to iterative training algorithms. DBN consists of multiple RBNs which is trained with a fast and greedy algorithm. The hyperparameters which requires user intervention are identified in this section.

2.9 Research Gap in Energy Storage Management

Real-time operation of ESS in electricity market has gained popularity in the research community in recent years due to the different electricity pricing strategies offered by the independent system operators. Instead of a flat tariff, grid operator can offer RTP or TOU tariff. RTP strategy employs different pricing based on the time of the day and the demand. TOU tariff employs different fixed pricing based on different periods of the day. Both RTP and TOU pricing strategies can incentivize consumers and power system operator [112].

The penetration of intermittent nature RES in power system are expected to increase over the next few decades [113]. Furthermore, large scale application of energy storage system remains an expensive option despite efforts and subsidies for storage from the government. As such, energy management system needs to be designed to reduce the average peak load and operating cost of the microgrid to remain attractive.

Several control strategies have been proposed for the energy management of ESS to minimize the fluctuation of the power profile introduced by RES and the operating cost. GA tuned fuzzy logic controller to reduce fluctuation introduced by wind power generation is proposed in [114]. This method only reduces the fluctuation introduced by wind power generation and does not reduce the operating cost. The ESS is used for wind power smoothing with a fuzzy logic controller with predefined membership function without considering operating cost is proposed in [115]. Similarly, the grid power profile fluctuation is reduced by controlling the ESS is proposed in [116]. Arbitrage operation and reducing peak load using expert knowledge FLC is proposed in [117]. A day-ahead/week-ahead scheduling of ESS to maximize revenue with TOU tariff is proposed in [14]. A bidding, scheduling and deployment of ESS solely for revenue maximization using stochastic optimization without considering any renewable energy sources and load is proposed in [118]. A daily cost minimization using convex optimization by considering a time-of-use tariff and day-ahead forecast of photovoltaic is proposed in [119].

2.9.1 Single Service of Energy Storage

Single service of energy storage has been proposed in the literature. The operation of energy storage is a finite resource optimization problem. As the ESS can operate on different time-scale depending on the type of service provided, e.g. minimizing the fluctuation of RES [114, 115] or operating cost [14, 119, 118] with time-of-use tariff.

Fuzzy Logic Controller (FLC) in microgrid operation have been proposed in [115, 116, 120–124]. ESS operation using FLC for voltage/frequency control [120–124]. The power difference between the demand and available renewable energy and, current capacity of the ESS is considered [116, 124]. ESS is also used for wind power smoothing without arbitrage operation [115].

Similar optimization approaches and objectives are taken into consideration, e.g., maximizing revenue / minimizing cost, power exchange between main grid and microgrid [14, 15]. However, these studies focus on day-ahead and week ahead scheduling based on forecasting of renewable energies, demand and electricity pricing to reduce the

end-user electricity bill or to smoothen the variation introduced by renewable energy sources [16, 115]. The electricity pricing considered is TOU rather than RTP which is highly stochastic [119]. The FLC approach only considers the SOC and difference between demand and RES and did not consider arbitrage operation as one of its objective [116, 124, 115].

In a dynamic environment where demand, availability of RES, and RTP are constantly changing, it is important that the control strategy is designed for arbitrage opportunities in an electricity market apart from providing ancillary services since ESS is costly and energy-limited resources. As such, many recent studies have been done in the operation of energy storage system based on forecasting of RES, demand, and pricing. Several methods such as MILP [14, 15, 125], quadratic programming [16], adaptive dynamic programming [17], and convex optimization [119] are proposed.

2.9.2 Multi-Service of Energy Storage

Apart from a single service, multiple services can be provided by a single storage system. In this case, it can be formulated as a multi-objective optimization or operation problem.

The multi-objective optimization proposed in [126–128] focuses on an aggregated sum of objective functions or reducing the distance of the cost functions to a predefined utopia point. As such only a single solution is found in a single iteration. Furthermore, the design of the EMS is purely based on the MOEA without any expert knowledge in the designing process which have a trade-off between accuracy and interpretability of a fuzzy system [129]. The net cost of electricity and any applicable peak demand cost vectors are reduced by minimizing the Euclidean distance to a predefined utopia point in the solution space [126]. A fuzzy energy management system to reduce the fluctuation of fuel cell current and hydrogen consumption of fuel cell and SC using a weighted sum of objectives is proposed in [127]. A dynamic programming approach to reduce economic cost and CO_2 emission is proposed in [128]. NSGA-II has been used for designing FLC parameters in MOO problems [130–133].

Chapter 3

Proposed Methodologies

3.1 Overview

This chapter presents the mathematical models of a grid-connected microgrid with renewable energy sources (RES) and energy storage system (ESS). After that, two methods are proposed in this chapter for the operation of ESS under the uncertainties of the load, real-time pricing (RTP) and RES.

First, section 3.2 presents the mathematical model of a grid-connected microgrid with RES and ESS.

Second, section 3.3 presents a day-ahead forecast and schedule of energy storage system using artificial neural networks (ANN) and mixed-integer linear programming (MILP) respectively. The objectives of MILP are minimizing of operating cost and reduction of the peak demand of the grid-connected microgrid.

Third, section 3.4.1 proposed a multi-service fuzzy logic-based energy management system (FEMS) for energy storage management. The proposed FEMS fuzzy rules and membership functions are designed based on expert knowledge. The services are energy arbitrage and peak shaving of the grid-connected microgrid.

Fourth, section 3.4.2 proposed an enhanced FEMS. The FEMS fuzzy membership functions are tuned offline using nondominated sorting genetic algorithm-II (NSGA-II). The fitness functions for the NSGA-II are energy arbitrage and peak shaving.

Finally, section 3.4.3 proposed an additional service on top of energy arbitrage and peak shaving. A reserve service (RS) is added to the operation of ESS. The minimum SoC of the ESS changes dynamically depending on different factors which are discussed in detail in section 3.4.3.

3.2 Grid-Connected Microgrid and Energy Storage Models

This thesis considers the problem of operating an ESS which is connected to a microgrid with renewable energy generation capability over a finite-time horizon, $t = 0, \Delta t, 2\Delta t, ..., T$, where Δt is the time step. The time interval is the electricity market trading period. All system variables, constraints, and decisions are made at discrete time intervals of equal and constant length. The remaining of this section describes the mathematical model of microgrid and ESS.

3.2.1 Grid-Connected Microgrid Model

An overview of a grid-connected microgrid test system is shown in Fig. 3.1. The system is similar to those considered in [124, 134, 117]. It consists of photovoltaic (PV) and wind power, load and ESS. The RES and ESS are connected to a DC bus via a unidirectional and bidirectional DC/DC converter. The DC bus is connected to the AC bus via a bidirectional DC/AC converter. The AC bus is connected to the main grid and the AC load. The DC/DC bidirectional conversion losses, for the energy storage system, is considered in this paper.

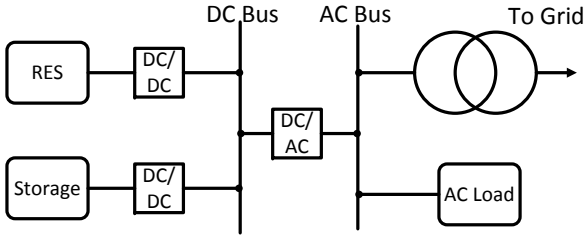

Fig. 3.1 Schematic of grid-connected microgrid

The power generated from wind turbine and PV are P_{wind} and P_{pv} respectively. The total renewable power, P_{res} generated in the microgrid can be calculated from (3.1).

$$P_{res}(t) = P_{wind}(t) + P_{pv}(t) \tag{3.1}$$

Due to the stochastic nature of wind and PV, the power generated may be more or less than actual load, P_{load}. The power difference between actual load and renewable energy is expressed as $P_{balance}$. A positive $P_{balance}$ means the actual load is more

than renewable power generated and a negative $P_{balance}$ means the renewable power generated is more than actual load from (3.2).

$$P_{balance}(t) = P_{load}(t) - P_{res}(t) \tag{3.2}$$

This difference is compensated by charging/discharging the ESS, P_{ess} from (3.3). P_{grid} is the resultant power that has to be met by the main grid.

$$P_{grid}(t) = P_{balance}(t) + P_{ess}(t) \tag{3.3}$$

3.2.2 Energy Storage Model

A generalized storage model is proposed in this thesis. It considers the charge and discharge efficiencies, output power limits and storage capacity of the ESS.

3.2.2.1 Charge and Discharge Efficiencies

The charge and discharge characteristics of the energy storage is shown from (3.4) to (3.6).

$$P_{ess}(t) = P_c(t) - P_d(t) \tag{3.4}$$

$$P_c(t) = \frac{p_c(t)}{\eta_c} \tag{3.5}$$

$$P_d(t) = p_d(t).\eta_d \tag{3.6}$$

where p, η and P are DC power, efficiency and AC power respectively. Subscripts c and d denotes charging and discharging. The energy losses during conversion between DC/AC and AC/DC is considered in (3.5) and (3.6). The net output power of ESS is considered in (3.4) in kW.

3.2.2.2 Output Power Limits

The maximum rated power for the energy storage system is considered in (3.7) to (3.8) in watt.

$$0 \leq P_c(t) \leq \bar{P}_c \tag{3.7}$$

$$0 \leq P_d(t) \leq \bar{P}_d \tag{3.8}$$

where $\bar{P}_c$ and $\bar{P}_d$ are the maximum charge and discharge rate of the ESS

3.2.2.3 Energy Storage State-of-Charge

The state-of-charge (SoC) of the ESS can be expressed as follows using coulomb counting technique:

$$SoC_{min} \leq SoC(t) \leq SoC_{max} \tag{3.9}$$

$$SoC_{model}(t) = SoC_{model}(t-1) + \frac{P_{ess}(t)\Delta t}{E_{max}} \tag{3.10}$$

where Δt is the discrete time interval for decision and $SoC_{model}(t)$ is expressed as a percentage.

3.2.3 Summary of Grid-Connected Microgrid and Energy Storage Models

This section presented a grid-connected microgrid model which considers RES, load and ESS. A generalized storage model is also presented in this section. These mathematical models are used for the rest of this thesis.

3.3 Day-Ahead Forecast and Scheduling of Energy Storage

In this section, a method to determine the day-ahead schedule for the ESS is proposed. The day-ahead energy forecast is obtained using ANN and the microgrid and storage model are formulated into two optimization problems.

First, a single objective optimization of minimizing the operating cost of the microgrid. Second, a multi-objective optimization of minimizing the operating cost and peak load of the microgrid. The second optimization problem is achieved by formulating one of the objective functions as an inequality constraint.

3.3.1 Day-Ahead Energy Forecasting

Extreme Learning Machine (ELM) and Deep Belief Network (DBN) are proposed for the day-ahead energy forecast in this subsection. To determine which ANN is suitable,

the day-ahead forecasting accuracy of load and computation time are used to determine the hyperparameters and evaluate the ANN. After the suitable ANN is identified, it is used to forecast the rest of the variables.

3.3.1.1 Extreme Learning Machine

ELM is a single-layer feedforward network as shown in Fig. 3.2. It consists of an input layer, X, hidden layer H, and finally output layer T. It has a normally distributed random input weight matrix, W.

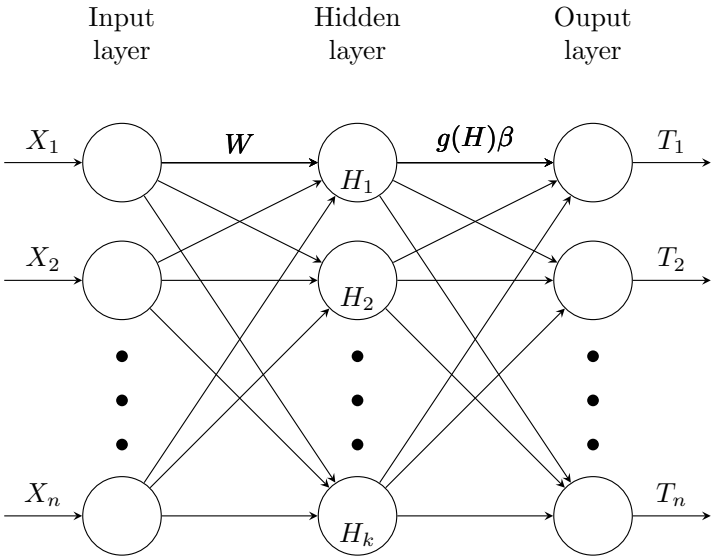

Fig. 3.2 Single layer feedforward network for training ELM

To train the ELM, the lagged observations of the variable are used as the input vector, X and expected output as the output vector, T. The output layer weights, β are determined analytically through the Moore-Penrose pseudo inverse.

Algorithm 1: Training ELM

Initialize: Training input and expected output, X and T;
Number of hidden nodes, k;
Activation function $\sigma(.)$

1. Generate a normally distributed weight matrix, W
2. Calculate the hidden layer weight matrix, H
3. Determine the output weight matrix analytically, β
4. Evaluate the forecasting accuracy of ELM

The input vector X represents the training dataset for ELM.
where n is the length of the lagged observation.

$$X = \begin{bmatrix} X_1 \\ \vdots \\ X_n \end{bmatrix}_{n \times 1} \tag{3.11}$$

The input layer and hidden layer are connected by a weight matrix, W.
where k is the number of hidden nodes.

$$W = \begin{bmatrix} W_{11} & ... & W_{1k} \\ \vdots & \ddots & \vdots \\ W_{j1} & ... & W_{jk} \end{bmatrix}_{j \times k} \tag{3.12}$$

To calculated the hidden layer matrix H, multiply the input layer and weight matrix as shown in (3.13).

$$H = XW \tag{3.13}$$

$$H = \begin{bmatrix} X_{11}W_{11} & ... & X_{1j}W_{1k} \\ \vdots & \ddots & \vdots \\ X_{n1}W_{j1} & ... & X_{nj}W_{jk} \end{bmatrix}_{n \times k} \tag{3.14}$$

After obtaining the hidden layer matrix, multiply it by the activation function to get the hidden layer output matrix, H_{out}, where σ is the activation function.

$$H_{out} = \sigma(H) \tag{3.15}$$

Finally, the output of a single layer feedforward network is T. The hidden layer and output layer are connected by a weight matrix, β.

$$\hat{T} = H_{out}\beta \tag{3.16}$$

The hidden layer output matrix is nonsquare matrix, hence does not have an exact solution. A Moore-Penrose pseudo inverse can guarantee least square solution.

There exist a β such that,

$$||H_{out}\hat{\beta} - T|| = \min_{\beta} ||H_{out}\beta - T|| \tag{3.17}$$

The smallest norm least squares solution can be obtained

$$\beta = H_{out}^{\dagger}T \tag{3.18}$$

where $H_{out}^{\dagger}$ is the Moore-Penrose pseudo inverse of H_{out}, which can be calculated through orthogonal projection.

$$H_{out}^{\dagger} = (H^T H)^{-1} H^T \tag{3.19}$$

The actual output T is a 1 $\times$ n vector.

$$T = \begin{bmatrix} T_1 \\ \vdots \\ T_n \end{bmatrix}_{n\times 1} \tag{3.20}$$

After the output layer weights β are determined, the ELM is evaluated with the testing set. The input and hidden layer weights from the training are kept, while the input vector is changed to the testing set. The predicted output, $\hat{Y}$ of the ELM is compared with the expected output, Y to evaluate the forecasting accuracy of the ELM. The hyperparameter for ELM is the number of hidden nodes.

3.3.1.2 Deep Belief Network

Figure 3.3 shows a two hidden layer DBN. Each hidden layer is treated as a restricted Boltzmann machine (RBM). The input layer is treated as the visible layer. The weights between the visible layer and next hidden layer are tuned with contrastive divergence procedure. After the weights are tuned, another set of hidden nodes are "stacked" on the first hidden layer. Now the first hidden layer is the visible layer. After all the layers are trained, the target or desired output are added as the output layer. This process is repeated until the desired stopping criterion is met.

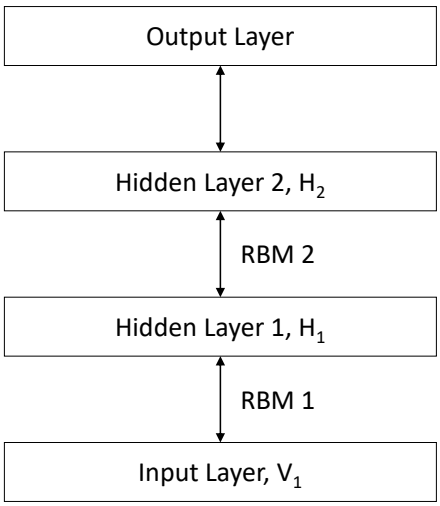

Fig. 3.3 Two hidden layer deep belief network

Algorithm 2: Training DBN

Initialize: Training input and expected output, X and T;
Number of hidden nodes, k;
Activation function $\sigma(.)$

1. Initialize the visible layer to training input, X
2. Positive and negative phase for RBM
3. Adjust the weights between visible and hidden layer
4. Add the targets to the final layer of the DBN and train with backpropagation algorithm.

A contrastive divergence-based method is used to train the DBN. It consists of two phases, a positive phase and a negative phase. During the positive phase, the probability of $P(H = 1|X)$,

$$P(H = 1|X) = \sigma(a_k + \sum_{1}^{k} X_{nj} W_{jk}) \tag{3.21}$$

where σ, a, X and W are the activation function, bias vector, input matrix and hidden layer weight matrix. k, n and j are the number of hidden layer nodes, input layer nodes and input variables.

During the negative phase, $P(X = 1|H)$,

$$P(X = 1|H) = \sigma(b_k + \sum_{1}^{k} H_{nj} W_{jk}) \tag{3.22}$$

where b is the bias vector.

The goal of contrastive divergence is to reconstruct the visible layer input onto the hidden layer output by making several forward and backward passes. Hence the error between X and H is calculated from (3.23).

$$\textbf{Error} = X - H \tag{3.23}$$

$$\Delta w_{jk} = \eta(< XH >_{data} - < X'H' >_{recon}) \tag{3.24}$$

where η is the learning rate.

Once the RBN is trained, another layer of hidden nodes, H_2 are added to the hidden layer, H_1 as shown in Fig. 3.3. Now H_1 is used as the input layer and H_2 is used as the hidden layer. The new RBM is trained using the same contrastive divergence procedure. This process is repeated until the stopping criterion is met. The hyperparameters for DBN are the number of epochs, number of nodes in each hidden layer and the number of RBM to be added in the DBN and learning rate.

3.3.1.3 Performance Evaluation for Forecasting

The forecasting accuracy is evaluated using mean absolute percentage error (MAPE) and root mean square error (RMSE).

MAPE is used to measure forecasting accuracy of the model and expressed as a percentage as shown in (3.25). The absolute difference between the estimated and

actual values are divided by the actual value. These values are summed up and divided by the total number of data points and finally converted into a percentage. A MAPE is always non-negative and a value of 0% represents a perfect forecast.

Intuitively, it seems like MAPE is straightforward and can be used to compare the forecasting accuracy of different methods. However, it cannot be used if there are zero values in the data. For instance, PV have no generation in the night, hence 0 kW would be the actual value, MAPE is unable to quantify this error in this case as there is a division by zero.

$$\text{MAPE} = \frac{100\%}{n} \sum_{t=1}^{n} \frac{|y_t - \hat{y}_t|}{y_t} \tag{3.25}$$

where $\hat{y}_t$, y_t and n are the estimated, actual values and total number of data points.

RMSE is used to measure the forecasting accuracy of the model as shown in (3.26). A RMSE is always non-negative and a value of 0 represents a perfect forecast, where the actual and estimated value are the same for every data points.

$$\text{RMSE} = \sqrt{\frac{\sum_{t=1}^{n} (\hat{y}_t - y_t)^2}{n}} \tag{3.26}$$

where $\hat{y}_t$, y_t and n are the estimated, actual values and total number of data points.

The value of RMSE is dependent on the scale of the data. It can be difficult to compare the forecast accuracy across different datasets. For instance, there is little meaning when comparing the forecast accuracy of demand data which is in kW range and electricity pricing data which is in $/MWh. Furthermore, if the dataset has a range of values from 0 to 1000, a RMSE of 10 would seem to be small, which signify a high forecasting accuracy. However, if the dataset has a range from 0 to 10, a RMSE of 10 would be large, which signify a low forecasting accuracy.

The size of the neural network and training data affects the computational time and scalability of the model. The computational time taken to train the network is also considered as a performance evaluation index.

3.3.2 Mixed Integer Linear Programming for Day-Ahead Scheduling of Energy Storage System

This thesis considers the problem of operating an ESS which is connected to a microgrid with renewable energy generation capability over a finite-time horizon, $t = 0, \Delta t, 2\Delta t, ..., T$, where Δt is the time step. Each time step is fifteen minutes and there are ninety-six time steps in a day.

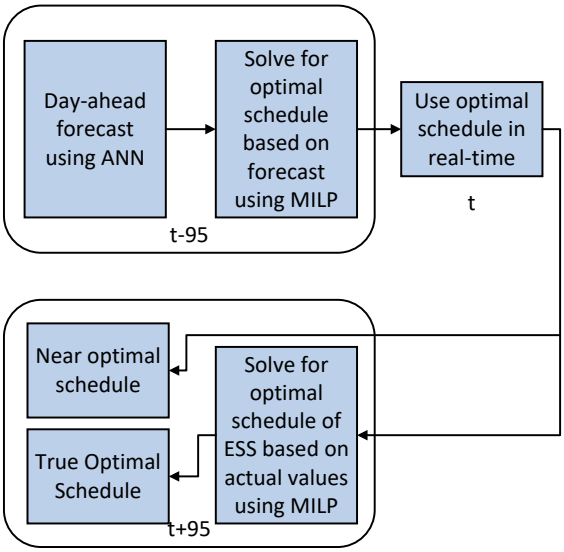

Fig. 3.4 Flow of day-ahead scheduling of energy storage system

The proposed near-optimal day-ahead scheduling of ESS is shown in Fig. 3.4. From $T = t - 95$, the day-ahead values of P_{load}, P_{pv}, P_{wind} and C_p are forecast using ANN. At $T = t$ getting the day-ahead values of P_{load}, P_{pv}, P_{wind} and C_p, the optimal day-ahead scheduling of ESS problem is formulated into a cost minimizing problem and solved using mixed-integer linear programming. The near-optimal schedule based on day-ahead forecast is used for the next day. The true optimal can be obtained by solving the cost minimizing problem with the actual value at $T = t + 95$.

The day-ahead schedule is near-optimal as there will always be error in the forecasting, which results in a near-optimal schedule. The true optimal schedule can be obtained after the realization of the uncertain variables at $T = t + 95$ and used as a comparison to the near-optimal schedule.

3.3.2.1 Minimizing Operating Cost

The grid-connected microgrid is operating under RTP and the total operating cost can be calculated using (3.27). As the focus of this thesis is the operation of ESS, the initial capital and maintenance cost are not considered.

$$f_1 = \sum_{t=1}^{T}[P_{balance}(t) + \frac{p_c(t)}{\eta_c} - p_d(t).\eta_d]C_p(t), \forall t \in T \tag{3.27}$$

where $C_p(t)$ is the current electricity price for time t.

By adding two binary variables, $U_c(t)$ and $U_d(t)$ to (3.7) and (3.8), and an additional constraint (3.28), ensures that the status of ESS is either charge or discharge.

$$U_d(t) + U_c(t) \leq 1, \forall t \in T \tag{3.28}$$

The decision variables for MILP are $p_c(t)$, $p_d(t)$, $U_c(t)$ and $U_d(t)$. MILP solves for the value of these variables for every time step to minimize the objective function. The MILP is formulated as follows:

$$\begin{aligned}
\min \quad & \sum_{t=1}^{T}[P_{balance}(t) + \frac{p_c(t)}{\eta_c} - p_d(t).\eta_d]C_p(t), \forall t \in T \\
\text{s.t.} \quad & 0 \leq \frac{p_c(t)}{\eta_c} \leq P_{c,max}U_c(t), \forall t \in T \\
& 0 \leq p_d(t).\eta_d \leq P_{d,max}U_d(t), \forall t \in T \\
& U_d(t) + U_c(t) \leq 1, \forall t \in T \\
& SoC_{min} \leq SoC(t) \leq SoC_{max}, \forall t \in T \\
& SoC_{model}(t) = SoC_{model}(t-1) + \frac{P_{ess}(t)\Delta t}{E_{max}}, \forall t \in T
\end{aligned} \tag{3.29}$$

3.3.2.2 Peak Load Reduction

The peak load of the grid-connected microgrid can be reduced by adding a nonequality constraint to P_{grid}, from (3.3).

$$P_{grid}(t) \leq P_{max}, \forall t \in T \tag{3.30}$$

where P_{max} is a constant to ensure the maximum value of P_{grid} is below this level.

Using the problem formulation in (3.29) and an addition inequality constraint (3.30), the MILP will solve the value of $p_c(t)$, $p_d(t)$, $U_c(t)$ and $U_d(t)$ for every time step

to minimize the objective function. The MILP is formulated as follows:

$$\begin{aligned}
\min \quad & \sum_{t=1}^{T}[P_{balance}(t) + \frac{p_c(t)}{\eta_c} - p_d(t).\eta_d]C_p(t), \forall t \in T \\
\text{s.t.} \quad & 0 \leq \frac{p_c(t)}{\eta_c} \leq P_{c,max}U_c(t), \forall t \in T \\
& 0 \leq p_d(t).\eta_d \leq P_{d,max}U_d(t), \forall t \in T \\
& U_d(t) + U_c(t) \leq 1, \forall t \in T \\
& SoC_{min} \leq SoC(t) \leq SoC_{max}, \forall t \in T \\
& SoC_{model}(t) = SoC_{model}(t-1) + \frac{P_{ess}(t)\Delta t}{E_{max}}, \forall t \in T \\
& P_{grid}(t) \leq P_{max}, \forall t \in T
\end{aligned} \tag{3.31}$$

The values of $P_{load}(t)$, $P_{res}(t)$ and $C_p(t)$ from $t = 0$ to $t = T$ is forecasted using ANN. The solution obtained by MILP represents the optimal schedule for $p_c(t)$ and $p_d(t)$ from $t = 0$ to $t = T$. The MILP formulation described here is implemented in AMPL and solved using CPLEX [135].

3.3.3 Summary of Day-Ahead Scheduling of Energy Storage

Two ANNs are presented in this section for forecasting. The hyperparameters required by each ANN are also identified. The performance evaluation methods are also presented in this section.

The uncertainty of the microgrid variables can be forecast using ANN, hence transforming the storage operation problem from a nondeterministic optimization to a deterministic problem. The multi-objective optimization using MILP achieved by changing one of the objective functions into a nonequality constraint.

Two deterministic optimization problem are proposed in this section. First, the operating cost of the grid-connected microgrid is minimized. Second, the peak load of the grid-connected microgrid is added as one of the nonequality constraint. The near-optimal schedule is used for the next day for the operation of ESS.

3.4 Multi-Service of Single ESS

In this section, a FEMS is designed with the historical data of the microgrid for energy arbitrage and peak demand reduction using a single ESS. These services are choosen as they operating in a similar time scales as shown in Table 2.1.

First, in subsection 3.4.1, instead of using a forecasting-based approach, the proposed FEMS is designed based on expert knowledge. The FLC rules are designed for energy arbitrage and to reduce the peak demand in the microgrid. The fuzzy membership functions should represent the distribution of the historical data. A uniformly distributed membership functions are usually chosen for simplicity purpose. However, it may not yield satisfactory performance when the standard deviation of the fuzzy variable is high. In this subsection, a median-σ method is proposed to design the membership function for the electricity market price. As it is highly volatile and non-stationary due to the dynamic market environment. Several performance evaluation indices are proposed in this subsection to measure the effectiveness of the FEMS. Furthermore, the proposed FEMS is compared with two benchmarking algorithms on a simulation level.

Second, subsection 3.4.2, proposed an offline tuning of the FEMS fuzzy membership functions using a Pareto based multi-objective evolutionary algorithm, NSGA-II. The best compromise solution is selected as the final solution and implemented in the fuzzy logic controller. A comparison with other control strategies with similar objectives are carried out on a simulation level. The proposed FEMS is experimentally validated on a real microgrid in the energy storage test bed at Newcastle University, UK.

Finally, subsection 3.4.3, the ESS provides an additional RS on top of the two services mentioned in subsection 3.4.1.

3.4.1 Multi-Service of Single ESS: Energy Arbitrage and Peak Shaving

In this subsection, a median-σ method is proposed to design the membership function for the electricity market price as it is volatile and non-stationary due to the dynamic market environment.

The main contributions of this section are listed as follows: 1) A decision making controller for ESS control designed with historical data of the microgrid hence omitting the need for forecasting. 2) End-user electricity bill and power exchange between main

and microgrid are reduced while meeting the demand without any demand side management techniques.

A Mamdani type fuzzy logic controller (FLC) is proposed as an energy management system to control the active power of ESS based on the power difference between RES and load, ESS SoC and electricity market pricing. An overview of the FEMS is illustrated in Fig. 3.5.

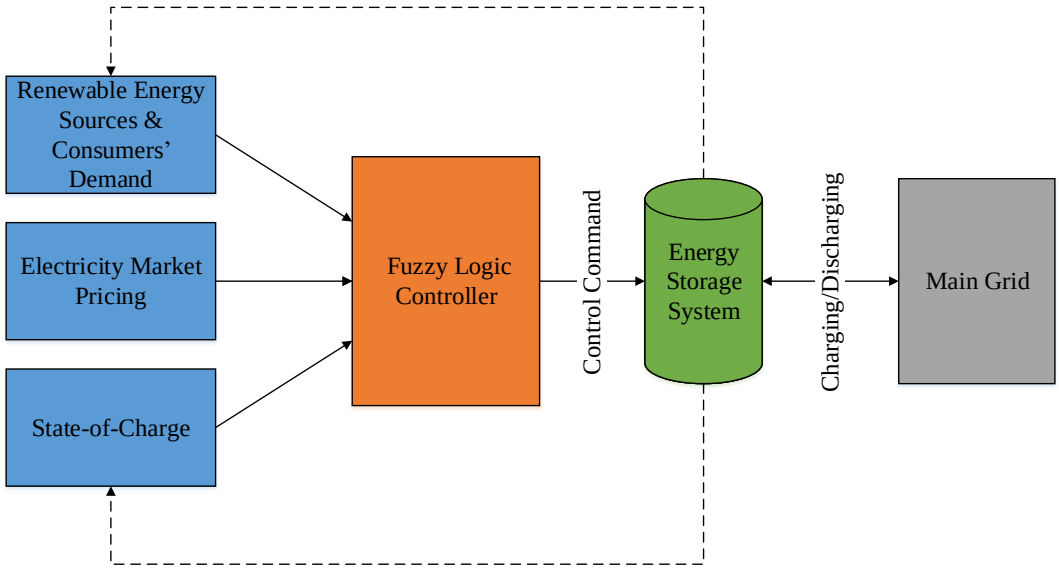

Fig. 3.5 Framework of proposed fuzzy logic-based energy management system

The proposed FEMS aims to:

1. Energy arbitrage operation of ESS
2. Reduce peak demand of the microgrid
3. Avoid over/under charging of ESS by maintaining its SoC within the upper/lower boundaries

The first and second aims are achieved by discharging the ESS during high demand or cost period and charge during low demand or cost period. The third aim is achieved by operating the ESS within its upper and lower limits.

The proposed FEMS is designed to reduce the consumers' electricity bill and reduce the peak demand microgrid. To numerically evaluate the proposed FEMS, a set of performance evaluation indices are proposed in the next subsection.

3.4.1.1 Design of Fuzzy Membership Functions

One important procedure in implementing a FLC is to determine the fuzzy membership functions. In this thesis, triangle and trapezoid membership functions are used. A uniformly distributed triangle membership functions are used for $P_{balance}$, P_{ess} and SoC. The three inputs are divided into five linguistic terms, negative big (NB), negative small (NS), zero (ZE), positive small (PS) and positive big (PB).

For $P_{balance}$, NB means renewable generation is higher than actual load from (3.2). ZE means renewable generation is equal to actual load and finally, PB means the load is a lot higher than the renewable generation. For SoC, NB means the SoC is very low, ZE means it is at half capacity, and PB means it is near full capacity. For P_{ess}, NB means a high discharging rate, ZE means idle, and PB means a high charging rate. Historical data of P_{res} and P_{load} are used to calculate $P_{balance}$. The range of $P_{balance}$ is used to determine the range of the fuzzy membership function.

For P_{ess} and SoC, the technical constraints from (3.7) to (3.9) of the ESS are considered when designing the membership functions. For P_{ess}, the range of the membership function is from the maximum discharge rate to the maximum charge rate. This ensures that the controller can quantify the output power limit of the ESS. For SoC, the membership function ranges from the upper to lower operating boundary of the ESS. This ensures that the controller operates the ESS within this limit.

For C_p, there are five linguistic terms for this input which is: negative (N), zero (ZE), positive small (PS), positive big (PB), and positive big big (PBB). The standard deviation of C_p is significantly higher than $P_{balance}$. Instead of having a uniformly distributed membership function for C_p, another approach is taken and explained in details below.

From Table 3.1, the real-time electricity price has a much higher standard deviation compared to $P_{balance}$. As such, a uniformly distributed triangle membership function does not represent the linguistic term properly.

Table 3.1 $P_{balance}$ and C_p parameters

	Max	Min	Median	Standard Deviation, σ
$P_{balance}$ (kW)	26.73	-16.74	5.05	6.65
C_p (\$/MWh)	929.31	1.44	128.10	46.02

The real-time electricity price for the year of 2014 is shown in Fig. 3.6. It is observed that C_p experienced significant numbers of peak and abrupt changes throughout the sampled period. The proposed method can be modified to suit different market data.

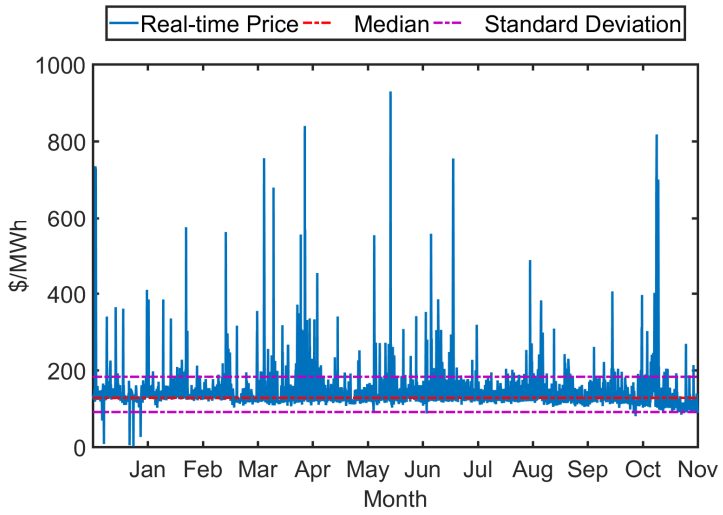

Fig. 3.6 Real-time electricity price for 2014, C_p

The median and standard deviation, σ, of C_p are used to design the membership functions. For C_p, N means low price(-1σ from the median), ZE means median price and PBB means extremely high price ($+3\sigma$ from the median). A trapezoid membership function is used to represent N and PBB while a triangle membership function is used to represent ZE, PS, and PB. Firstly, the median price of C_p is used to represent the peak of ZE. Secondly, since the majority of the price is within $\pm 1\sigma$, hence it is used to represents the peak of N and PS respectively. Thirdly, the peak of PB is represented by $+2\sigma$ since the occurrence is significantly lower. Finally, the peak of PBB is represented by any prices beyond $+3\sigma$.

3.4.1.2 Design of Fuzzy Rules

The proposed FLC has the liberty to buy(charge) and sell(discharge) power from the main grid when $P_{balance}$ is zero to reduce the end user operating cost. This set of fuzzy rules are designed to yield economic rewards by charging when $P_{balance}$ is zero and the price is low and discharge when the price is high. In this manner, P_{grid} will slightly increase/decrease due to the additional charging and discharging of ESS when $P_{balance}$

is zero. On top of this, to reduce the fluctuation of the grids' power profile, the storage discharges when renewable energy is absent and charges when there is an excess.

The ESS will operate in two different modes based on the value of $P_{balance}$. The $P_{balance}$ can take one of the three states; positive, negative or zero as mentioned in Section 3.2.1. When $P_{balance}$ is zero, it will operate in arbitrage mode, and when $P_{balance}$ is positive or negative, it will operate to reduce power exchange mode.

When $P_{balance}$ is zero, fuzzy rules number 51 to 75 enable the ESS to operate in arbitrage condition. To discharge when the price is high, an example shown in Table 3.2, rule number 53 corresponds to:

IF $P_{balance}$ is ZE and SoC is PB and C_p is PS THEN P_{ess} is NS.

There is no difference between the supply and demand, battery capacity is near its maximum capacity, and the price is high, the ESS will discharge.

Similarly, to charge when the price is low, an example shown in Table 3.2, rule number 71 corresponds to:

IF $P_{balance}$ is ZE and SoC is NB and C_p is N THEN P_{ess} is PB.

There is no difference between the supply and demand, battery capacity is near its minimum capacity, and the price is low, the ESS will charge.

When $P_{balance}$ is positive or negative, fuzzy rules number 1 to 50 and 76 to 125 reduces the power exchange between the main and microgrid. To reduce the peak demand of the microgrid, in the example shown in Table 3.2, rule number 1 corresponds to:

IF $P_{balance}$ is PB and SoC is PB and C_p is N THEN P_{ess} is NB.

When the load is more than RES, and the battery capacity is near its maximum capacity, the ESS will discharge at a high rate to compensate for the shortfall of renewable.

Similarly, when $P_{balance}$ is negative, it means that there is a surplus of RES. In example shown under Table 3.2, rule number 125 corresponds to:

IF $P_{balance}$ is NB and ESS is NB and C_p is PBB THEN P_{ess} is PB.

This means that when there is a surplus of RES, and the battery capacity is near its minimum capacity, the ESS will charge at a high rate to absorb the surplus RES.

Extending this reasoning to other linguistic terms results to the fuzzy rules in Table 3.2.

Table 3.2 Proposed fuzzy logic controller rules

$P_{balance}$ is positive, $P_{load} > P_{res}$					$P_{balance}$ is zero, $P_{load} = P_{res}$					$P_{balance}$ is negative, $P_{load} < P_{res}$				
No.	Pbalance	SoC	Price	Pess	No.	Pbalance	SoC	Price	Pess	No.	Pbalance	SoC	Price	Pess
1	PB	PB	N	NB	**26**	PS	PB	N	NB	**51**	ZE	PB	N	NB	**76**	NS	PB	N	ZE	**101**	NB	PB	N	ZE
2			ZE	NB	**27**			ZE	NB	**52**			ZE	NB	**77**			ZE	NS	**102**			ZE	NS
3			PS	NB	**28**			PS	NB	**53**			PS	NB	**78**			PS	NB	**103**			PS	NB
4			PB	NB	**29**			PB	NB	**54**			PB	NB	**79**			PB	NB	**104**			PB	NB
5			PBB	NB	**30**			PBB	NB	**55**			PBB	NB	**80**			PBB	NB	**105**			PBB	NB
6		PS	N	NB	**31**		PS	N	NB	**56**		PS	N	PS	**81**		PS	N	PS	**106**		PS	N	PS
7			ZE	NB	**32**			ZE	NB	**57**			ZE	PS	**82**			ZE	PS	**107**			ZE	PS
8			PS	NB	**33**			PS	NB	**58**			PS	NS	**83**			PS	PS	**108**			PS	PS
9			PB	NB	**34**			PB	NB	**59**			PB	NB	**84**			PB	PS	**109**			PB	PS
10			PBB	NB	**35**			PBB	NB	**60**			PBB	NB	**85**			PBB	PS	**110**			PBB	PS
11		ZE	N	NB	**36**		ZE	N	NS	**61**		ZE	N	PS	**86**		ZE	N	PS	**111**		ZE	N	PB
12			ZE	NB	**37**			ZE	NS	**62**			ZE	PS	**87**			ZE	PS	**112**			ZE	PB
13			PS	NB	**38**			PS	NB	**63**			PS	NS	**88**			PS	PS	**113**			PS	PB
14			PB	NB	**39**			PB	NB	**64**			PB	NS	**89**			PB	PS	**114**			PB	PB
15			PBB	NB	**40**			PBB	NB	**65**			PBB	NB	**90**			PBB	PS	**115**			PBB	PB
16		NS	N	NS	**41**		NS	N	NS	**66**		NS	N	PB	**91**		NS	N	PB	**116**		NS	N	PB
17			ZE	NS	**42**			ZE	NS	**67**			ZE	PS	**92**			ZE	PB	**117**			ZE	PB
18			PS	NS	**43**			PS	NB	**68**			PS	NS	**93**			PS	PB	**118**			PS	PB
19			PB	NS	**44**			PB	NB	**69**			PB	NS	**94**			PB	PB	**119**			PB	PB
20			PBB	NS	**45**			PBB	NB	**70**			PBB	NB	**95**			PBB	PB	**120**			PBB	PB
21		NB	N	ZE	**46**		NB	N	ZE	**71**		NB	N	PB	**96**		NB	N	PB	**121**		NB	N	PB
22			ZE	ZE	**47**			ZE	ZE	**72**			ZE	PS	**97**			ZE	PB	**122**			ZE	PB
23			PS	ZE	**48**			PS	ZE	**73**			PS	NS	**98**			PS	PB	**123**			PS	PB
24			PB	ZE	**49**			PB	ZE	**74**			PB	NS	**99**			PB	PB	**124**			PB	PB
25			PBB	ZE	**50**			PBB	ZE	**75**			PBB	NS	**100**			PBB	PB	**125**			PBB	PB

3.4.1.3 Performance Evaluation Indices

To quantify the effectiveness proposed controllers, several performance evaluations indices are proposed in this subsection.

Three performance evaluation indices to quantify the effectiveness of the proposed controllers are defined in this subsection. They are standard deviation, σ, operating cost and load factor.

3.4.1.4 Standard Deviation of Microgrid Power Profile

Standard deviation is used to measure the variation in P_{grid} away from its mean. As shown in (3.3), P_{grid} is the resultant power that has to be met by the main grid. The variation in the power profile is reduced by reducing the standard deviation, σ.

$$\sigma = \sqrt{\frac{\sum_{t=1}^{T}(P_{grid}(t) - P_{grid}, \mu)^2}{T}} \tag{3.32}$$

where t is the t^{th} sample and T is the total number of samples.

3.4.1.5 Operating Cost of Grid-Connected Microgrid

To quantify the amount economic benefits of the proposed controllers, (3.33) is used to calculate the operating cost. It consists of $P_{balance}, P_c$, and P_d. Which are the resultant power of the microgrid, and charging and discharging rate of the ESS. The proposed controllers consider real-time pricing, C_p, in \$/MWh as one of its input to determine the charge and discharge rate. This index should be reduced.

$$Cost = \sum_{t=1}^{T}[P_{balance} + P_c(t) - P_d(t)]C_p(t) \tag{3.33}$$

As the focus of this thesis is the operation of ESS. The initial capital and maintenance cost of the ESS are considered in the planning phase of the microgrid hence it is omitted in the operation phase [136]. Also, the arbitrage operation of ESS will not have a considerable effect on the electricity market price. As such, the microgrid can freely purchase and sell electricity from the main grid at time t at the same market price, $C_p(t)$.

3.4.1.6 Load Factor of Microgrid Power Profile

Load factor calculates the ratio between average and peak load over a period of time, τ.

$$LF = \frac{|P_{grid}, \mu.\tau|}{|P_{grid}, max.\tau|} \tag{3.34}$$

where P_{grid}, μ is the average power and P_{grid}, max is the maximum power consumption over the time period of interest, τ. Where τ is the monthly billing period.

The load factor (LF) is always less than one and a higher load factor signify the load profile over the period of interest is close to constant. Low load factor signifies an erratic power profile. The LF can be increased in two ways; decrease P_{grid}, max or increase P_{grid}, μ. The former is favorable because operating cost increases when P_{grid}, μ increases.

The proposed FEMS is implemented in MATLAB/Simulink and executed on a workstation with an Intel XEON E3-1271 CPU running at 3.60 GHz.

3.4.1.7 Implementation of Microgrid and ESS Model using Simulink

The proposed microgrid and energy storage model are implemented in MATLAB/ Simulink environment and are discussed in this subsection.

Fig. 3.7 shows the simulink diagram of the proposed grid-connected microgrid. The historical data of P_{load}, P_{pv}, P_{wind} and C_p are imported from MATLAB workspace into the simulink. The energy storage efficiency and SoC estimator blocks are shown in Fig. 3.8.

Fig. 3.8a shows the efficiency block for ESS according to (3.4). This block considers a constant charge and discharge efficiencies for the storage. The constant block η_c and η_d can be replaced with a lookup table for different efficiencies at different power levels.

Fig. 3.8b shows the SoC estimation block from (3.10). It considers the current $P_{ess}(t)$ and previous $SoC(t-1)$ to estimate the current $SoC(t)$.

The simulink models are created to read the microgrid data from the MATLAB workspace to the simulink. These data are processed by the fuzzy logic block in the simulink. The output of the fuzzy block is used to estimate the SoC of the storage system and fed back as an input. P_{grid} from the simulink model is used to evaluate the effectiveness of the proposed FEMS using (3.32) and (3.34).

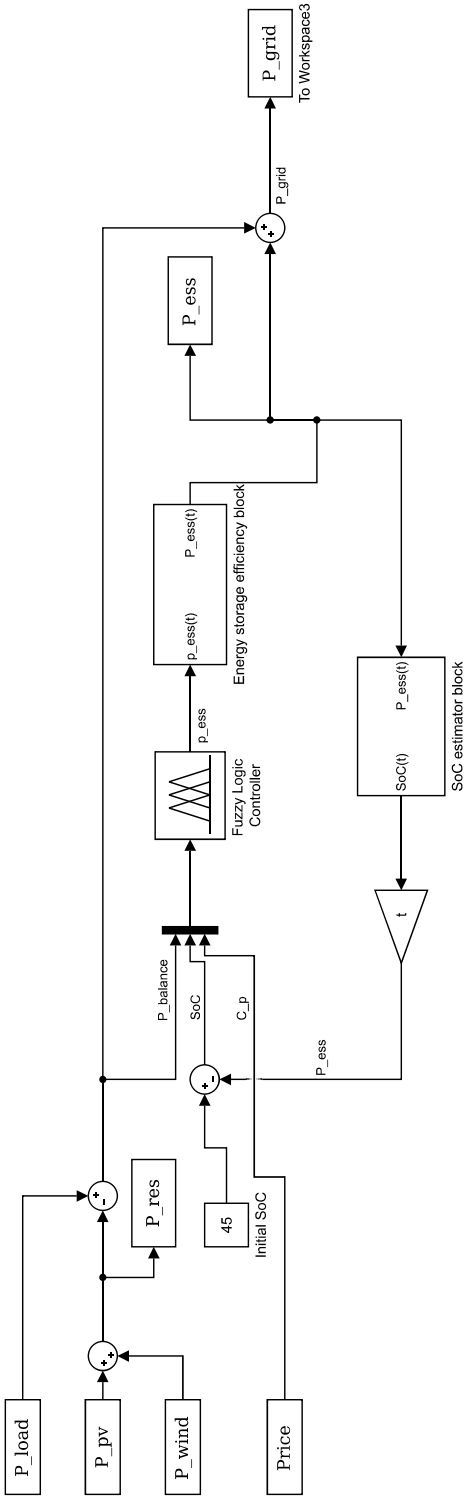

Fig. 3.7 Simulink diagram of proposed microgrid

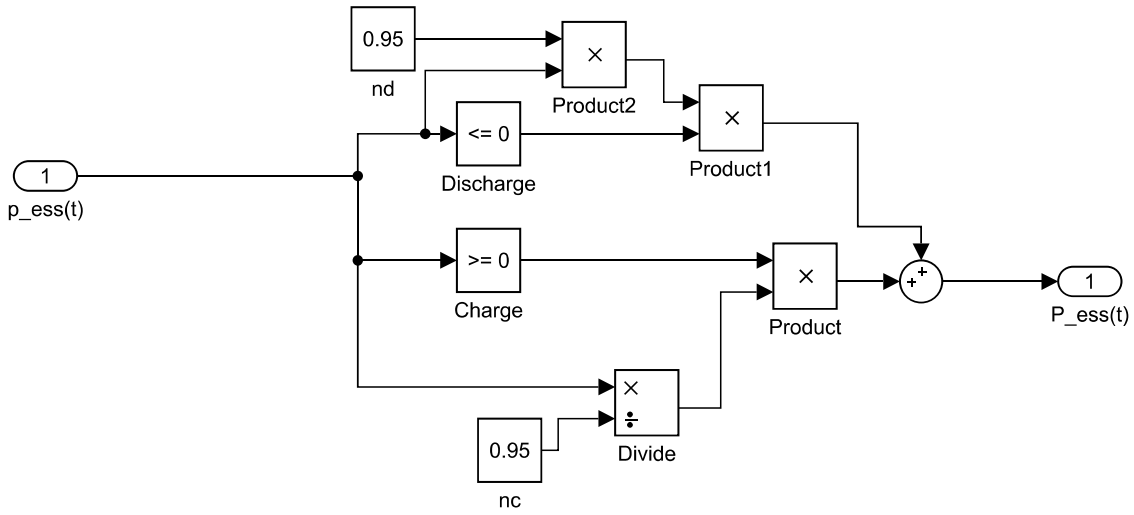

(a) Energy storage efficiency block

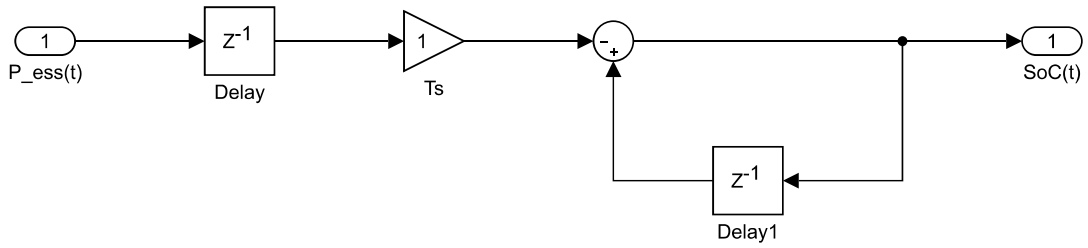

(b) State-of-charge estimator block

Fig. 3.8 Simulink subsystem from Fig.3.7

3.4.2 Enhanced Fuzzy Logic Based Energy Management System

The fuzzy membership functions and rules are designed by expert knowledge in the previous subsection. The effectiveness of the proposed FEMS is satisfactory however it can be improved by optimizing the fuzzy membership functions placement. This subsection presents a MOEA method to tune the membership functions of the proposed FEMS. To maintain interpretability, only the fuzzy membership functions are tuned in this subsection while the fuzzy rules are determined through expert knowledge.

Conventionally, when using computational evolutionary algorithms to solve an optimization problem, the solutions are usually randomly generated and refined over many generations. However, in this proposed methodology, the expert knowledge is added into the initial population of the genetic algorithm.

The main contributions of this subsection are listed as follows. (1) Minimizing operating cost and average peak load (APL) of microgrid simultaneously by tuning the proposed fuzzy logic-based energy management system using NSGA-II. (2) Expert knowledge is integrated into the design process of optimizing FEMS (3) Pareto optimal solutions are found using NSGA-II, and the best compromise solution is selected without the imprecise nature of the decision maker's judgment. (4) Real- time simulation and experimental validation of the proposed controller.

The first and second aims are achieved by discharging the ESS during high demand or cost period and charge during low demand or cost period. The third aim is achieved by operating the ESS within the upper and lower limits. The proposed FLC is designed to reduce the consumers' electricity bill and peak demand of the microgrid.

NSGA-II is fast and efficient in finding the Pareto-front compared to other multi-objective evolutionary algorithms such as Pareto-archived evolution strategy (PAES) and strength Pareto EA (SPEA) [79]. NSGA-II is implemented and used offline to optimize the location of the membership functions by minimizing the operating cost and APL of the grid-connected microgrid while satisfying the constraints in Section 3.2.

Fig. 3.9 shows the computational flow of NSGA-II. Firstly, the initial population which consists of chromosomes are randomly generated. Secondly, the fitness of each chromosome is evaluated using fitness function. Thirdly, chromosomes are ranked according to their domination count and crowding distance. Fourthly, chromosomes with a lower domination count are selected. Finally, the selected chromosome undergo

genetic operation to create the next generation of chromosomes. This process is repeated until the maximum number of generations is reached.

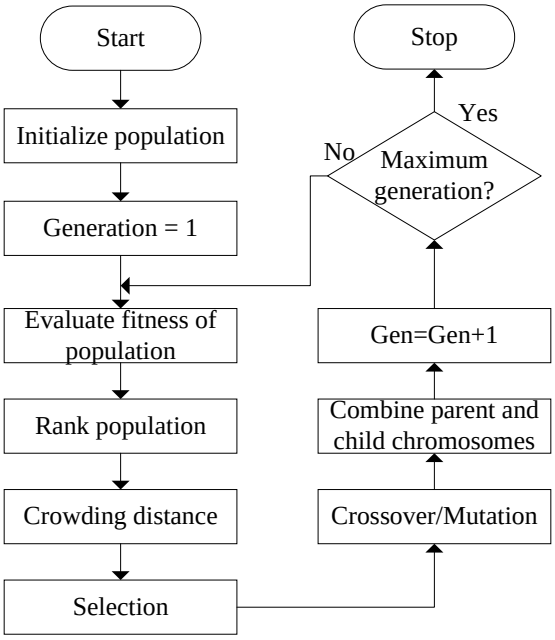

Fig. 3.9 Computational flow of NSGA-II

3.4.2.1 Chromosomes Design

The type of encoding and the total number of membership functions determines the length of each chromosome. The membership functions are coded as a string of real numbers. As precision is lost when the solutions are coded in binary and incrementing to a neighboring solution require many bits change [81].

Five membership functions are used to represent different linguistic term for each input variable of the FLC. The membership functions tuned in this work are triangle and trapezoid. The membership functions are encoded into chromosomes which represent a potential solution.

Let chromosome be $C_{j,q}^{g}$,

$$C_{j,q}^{g} = \overbrace{x_1, \underbrace{x_2, x_3,}_{M_2} x_4,}^{M_1}, ..., x_n \tag{3.35}$$

where q is the q^{th} chromosome within generation g for j^{th} variable.

Fuzzy variable $P_{balance}$, SoC and P_{ess} consists of five triangles membership functions. The triangle membership function is represented by a vector of three elements. From (3.36), the left span, center and right span of the triangle are a, b and c respectively.

$$f(x, a_n, b_n, c_n) = max\Big(min\Big(\frac{x - a_n}{b_n - a_n}, \frac{c_n - x}{c_n - b_n}\Big), 0\Big) \tag{3.36}$$

Five triangle membership functions are used for $P_{balance}$, SoC and P_{ess} as shown in Fig. 3.10. From Table 3.3, the center, b_1 and right span, c_1 of the first linguistic term, M_1 is equal to the left span, a_2 and center b_2 of the second linguistic term, M_2. This is to ensure that there is sufficient overlap between adjacent linguistic term. Continuity is lost if the overlap is too small and linguistic term is redundant if overlap is too big. In this manner, five triangle membership functions can be represented with seven parameters, g_1 to g_7.

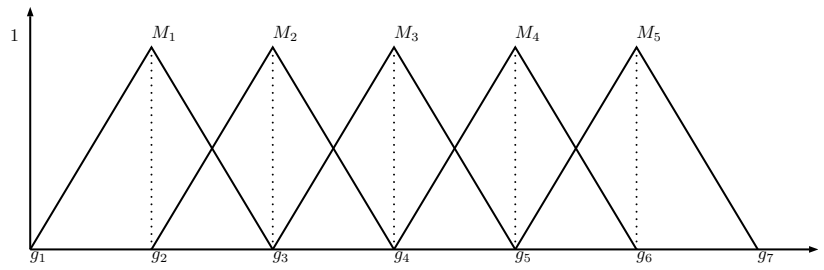

Fig. 3.10 $P_{balance}$ and ESS membership functions

A randomly generated vector of 7 elements, g_1 to g_7, can represent all the placement of 5 membership functions for $P_{balance}$ and ESS as shown in Table 3.3.

Table 3.3 Chromosomes encoding of $P_{balance}$ and ESS

$C^g_{j,q}$	g_1	g_2	g_3	g_4	g_5	g_6	g_7
M_1	a_1	b_1	c_1				
M_2		a_2	b_2	c_2			
M_3			a_3	b_3	c_3		
M_4				a_4	b_4	c_4	
M_5					a_5	b_5	c_5

Table 3.4 shows an example of encoding the fuzzy variable, $P_{balance}$. The range of $P_{balance}$ from the historical data are 26.76 kW to -18.3 kW. These values are used to denote the range of the fuzzy membership functions.

Table 3.4 Encoding of $P_{balance}$

$C^g_{j,q}$	g_1	g_2	g_3	g_4	g_5	g_6	g_7
M_1	-18.3	-10.79	-3.28				
M_2		-10.79	-3.28	4.23			
M_3			-3.28	4.23	11.74		
M_4				4.23	11.74	19.25	
M_5					11.74	19.25	26.76

Fuzzy variable C_p consist of 3 triangle membership functions and 2 trapezoid membership functions. The trapezoidal membership function is represented by a vector of 4 elements. From (3.37), the left and right span are a and d and the "shoulders" of the trapezoid are b and c.

$$f(x, a_n, b_n, c_n, d_n) = max\Big(min\Big(\frac{x - a_n}{b_n - a_n}, 1, \frac{d_n - x}{d_n - c_n}\Big), 0\Big) \tag{3.37}$$

Similar to the chromosome design of $P_{balance}$ and ESS, from Table 3.5, the "right shoulder", c_1 and right span, d_1 of the first linguistic term M_1 is equal to the left span, a_2 and center, b_2 of the second linguistic term M_2. In this manner, two trapezoid and three triangle membership functions can be represented with nine parameters, g_1 to g_9.

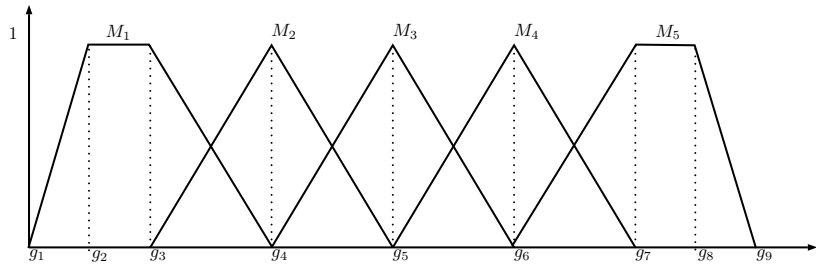

Fig. 3.11 C_p membership function

A randomly generated vector of 9 elements, g_1 to g_9 can represent all the placement of 5 membership functions for C_p as shown in Table 3.5.

Table 3.5 Chromosomes encoding of C_p

$C^k_{j,q}$	g_1	g_2	g_3	g_4	g_5	g_6	g_7	g_8	g_9
M_1	a_1	b_1	c_1	d_1					
M_2			a_2	b_2	c_2				
M_3				a_3	b_3	c_3			
M_4					a_4	b_4	c_4		
M_5						a_5	b_5	c_5	d_5

3.4.2.2 Initial Population

The chromosomes are randomly generated and subjected to the following constraints:

$$SoC_{min} \leq SoC(t) \leq SoC_{max} \tag{3.38}$$

$$P_{balance,min} \leq P_{balance}(t) \leq P_{balance,max} \tag{3.39}$$

$$C_{p,min} \leq C_p(t) \leq C_{p,max} \tag{3.40}$$

$$\tag{3.41}$$

Constraint (3.38) is the upper and lower allowable operating SoC of the ESS. By operating the ESS within this boundary can prevent over and under charging [137]. Constraint (3.39) and (3.40) are the maximum and minimum values of $P_{balance}$ and C_p which are obtained from the historical data.

The maximum and minimum boundaries of these constraints can be modified to suit other storage technology, electricity market price and microgrid configuration according to the available historical data.

3.4.2.3 Fitness Function

The fitness function evaluates the quality of each chromosome in the current generation. A poorly designed fitness function will result in a weak solution. The objective of the proposed FEMS is to reduce the overall operating cost and average peak load by charging and discharging the energy storage at appropriate times. The overall operating cost of the microgrid can be calculated by (3.42).

$$f_1 = \sum_{t=1}^{T} P_{grid}(t).C_p(t) \tag{3.42}$$

where C_p is the wholesale electricity price. The microgrid can freely purchase and sell electricity from the main grid at time t at the same market price, $C_p(t)$.

a) $P_{grid}(t) > 0$ if electricity is purchased from the grid;

b) $P_{grid}(t) < 0$ if electricity is sold back to the grid.

The average peak load of the power profile is calculated using (3.43).

$$f_2 = \frac{\sum_{m=1}^{M} P_{grid,max}(m)}{M} \tag{3.43}$$

where M is the total number of months.

The objective of NSGA-II is to tune the membership functions to minimize operating cost, and average peak load. Hence (3.42) and (3.43) are used as the fitness function to evaluate each chromosome.

There are two objective functions in this work, as such it can be formulated as a multi-objective optimization problem. A multi-objective optimization problem can be formulated as follows:

$$\begin{aligned} \min \quad & (f_1(x), f_2(x), ..., f_k(x)) \\ \text{s.t.} \quad & \forall x \in X \end{aligned} \tag{3.44}$$

where k is the objective function and x is the solution. For instance, this work considers (3.42) and (3.43) as the objective functions.

Let the fitness functions f_1, f_2 be (3.42) and (3.43). Apart from the fitness function, domination count and crowding distance are computed to further evaluate each solution.

3.4.2.4 Domination Count and Crowding Distance

In multi-objective optimization, when considering the quality of two solutions, p and q with multiple objective functions, solution p is considered to dominate solution q iff:

1. $f_i(p) \leq f_i(q)$ for all indices $i \in 1, 2, ..., k$ and

2. $f_j(p) < f_j(q)$ for at least one index $j \in 1, 2, ...k$

where p and q are two different solutions and i and j are two fitness functions. When solution p is compared with q, if the fitness function for all objectives for p is less than or equal to q and p is less than q for at least one objective, p dominates q. If these

criteria are not met, p and q are nondominant and they belong to the same Pareto front.

All solutions not dominated by any other solutions are assigned a domination count of 0. All solutions that are only dominated by solutions with domination count of 0 are assigned a domination count of 1. This process is repeated until all the solutions have a domination count. All solutions with the same domination count are considered equally good as they are on the same Pareto front. In order to further differentiate the solution with the same domination count, a second entity, crowding distance is introduced.

Within the same Pareto front, the crowding distance is calculated. A higher crowding distance signifies a less crowded region, and vice-versa. When comparing two solutions with the same domination count, the solution with a higher crowding distance is the better solution. In this manner, the sorting algorithm favors a more diverse solution and avoid clustering on the Pareto front.

3.4.2.5 Best Compromise Solution

After the domination count and crowding distance are computed, fuzzy set theory is implemented to determine the best compromise solution from the set of Pareto optimal solution [95]. For each solution in i^{th} objective function, the respective fitness function is fuzzified using (3.45).

$$\mu_i = \begin{cases} 1 & f_i \leq f_i^{min} \\ \frac{f_i^{max} - f_i}{f_i^{max} - f_i^{min}} & f_i^{min} < f_i < f_i^{max} \\ 0 & f_i \geq f_i^{max} \end{cases} \tag{3.45}$$

For each minimizing objective function, the lowest objective is assigned a value of 1 from (3.45). The normalized membership function μ^k for each nondominant solution is calculated using (3.46).

$$\mu^k = \frac{\sum_{i=1}^{N_{obj}} \mu_i^k}{\sum_{k=1}^{M} \sum_{i=1}^{N_{obj}} \mu_i^k} \tag{3.46}$$

where M is the total number of nondominant solution. The solution with the highest value of μ^k is the best compromise solution.

3.4.2.6 Selection of Parent Chromosomes

Parent chromosomes are selected using binary tournament selection based on domination count and crowding distance in MOO [138].

From Algorithm 3, binary tournament selection randomly chooses a pair of chromosomes from the population . The domination count of the selected pairs is compared and the lower one is selected. If both chromosomes have the same domination count, the one with the higher crowding distance is selected. Binary tournament selection algorithm allows the less-fit chromosome to be chosen because the fitness is relative to the other selected chromosome instead of the absolute fitness of the population.

Algorithm 3: Binary Tournament Selection

```
From population P, select λ = {s_1, ..., s_λ} ;
s = 1;
for s ≤ λ do
    Randomly select two chromosomes;
    Compare domination count and crowding distance;
    Put fitter chromsome into λ;
    s = s + 1;
end
```

Elitism is ensured by selecting the solution with the lowest domination count and highest crowding distance in the Pareto front and adding it to λ. Where λ is the total number of selected chromosomes for crossover and mutation.

3.4.2.7 Crossover of Chromosomes

Crossover produces the next generation of chromosomes based on the fitter chromosomes of the current generation. The literature proposed several methods for crossover and mutation, and it depends on how the chromosomes are encoded. A Simulated Binary Crossover (SBX) is used in this thesis [139]. Let $C^g_{j,1}$ and $C^g_{j,2}$ be the two fittest chromosome of the g^{th} generation and j^{th} variable.

$$C_{j,1}^{g} = (c_1, ..., c_h, ..., c_z) \tag{3.47}$$

$$C_{j,2}^{g} = (c'_1, ..., c'_h, ..., c'_z) \tag{3.48}$$

$$C_{j,1}^{g+1} = \frac{1}{2}[(1-\beta)C_{j,1}^{g} + (1+\beta)C_{j,2}^{g}] \tag{3.49}$$

$$C_{j,2}^{g+1} = \frac{1}{2}[(1+\beta)C_{j,1}^{g} + (1-\beta)C_{j,2}^{g}] \tag{3.50}$$

$$\beta = \begin{cases} (2\epsilon)^{\frac{1}{\psi+1}} & \text{if } \epsilon \leq 0.5 \\ (\frac{1}{2(1-\epsilon)})^{\frac{1}{\psi+1}} & \text{otherwise} \end{cases} \tag{3.51}$$

where ϵ is a randomly generated number between 0 and 1, ψ is a distribution index which determines how similar the offspring is to the parent and β is the spread factor. The offspring solution of a large ψ are close to the parent solution and the offspring solution of a small ψ are away from the parent solution.

3.4.2.8 Uniform Mutation of Chromosomes

A uniform mutation operator replaces the value of the chosen gene with a value generated between the upper and lower limit of the chromosome from (3.52). Whether the chromosome will undergo a mutation is determined by mutation probability, ρ_m. After the mutation occurs, sort the chromosome in ascending order for the fuzzy membership functions to overlap.

$$\epsilon_j = [(max - min)rand + min] \tag{3.52}$$

where j is the j^{th} variable.

3.4.3 Multi-Service of Single ESS: Reserve Service

After the membership functions of the FEMS are tuned using NSGA-II, an additional RS is added to the operation of ESS. The proposed methodology in this subsection uses a single energy storage to provide multiple streams of benefits: RS, energy arbitrage and reduce peak demand of the microgrid.

Fig. 3.12 shows the operation of the FEMS. The operation mode depends on the reserve signal, P_{reserve} and SoC.

$P_{reserve}$ dictates the amout of power to be delivered by the ESS to the main grid as RS. As such the ESS will operated under *Reserve Operation*, else it will operate under *FEMS Operation*, which is the FEMS proposed in the previous subsection.

The minimum operating SoC are different in reserve and FEMS operation. In reserve operation, the minimum SoC is 10% while in FEMS operation, the minimum SoC is 40%. This is to ensure that there will always be enough energy to meet the reserve operation.

In an event where the minimum SoC is less than 40% after a reserve operation, the ESS will operate in *Recovery Operation*, where it charges the ESS during low price period. The details of each operation are discussed in the rest of this subsection.

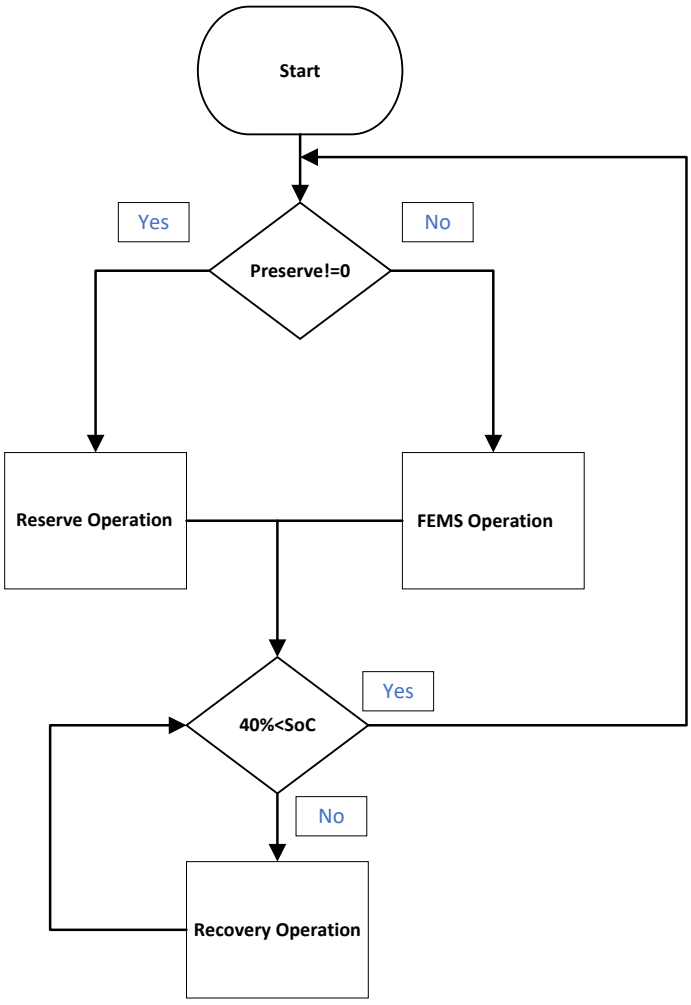

Fig. 3.12 Different operation modes of ESS

3.4.3.1 Reserve Operation Mode

Reserve operation mode provides a RS to the grid operator. Reserve service is a contracted balancing service for the grid operator to manage the actual demand when the demand is greater than forecast or generation unavailability. In this operation mode, the controller will follow the protocol listed by the grid operator. The requirements for STOR are as follows:

- A minimum of 90 % of the contracted reserve must be delivered
- A RS provider must be able to deliver at least 3 times per week
- Providers should be able to response to an instruction within a maximum of 240 minutes
- A RS provider must be able to sustain the response for a minimum of 2 hours and have a recovery period of not more than 1200 minutes (20 hours)

The payment from the grid operator are as follows:

- Availability - Paid for the hours in which the service has been made available, in \$/kW/h
- Utilization Fee - Paid for the energy delivered when requested, in \$/kWh

The availability window or reserve window is a period where the service provider must be available to operate at the contracted power when requested. The grid operator may not always have a RS request; however, the service provider should be ready when required.

The utilization of the service is where the grid operator issues a RS request. The service provider must start to provide the contracted power within the response time and sustain for a minimum of 2 hours. The percentage of delivered reserve is calculated using (3.53).

$$\text{Percentage of delivered reserve} = \frac{\text{Delivered service request (kWh)}}{\text{Service request (kWh)}} \times 100\% \quad (3.53)$$

3.4.3.2 FEMS Operation Mode

The ESS operates in energy arbitrage and reduce peak demand when it is not providing any reserve services. The detailed explanation of this operation mode is described in

subsection 3.4.1 and 3.4.2. Instead of a constant minimum SoC, the minimum SoC of the ES during normal mode changes dynamically depending on the time to reserve window. As such the ES have a wider operating SoC during normal and recovery operation and a narrower SoC during RS operation.

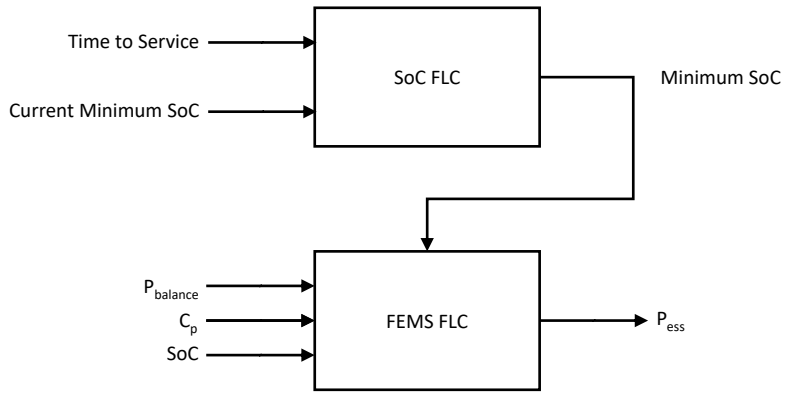

Fig. 3.13 Dynamic minimum SoC during normal operation

Fig. 3.13 shows two FLC. The SoC FLC has two inputs and one output. They are time to service (TTS), current minimum SoC and updated current SoC respectively. This SoC FLC is used to determine the minimum SoC for the FEMS FLC. The linguistic terms for TTS are far, moderate and near, current minimum SoC and updated minimum SoC are low medium and high. For TTS, the linguistic terms are used to quantify the time to the start of the contracted service period. The FLC rules are designed to have a higher minimum SoC at the start of the service to ensure that there is sufficient energy for the reserve request and a lower minimum SoC at the end of the service.

Table 3.6 shows the fuzzy rules for the first fuzzy logic controller. For instance, from rule number 1, when the time to reserve window is far and current minimum SoC is low, new minimum SoC will be low.

3.4.3.3 Recovery Operation Mode

If the SoC of the storage falls below the minimum SoC after a reserve request, the ESS will operate in this mode. The focus of this mode is to prepare the ESS for the next service request.

The controller only charges when the price is low. It also charges when P_{balance} is negative. Fuzzy rules 21-25 and 46-50 of Table 3.2 are modified for this operation mode.

Table 3.6 Fuzzy rules to determine minimum SoC

Fuzzy Rule	Time to Service	Current SoC	New SoC
1	Far	Low	Low
2	Far	Medium	Low
3	Far	High	Low
4	Moderate	Low	Medium
5	Moderate	Medium	Medium
6	Moderate	High	Medium
7	Near	Low	High
8	Near	Medium	High
9	Near	High	High

3.4.3.4 Summary of Operation Modes

These three operation modes have different tasks and minimum SoC for the energy storage and they are summarized in Table 3.7. During the reserve window, the FEMS continues to operate in normal mode if there is no reserve request from the grid operator. The ESS switches from FEMS operation mode to reserve operation mode when the grid operator sends a reserve request.

Table 3.7 Summary of operation modes

Mode	Minimum SoC (%)	Task
Reserve service	10	Provide constant power for 2 hours when requested during the contracted period
Normal	10 to 40	Provide energy arbitrage and reduce peak demand
Recovery	10	Restore SoC to minimum level

3.4.4 Summary of Multi-Service of Single ESS

First, energy arbitrage and peak shaving are proposed as two services for the ESS in Section 3.4.1. The design of the FEMS, performance evaluation indices and Simulink models are presented as well.

Second, the membership functions of the FEMS are tuned using NSGA-II in Section 3.4.2. The performance evaluation indices from Section 3.4.1 are modified and used as the fitness functions for NSGA-II.

Finally, RS is added as the third service for the ESS. Instead of a constant minimum SoC, a dynamic minimum SoC allows the ESS to be utilized more during normal operation while having enough energy to meet the RS.

3.5 Summary of Proposed Methodologies

The results and discussions of the proposed methodologies in this chapter are shown in the respective chapter or sections from Table 3.8.

Table 3.8 Summary of proposed methodologies

Proposed Methodology	Service of ESS			Results and Discussions
	Energy Arbitrage	Peak Shaving	Reserve Service	
Section 3.3	✓	✓		Chapter 4
Section 3.4.1	✓	✓		Section 5.2
Section 3.4.2	✓	✓		Section 5.3
Section 3.4.3	✓	✓	✓	Section 5.4

Chapter 4

Day-Ahead Forecast and Scheduling of Energy Storage

4.1 Overview

This chapter presents a day-ahead scheduling of energy storage based on forecasting and mixed-integer linear programming (MILP) proposed in Section 3.3. The day-ahead values of load, renewable generation and real-time electricity price are forecast with artificial neural network (ANN). The day-ahead forecasting performance of extreme learning machine (ELM) and deep belief network (DBN) are evaluated in this chapter. After the day-ahead energy forecast are obtained, this information is used to formulate the scheduling of energy storage into a MILP problem. The schedule is used in real-time operation of the energy storage system (ESS).

4.2 Day-Ahead Energy Forecast using Artificial Neural Network

This section compares the different methods of ANN forecast. The methods are ELM and DBN. The hyperparameters of the ANNs are heuristically tuned for day-ahead forecast of load. Day-ahead forecast of load is used as it is more predictable compared to highly stochastic renewable energies and electricity price. After the method of forecasting is determined, it is used to forecast PV, wind and electricity prices which are highly stochastic compared to load.

4.2.1 Hyperparameters Tuning for Artificial Neural Network

Among the hyperparameters mentioned in Table 2.2, only the number of hidden nodes and hidden layers are tested in this section. For consistency during comparison between different ANN models, the size and division of datasets and performance evaluators are fixed. Apart from using MAPE and RMSE to measure the performance of the model, the computation time taken to train the model is also considered.

Some of the parameters of the ANN models are randomly generated, for instance the input layer weight matrix of ELM, the performance of the model may vary even if the hyperparameters are the same. As such, after the hyperparameters of these models are determine, 10 trials are conducted to investigate the effects of the randomly generated parameters.

After the hyperparameters of these models are determined, the final model is trained 10 times to understand the stability of the model. These parameters are used to evaluate and conclude which ANN model are more suitable for forecasting.

The half hourly load data are obtained from Energy Market Authority [140], from 6 February 2012 to 6 February 2013. The data set consist of 17,520 data points. This dataset is split into training and testing set with a ratio of 50:50. The training set is used to heuristically tune the neural network hyperparameters while the testing set is used to validate the model performance.

Having more than a year of data for training does not have significant improvement in the forecasting accuracy [141]. Furthermore, having more training data will increase the computational time when training the network.

ELM is implemented using MATLAB M-script. DBN is implemented using DeebNet Toolbox in MATLAB from [142]. These models executed on a workstation with an Intel XEON E3-1271 CPU running at 3.60 GHz with 32 GB of system memory.

4.2.2 Day-Ahead Forecast using Extreme Learning Machine

The hyperparameters of ELM are number of hidden nodes. The RMSE, MAPE and computational time are recorded.

The number of hidden nodes is increase from 500 to 20000 with an increment of 500, the RMSE and MAPE of the model gradually decrease as shown in Fig. 4.1. From 7,500 to 15,000 hidden nodes, error fluctuates between 360 and 365 for RMSE and 4.9% and 5.1% for MAPE. The computational time increases drastically as the number of hidden nodes increases, as such 7500 is chosen as the number of hidden nodes for

ELM. This fluctuation in forecasting accuracy is due to the randomly generated input weight matrix. The total computational time taken to increase the number of hidden nodes from 500 to 20000 is 7463s.

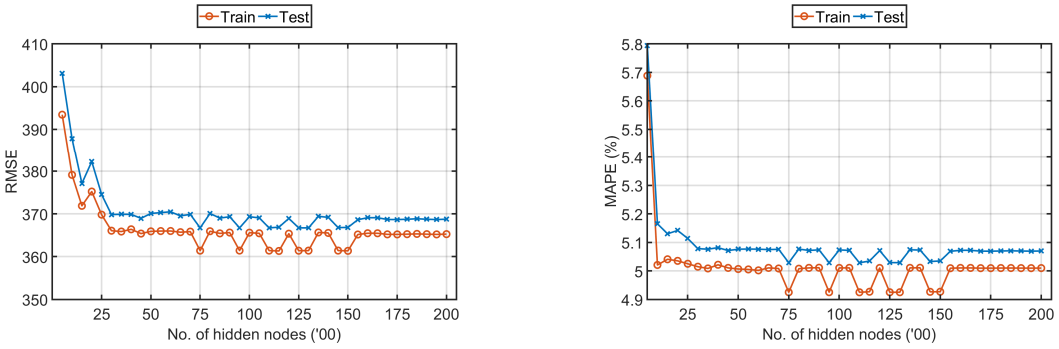

(a) RMSE vs No. of Hidden Nodes (b) MAPE vs No. of Hidden Nodes

Fig. 4.1 RMSE and MAPE for ELM

When using the equation from [110], it shows unsatisfactory forecasting performance as the number of hidden nodes is too small when compared to the training data size which resulted in an underfit. Underfit is where the training error is larger than the testing error. It suggests that the model have poor predicting power.

The number of hidden nodes is set as 7500 and the training of ELM is repeated for 10 times to investigate the effect of random input weights. Fig. 4.3 shows a similar phenomenon as increasing the number of hidden nodes where the forecasting accuracy fluctuates. The performance of ELM is stable on a wide range of hidden nodes as shown in Fig. 4.1 and 4.3. The fluctuation is not large and is bounded between a relatively small range. The time taken to train an ELM with 7500 hidden nodes is 215s.

4.2.3 Day-Ahead Forecast using Deep Belief Network

There are several hyperparameters for deep belief network to be determine. The number of hidden nodes and layers are determined in this subsection. Similar to ELM, the RMSE, MAPE and computational time are recorded.

First, the number of epochs for each layer is set to 200 for RBM and 500 for the final layer. Second, another RBM is added to DBN and the number of hidden nodes is increased from 100 to 2000 with an interval of 100. After the number of hidden nodes is determined for the first layer, a second RBM is added and the number of hidden

nodes is increased from 100 to 2000 with an interval of 100. This process is repeated for the third RBM to investigate the effect of hidden nodes and number of RBM.

The results from the first RBM is shown in Fig. 4.2a and 4.2b. The RMSE and MAPE are fairly consistent as the number of hidden nodes is increasing. From 100 to 2000 hidden nodes, the error fluctuates between 358.5 and 359.4 for RMSE and 4.85% and 4.86% for MAPE. The total computation time taken to increase the number of hidden nodes is 2506s. Since the lowest RMSE and MAPE occurs at 100 hidden nodes, the number of hidden nodes is set as 100 for the first RBM.

The second RBM is added on top of the first RBM and the results are shown in Fig. 4.2c and 4.2d. The RMSE and MAPE have a greater fluctuation as the number of hidden nodes increases. From 100 to 2000 hidden nodes, the error fluctuates between 358 and 361.2 for RMSE and 4.83% and 4.85% for MAPE. The total computational time taken is significantly higher at 7915s. The number of hidden nodes is set as 300 for the second RBM.

The third RBM is added on top of the second RBM and the results are shown in Fig. 4.2e and 4.2f. The RMSE and MAPE are similar to a DBN with two RBM and there is no significant improvement in forecasting accuracy by adding the third RBM. As such two RBM is used as the final model.

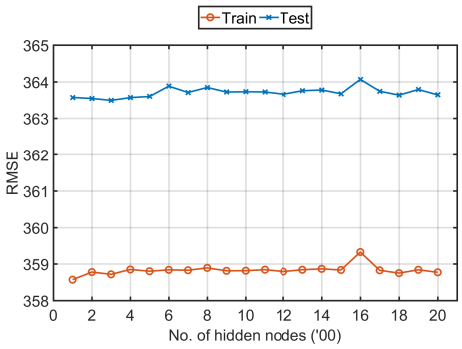

(a) RBM 1: RMSE vs no. of hidden nodes

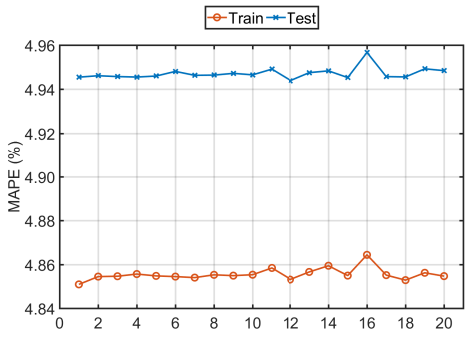

(b) RBM 1: MAPE vs no. of hidden nodes

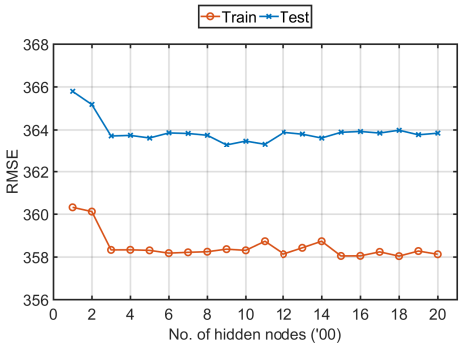

(c) RBM 2: RMSE vs no. of hidden nodes

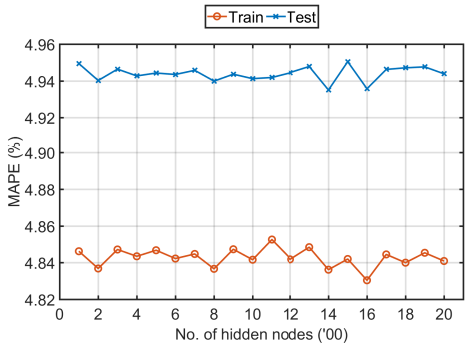

(d) RBM 2: MAPE vs no. of hidden nodes

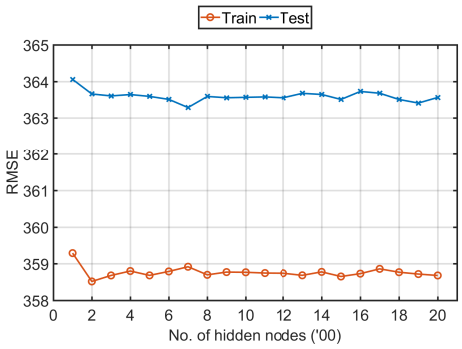

(e) RBM 3: RMSE vs no. of hidden nodes

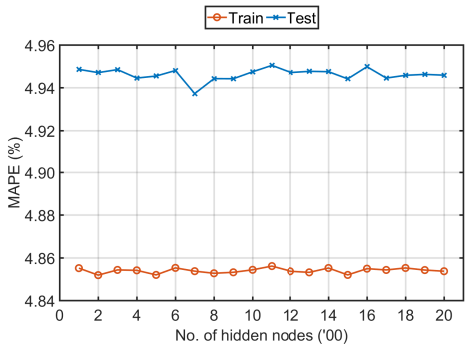

(f) RBM 3: MAPE vs no. of hidden nodes

Fig. 4.2 RMSE and MAPE for different RBM

4.2.4 Comparison between ELM and DBN

After the hyperparameters of ELM and DBN are heuristically determine through cross-validation, each model is trained 10 times to investigate the stability of the models.

Fig. 4.3 shows the simulation results of ELM and DBN after 10 trials. The forecasting accuracy are bounded within a certain range and does not have drastic changes from the different trials. This shows that the randomly generated parameters of each model during initialization is managed by tuning of the hyperparameters.

The training error for ELM and DBN are almost equal to the testing error. This gives the model the ability to generalize. If the training error is smaller than testing error, over-fitting occurs. This gives the model a poor generalizing performance. If the training error is greater than the testing error, under-fitting occurs. This also gives a poor generalizing performance.

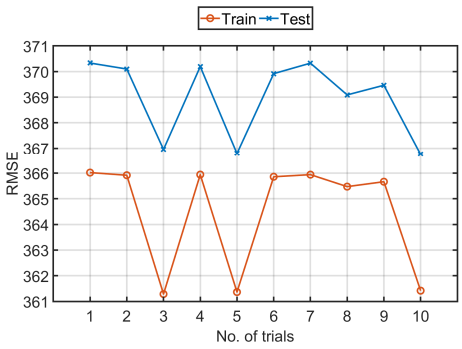

(a) ELM: RMSE vs no. of trials

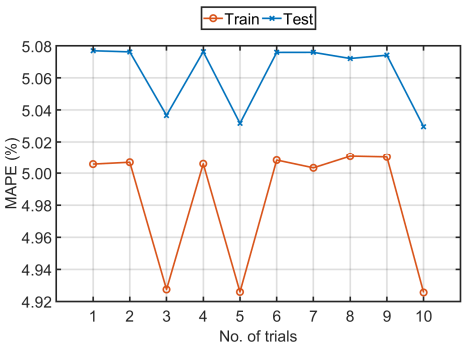

(b) ELM: MAPE vs no. of trials

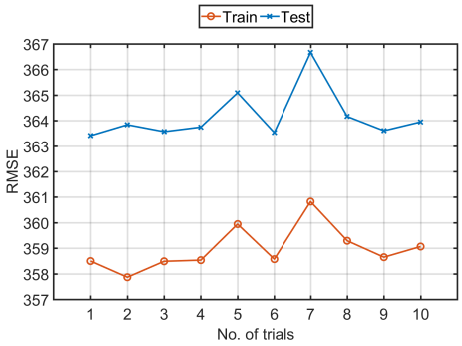

(c) DBN: RMSE vs no. of trials

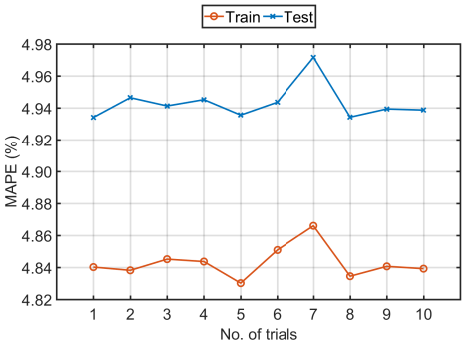

(d) DBN: MAPE vs no. of trials

Fig. 4.3 10 Trials for ELM and DBN

The day-ahead forecasting results of the demand are shown in Fig. 4.4. The forecast of ELM and DBN are relatively similar to the load pattern. During training, the model is tuned to fit the training data while testing set is used to test the model. Hence Fig. 4.4a closely resemblance the actual data while Fig. 4.4b is further away from the actual data.

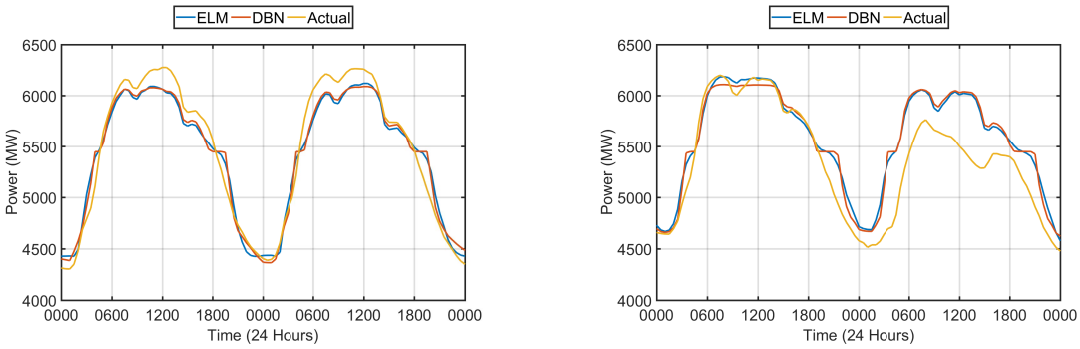

(a) Actual and forecast of training data

(b) Actual and forecast of testing data

Fig. 4.4 Comparison of day-ahead demand forecast between ELM and DBN

4.2.5 Summary of Day-Ahead Energy Forecast

The forecasting performance of ELM and DBN are similar in terms of RMSE and MAPE. Even though DBN has a slightly lower RMSE and MAPE, there are many hyperparameters to be tuned. The time taken to choose these hyperparameters are significantly higher than ELM.

ELM only requires the number of hidden nodes to be tuned. While DBN requires the number of hidden nodes for each RBM. This excludes the tuning of the number of epochs for each RBM and the final output layer. Since the improvement of DBN is marginal over ELM, ELM is chosen for simplicity in implementation and good generalization performance.

4.3 Day-Ahead Scheduling of Energy Storage

Many studies have been done in operation of energy storage system in the electricity market. Several methods such as mixed integer linear programming (MILP) and dynamic programming are proposed in [143, 144] respectively. However, [143] focuses on a three-tier, on-peak, semi-peak and off-peak, time-of-use (TOU) tariff and [144]

focuses on day-ahead pricing instead of real-time electricity price. The revenue is maximized without reducing the power exchange between the main grid and microgrid in [144]. The fluctuation introduced by RES are flattened in [145]. The cost associated with the power exchange between the main grid and microgrid is modeled as a quadratic cost function, and excess power from the microgrid cannot be sold back to the main grid. The ESS capacity and charging/discharging rate are non-continuous (discretized). Demand side management techniques require changes to the consumers' usage pattern [146].

Compared to the literature, this method considers a near-optimal day-ahead scheduling of energy storage system using MILP to minimize the operating cost and reduce the peak demand. This method also considers real-time electricity pricing in the MILP formulation. The charge and discharge rate of the ESS are also continuous and require no change to the consumers' usage pattern.

First, the day-ahead energy forecast is obtained using ELM. Second, the forecast is used for MILP scheduling with the operating cost of the microgrid as the cost function. Finally, an additional inequality constraint is added to the MILP formulation to reduce the peak demand. The forecast schedule is compared with a microgrid without ESS and the optimal schedule (no error in forecast) to investigate the impact of forecasting error in the scheduling.

The rating of the test system is shown in Table 4.1. The test data used in this thesis are obtained from National Renewable Energy Laboratory (NREL) [147] and wholesale electricity prices from Energy Market Company Singapore (EMCSG). A year of data is used in this thesis and are sampled at a 15-minute interval. The resulting dataset consists of 35040 data points.

Table 4.1 Microgrid parameters for test system

Parameter	Values
PV Array	13.68 kWp
Wind Turbine	12 kWp
Load	26.8 kWp
t	0.25 (15 minutes)
T	2976 (31 days)
Energy storage capacity	90 kWh
Maximum charge and discharge rate	15kW
Upper and lower limit	90%, 4%
Charge and discharge efficiency, η_c, η_d	0.95

4.3.1 Day-Ahead Energy Forecast using ELM

One year of historical data is used to train the ELM for day-ahead forecasting. The day-ahead forecast can be obtain after the ELM is trained. The forecasting error is calculated as root-mean-square error (RMSE). It should be noted that RMSE is relative to the values of each data. The value of C_p is relatively smaller than the rest of the parameters which resulted in a smaller RMSE.

Table 4.2 Day-ahead forecast RMSE

Variable	Training RMSE	Testing RMSE
P_{load}	1.8927	2.3754
P_{pv}	2.0383	2.5638
P_{wind}	4.4472	5.2223
C_p	0.0699	0.0526

From Table 4.2, the RMSE of P_{pv} and P_{wind} are higher than P_{load} even though they are in similar range in terms of kW. This shows that it is difficult to obtain accurate forecast of stochastic renewable energy sources. The day-ahead forecast of these variables are used for MILP scheduling.

4.3.2 Day-Ahead Scheduling for Minimizing Operating Cost

The operation cost of the microgrid for a day is shown in Table 4.3. The forecast schedule cost is \$89.58 while the optimal schedule cost is \$41.21. Even though the difference in operating cost between the forecast and optimal schedule is \$48.37, the forecast schedule manages to reduce the operating cost by \$37.98 when compared to no ESS.

Table 4.3 Cost minimization

	Cost (\$)	$P_{grid,max}$(kW)
No ESS	127.56	20.75
Forecast schedule	89.58	32.78
Optimal schedule	41.21	36.54

The fluctuation of the microgrid power profile significantly increased when the operating cost is minimized. Furthermore, the peak demand of the microgrid also

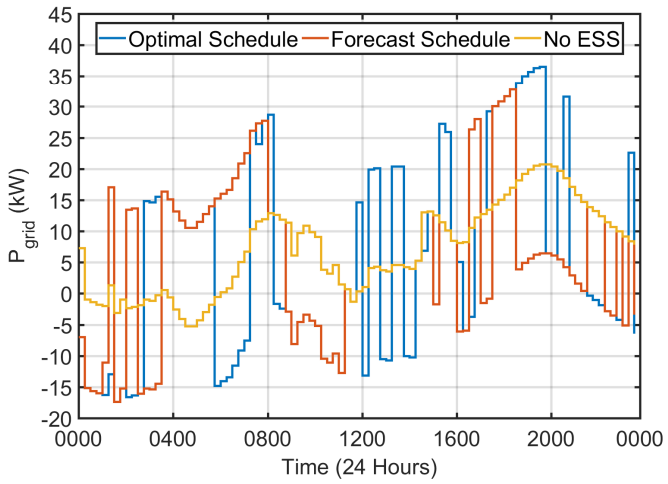

Fig. 4.5 P_{grid} for minimizing operating cost

increased from 20.75kW to 32.78kW and 36.54kW for actual and optimal respectively. The operating cost is minimized at the expenses of a higher peak load.

From Fig. 4.5, the microgrids' power profile experiences many peaks and trough throughout the daily operation due to the forecast and optimal schedule. The increased in fluctuation is unfavorable to the grid operator even though the operating cost is reduced for the microgrid.

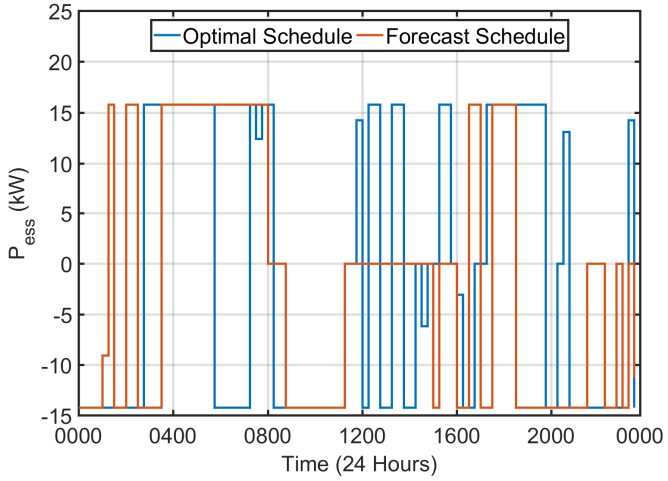

Fig. 4.6 P_{ess} schedule for minimizing operating cost

From Fig. 4.6, the ESS experienced frequent charging and discharging at the maximum rate. Not only does it greatly reduce the life-cycle of the ESS, but it will also

increase the fluctuation on the microgrid. To reduce the usage of ESS and fluctuation in power profile, the inequality constraint from (3.30) is introduced.

4.3.3 Day-Ahead Scheduling for Peak Load Reduction

From the historical data of the microgrid, the peak demand of the microgrid, $P_{grid,max}$ is 20.75kW. An additional inequality constraint, P_{max} , is formulated into the MILP optimization for cost minimization. The value of P_{max} is increased from 0 kW to 21 kW with an increment of 1 kW. From 0 kW to 6 kW, the MILP is unable to solve for a solution. Hence 7 kW is the minimum value for P_{max}.

Table 4.4 Peak load reduction

	Cost ($)	$P_{grid,max}$(kW)
No ESS	127.56	20.75
Forecast schedule	90.60	24.67
Optimal schedule	45.84	7.00

When compared to the optimal schedule in Table 4.3, the optimal schedule with peak load reduction has a slightly higher operating cost of $45.84 while a much lower peak load of 7 kW. From the forecast schedule, the peak load is reduced from 32.78 kW to 24.67 kW even though it is still much higher than 7kW.

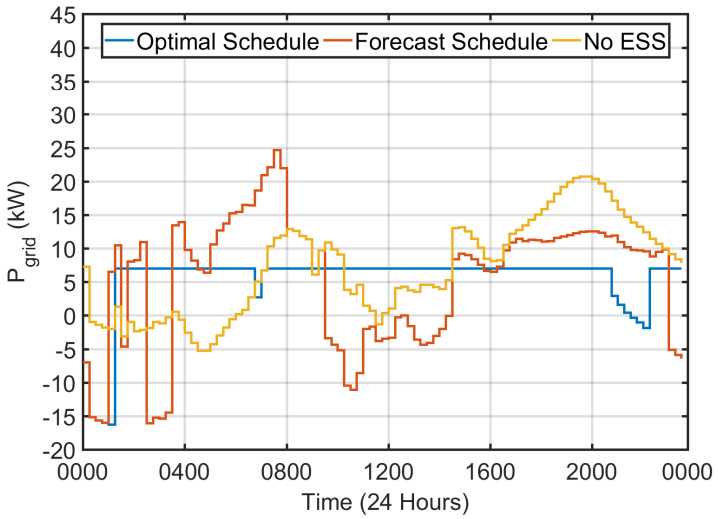

Fig. 4.7 P_{grid} for peak load reduction

The effect of forecasting error is more prominent when an additional inequality constraint is added to the minimization problem. From Fig. 4.7, it is obvious that the forecast schedule of ESS is unable to reduce the peak load to 7kW due to the error in the forecast.

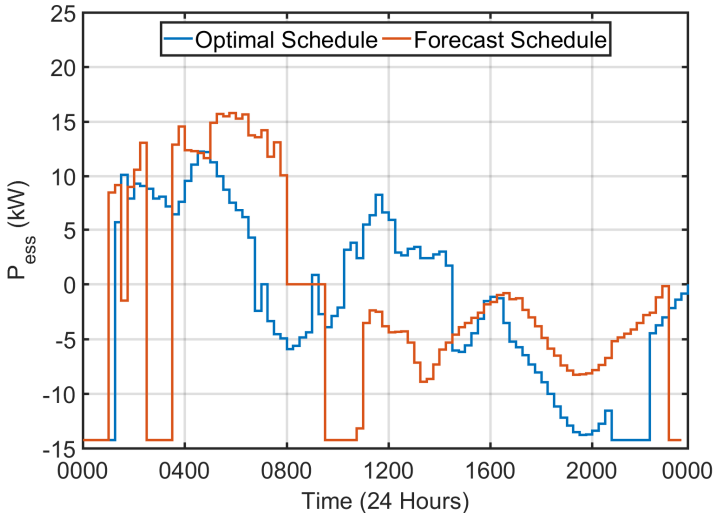

Fig. 4.8 P_{ess} schedule for peak load reduction

By comparing the results from Table 4.3 and 4.4, in cost minimization, the optimal schedule operating cost for the microgrid is $41.21. After adding inequality constraint, P_{max}, the operating cost increased to $45.84. The peak demand for the microgrid is reduced from 36.54 kW to 7 kW at the expense of a slightly higher operating cost. When comparing the operating cost of forecast schedule, the operating cost increased from $89.58 to $90.60. The peak demand for the microgrid is reduced from 32.78 kW to 24.67 kW.

Even though the forecast schedule is not the optimal schedule, it reduces the operating cost and peak load of the microgrid when compared to a microgrid without ESS. Furthermore, by adding an inequality constraint from (3.30) can reduce the maximum peak load and life cycle of ESS.

4.3.4 Summary of Day-Ahead Scheduling of Energy Storage

A single solution is found using the MILP scheduling method. A MILP scheduling for ESS scheduling based on the day-ahead forecast is investigated. A multi-objective optimization using MILP are formulated. The first objective is minimizing of operating

cost of the microgrid. This is achieved by using the operating cost as the cost function of the MILP. The second objective, reduction of peak demand is added as an inequality constraint during the MILP formulation. Empirical evidence shows that the proposed methodology reduces the operating cost and peak demand of the microgrid. The impact of forecasting errors resulted in a near-optimal solution rather than an optimal solution.

4.4 Summary

This section evaluated the forecasting performance of two ANNs. The forecasting accuracy of DBN is marginally better than ELM. However, there are more hyperparameters to be determine in DBN. Hence ELM is chosen as it requires less user intervention to determine its hyperparameter.

The proposed methodology heavily relies on the accurate day-ahead energy forecast which can be difficult to obtain. Furthermore, without introducing further parameters such as weighted sum to the MILP formulation, multi-objective optimization cannot be achieved. Multi-objective optimization can only be achieved by adding additional constraints to the problem formulation. Also, the maximum value of the constraint is determined heuristically.

The next chapter proposed a fuzzy logic-based energy management system which is designed with the microgrid historical data and does not rely on forecasting techniques. Furthermore, multi-objectives are considered in the design of fuzzy rules using expert knowledge.

Chapter 5

Multi-Service of Single ESS

5.1 Overview

This chapter investigates the multi-service of single ESS proposed in Chapter 3.4.1, 3.4.2 and 3.4.3. The proposed methodologies are implemented and validated in simulation using a test system.

The rating of the test system is shown in Table 5.1. The test data used in this chapter are obtained from National Renewable Energy Laboratory [147] and wholesale electricity prices from Energy Market Company Singapore (EMCSG). A year of data was used in this paper and are sampled at a 15-minute interval. The resulting dataset consists of 35040 data points. The test system is implemented using MATLAB/Simulink and consists of photovoltaic, wind, ESS and load as shown in Table 5.1.

Table 5.1 Microgrid parameters for test system

Parameter	Values
PV Array	13.68 kWp
Wind Turbine	12 kWp
Load	26.8 kWp
t	0.25 (15 minutes)
T	2976 (31 days)
Energy storage capacity	90 kWh
Maximum charge and discharge rate	15kW
Upper and lower limit	90%, 4%
Charge and discharge efficiency, η_c, η_d	0.95

5.2 Multi-Service of Single ESS: Energy Arbitrage and Peak Shaving

The first eleven months of data were used to design the fuzzy membership functions and the last month of data is used to validate the proposed fuzzy logic controller. The range of the fuzzy membership functions is shown in Table 5.2.

Table 5.2 Fuzzy membership functions range from historical data

Fuzzy Variables	Min	Max
$P_{balance}$ (kW)	-18.3	26.76
ESS (kWh)	4.0	90.00
C_p (\$/MWh)	1.44	929.31
P_{ess} (kW)	-15	15

The median-σ tuned C_p membership functions are shown in Fig. 5.1. The membership functions of C_p and histogram are superimpose for clarity. Even though the difference between C_p, max and C_p, min is relatively large, majority of its distribution falls within $\pm 1\sigma$.

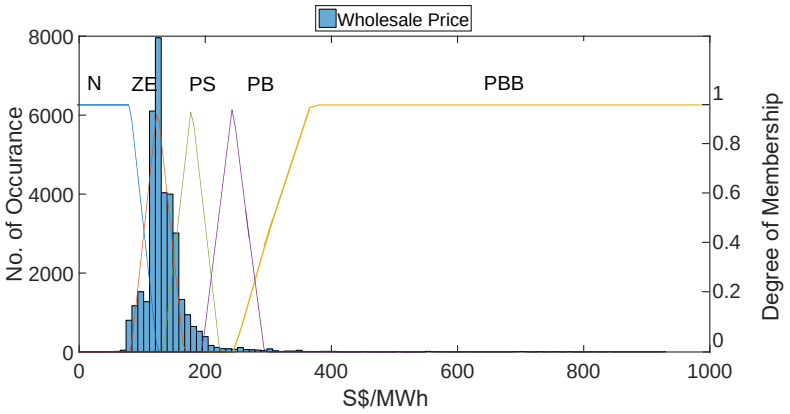

Fig. 5.1 Superimpose of C_p membership functions and histogram of C_p

The performance of the proposed fuzzy logic-based energy management system (FEMS) is compared with a microgrid without ESS, SAEC, and MILP in terms of operating cost, load factor and standard deviation.

5.2.1 Benchmark Algorithms

The proposed FEMS is compared using the proposed performance evaluation indices from Section 3.4.1.3, with two other controllers, self-adaptive ESS controller (SAEC) and mixed-integer linear programming (MILP) scheduling.

5.2.1.1 Benchmark Algorithm I: Self-Adaptive ESS Controller

The proposed FEMS is compared against a Self-Adaptive ESS Controller (SAEC). This controller is explained in detail here. The SAEC evaluates the requirement of the microgrid and decides the charge or discharge rate of the ESS. This is achieved by the following:

a) Determine the state of the ESS (Charge/Discharge/Idle)

b) Determine the charge or discharge rate

The controller determines the state of the ESS, whether to charge, discharge or idle. If the state of the ESS is charge or discharge, the rate of charging or discharging is determined.

Fig. 5.2 shows an overview of the control strategy of SAEC. The top half of the diagram shows how the state of ESS is determined and the bottom half of the diagram shows how the rate of charging/discharging is determined. For instance, if $P_{balance}$ is positive, P_{load} is more than P_{res}, there is a need to discharge ESS to make up for this shortfall. After deriving the state of ESS as "discharge", the discharging rate is determined. For discharging rate, if $P_{balance}$ is more than the maximum discharging rate, $\bar{P}_d$, then the discharging rate will be $\bar{P}_d$, else discharging rate will be equal to the shortfall, $P_{balance}$.

In this manner, the proposed controller can adequately compensate any surplus or shortfall by charging or discharging at the required rate without exceeding the power limits and capacity constraints in (3.7) to (3.9). The SAEC is also able to sell excess power that is not required by the microgrid to the main grid to reduce the operating cost. However, it is unable to exploit the arbitrage pricing as it does not consider the electricity price as its input. The SAEC described in this section is implemented in MATLAB as M-script.

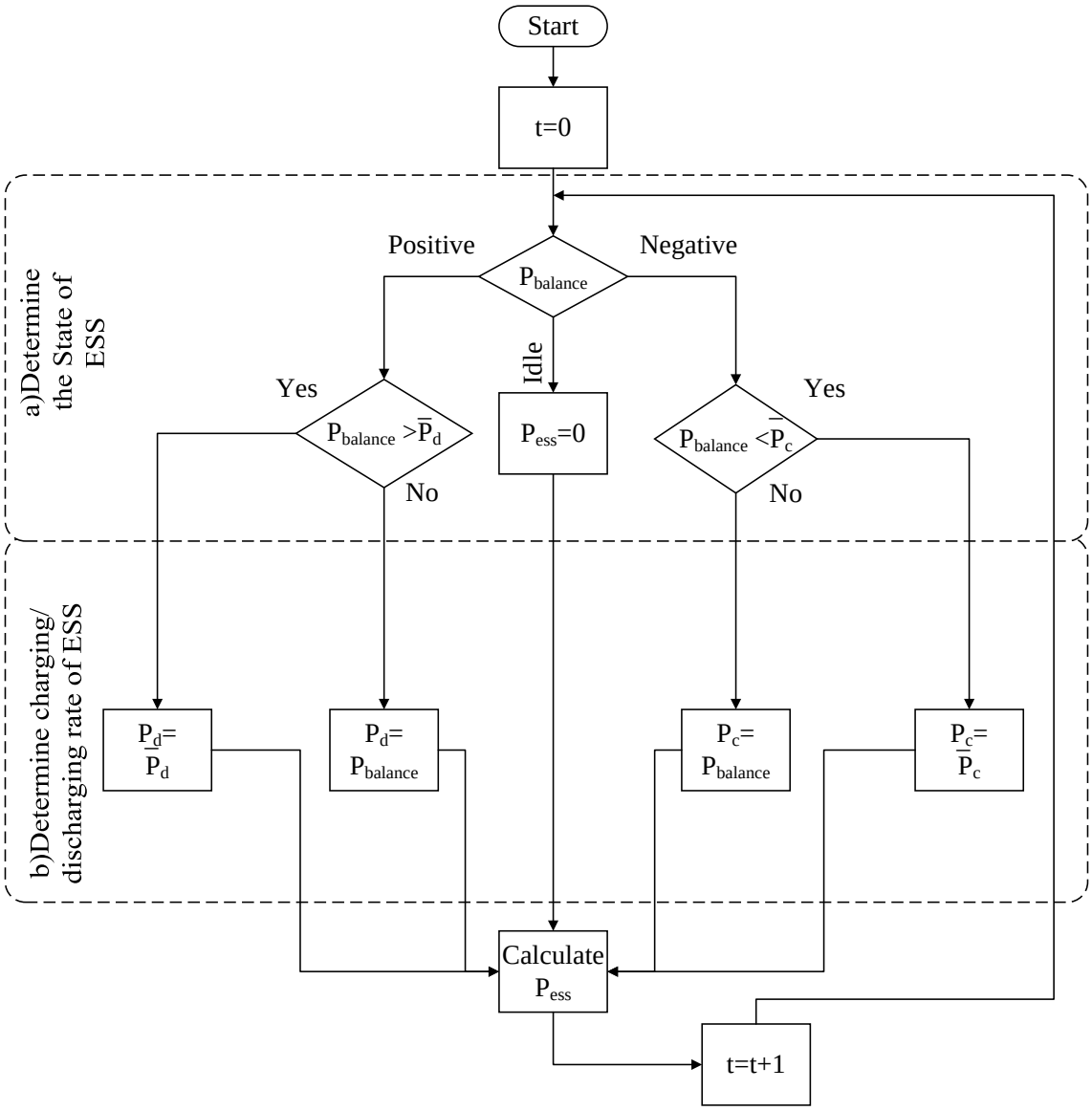

Fig. 5.2 Self-Adaptive ESS control (SAEC) strategy

5.2.1.2 Benchmark Algorithm II: MILP Scheduling

The proposed FEMS is also compared against a MILP scheduling to find a single optimum solution. This MILP scheduling is different from one proposed in the previous chapter as it assumed that the values of $P_{load}(t)$, $P_{res}(t)$ and $C_p(t)$ from $t = 0$ to $t = T$ can be forecast without any error. The mathematical model introduced earlier in Section 3.3 is used to formulate into a MILP minimizing problem.

5.2.2 Comparison Between Proposed FEMS, SAEC and MILP

The last month of data is used to compare and validate the proposed controller. The results of the test data are presented in this subsection. Fig. 5.3 and 5.4 shows the grid power profile and ESS power, for the first day of the test data.

The grid power profile of a microgrid without ESS, SAEC, MILP, and the proposed FEMS is shown in Fig. 5.3. It can be observed that the grid power profile of the proposed controller is the smoothest compared to SAEC and MILP. The grid power profile for MILP has many peaks and trough throughout the day which is undesirable to the grid operator. In contrast, the proposed controller grid power profile is fairly consistent compared to SAEC and MILP.

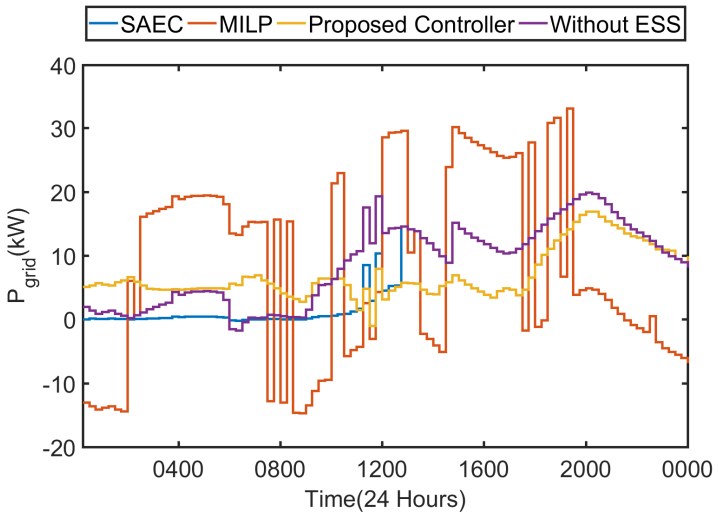

Fig. 5.3 Power profile for different control strategies

The peak demand increases under MILP which is even higher than a microgrid without an ESS. This result in a trade-off between lower operating cost and a higher

variation in power profile for MILP. The integration of RES and ESS should reduce the operating cost and peak demand. Frequent abrupt changes in the power exchange between main and microgrid are unfavorable to the grid operator. This is especially important with the integration of high intermittent RES such as wind power. The power profile of MILP and the proposed controller demonstrates the importance of a controller specifically designed to reduce the peak demand.

From Table 5.4, when the proposed controller is compared to SAEC, the operating cost and standard deviation is 1.87% and 22.79% higher than the proposed controller respectively. The load factor is 10.34% lower than the proposed controller. In terms of operating cost, load factor and standard deviation, the proposed controller can achieve a lower operating cost and peak demand.

When the proposed controller is compared to MILP, it is important to reiterate that the solution obtained from MILP is the optimum solution and assumes that all the values $P_{load}(t)$, $P_{pv}(t)$, $P_{wind}(t)$ and $C_p(t)$ are known in advance. Even though the operating cost is 13.69% lower than the proposed controller, the load factor of MILP is 37.5% lower than the proposed controller. The standard deviation is 187.27% higher.

The proposed FEMS can reduce the operating cost without increasing the peak demand of the microgrid. Furthermore, it only requires the current values of $P_{load}(t)$, $P_{pv}(t)$, $P_{wind}(t)$ and $C_p(t)$ to compute P_{ess} instead of relying on the day-ahead forecast.

The charge and discharge rate of ESS, P_{ess} is shown in Fig. 5.4. It can be observed that MILP frequently charge and discharge at the maximum rate while the proposed controller charge and discharge at a much lower rate.

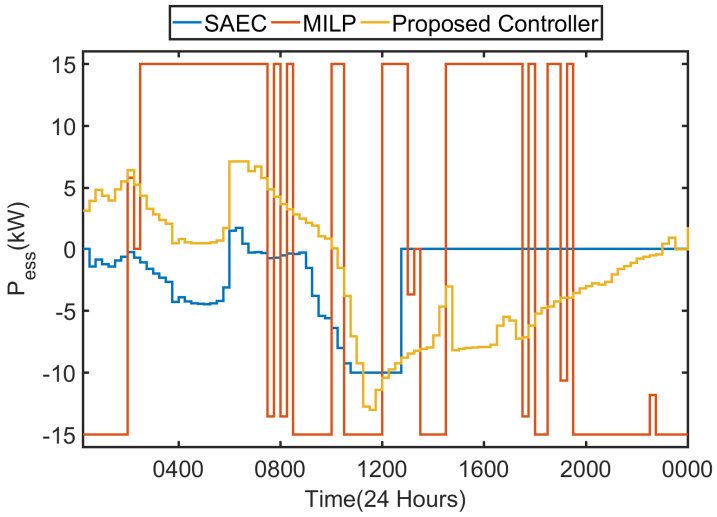

Fig. 5.4 P_{ess} profile for different control strategies

The number of life cycle of ESS can be estimated with (5.1) and the results are shown in Table 5.3.

$$\text{Life cycle} = \frac{\sum_{t=1}^{t=T} |P_{ess}(t)|}{ESS} \tag{5.1}$$

where ESS is the full capacity of the storage system in kWh.

As shown in Table 5.3, the estimated life cycle of ESS under MILP is significantly higher than the proposed controller even though the ESS is only used for a month. Frequent charging and discharging at the maximum rate will have an adverse effect on the energy storage lifespan.

Table 5.3 Estimated number of life cycle of ESS

Controller	No. of life cycle
MILP	474.70
Proposed Controller	124.50

In a multi-objective optimization problem, each performance evaluation indices is an objective function. It can be formulated as follows:

$$\begin{aligned} \min \quad & (f_1(x), f_2(x), ..., f_k(x)) \\ \text{s.t.} \quad & \forall x \in X \end{aligned} \tag{5.2}$$

where k is the objective function and x is the solution. For instance, this subsection considers (3.32), (3.34) and (3.42) as the performance evaluation indices. Let the objective functions f_1, f_2 and f_3 be (3.32), (3.34) and (3.42). As (3.34) is a maximizing objective function, it can be change into a minimizing objective function by inverting the objective function.

In general, there are two approaches for multiobjective optimization. The first approach is using a weighted sum to sum up the two objective functions into a single figure of merit. However, the weight of each objective function is heuristically determined and may not guarantee an optimum solution compared to single objective optimization. The second approach is finding the solutions on the pareto front. The solutions are sorted into their respective Pareto front as discussed in [148].

Solution p is considered to dominate solution q iff:

1. $f_i(p) \leq f_i(q)$ for all indices $i \in 1, 2, ..., k$ and
2. $f_j(p) < f_j(q)$ for at least one index $j \in 1, 2, ...k$

The solutions of without ESS, SAEC, MILP and proposed controller are sorted into their respective pareto front and shown in Table 5.4.

Table 5.4 Performance evaluation indices

Controller	Cost(\$), f_1	$\frac{1}{LF}$, f_2	σ, f_3	Pareto Front
Without ESS	2205.54	3.45	7.84	3
SAEC	2182.06	3.45	7.02	2
MILP	1847.90	5.00	15.57	4
Proposed Controller	2141.23	3.12	5.42	1

Fig. 5.5 shows the search space for three objective functions. The optimum region is located at the bottom center of the search space. From the Pareto front sorting, the proposed controller belongs to the first Pareto front, which is considered to be the optimum solution as it dominates all the other solutions. While SAEC, Without ESS and MILP takes the second, third and last Pareto front respectively.

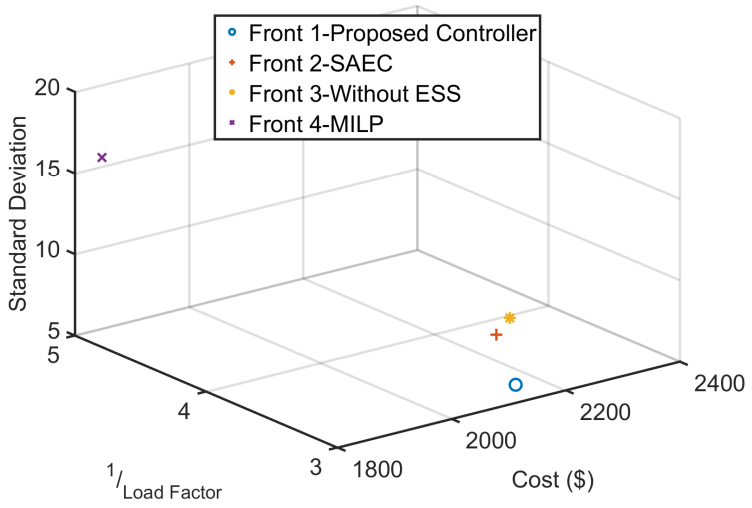

Fig. 5.5 Three objective functions solution space

Fig. 5.6 shows one day operation of the proposed FEMS. From 0000 to 0800, the energy storage is at half capacity, while $P_{balance}$ is close to zero and the electricity market price is low. Hence the proposed controller capitalizes on this arbitrage opportunity to charge the energy storage at a low price.

From 0800 to 1200, as the morning peak demand begins to ramp up, and the electricity market price is high, the energy storage begins to discharge to reduce the peak load. From 1600 to 2000, the electricity price increases with the evening peak demand and the energy storage continue to discharge to reduce the operating cost. As the energy storage capacity approaches the lower limits, the discharge rate gradually reduces to zero to prevent it from over discharging. This process is repeated for the day-to-day operation of the energy storage to reduce the operating cost and peak demand of the microgrid.

The proposed controller is designed based on the historical data of $P_{load}(t)$, $P_{pv}(t)$, $P_{wind}(t)$ and $C_p(t)$ and does not rely on forecasting. Compared to MILP scheduling, which relies on accurate forecast. It is especially important to design a controller that does not rely on forecasting as it is challenging to obtain an accurate forecast for highly stochastic natured variables such as wind and electricity pricing [27]. In this highly dynamic and uncertain operating environment, the proposed controller can reduce the end-user operating cost without increasing its reliant on the main grid as shown in Table 5.4.

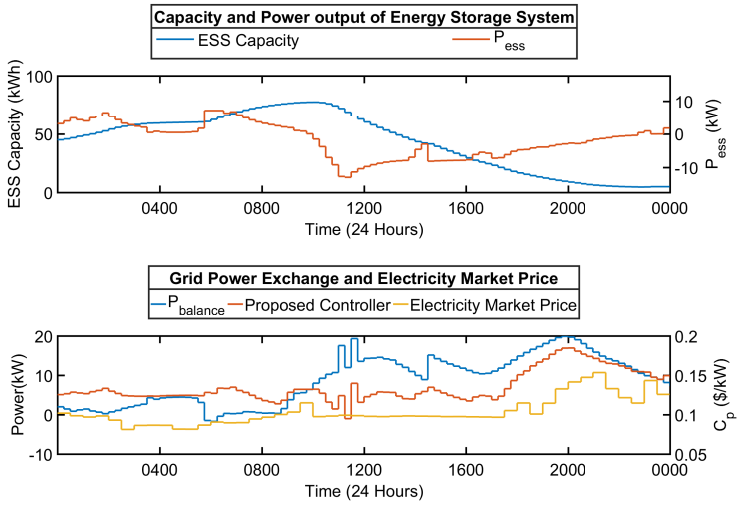

Fig. 5.6 One day operation of proposed FEMS. Top: ESS capacity and ESS power output. Bottom: $P_{balance}$, P_{grid} of proposed controller and electricity market price

5.2.3 Summary of FEMS

In this subsection, a FEMS that considers the mismatch between supply and demand, state-of-charge of ESS, and electricity price to determine the charge and discharge rate of ESS has been proposed. The proposed controller aims to reduce the operating cost and peak demand of the microgrid. The performance evaluating indices can accurately quantify the aims of the proposed controller. The operation cost is calculated and the power exchange between the main and microgrid can be measured with load factor and standard deviation. A decrease in load factor and increase in standard deviation signify a more erratic power profile. A comparison between SAEC and MILP using the performance evaluating indices have shown that the proposed controller can achieve a better solution.

5.3 Enhanced Fuzzy Logic Based Energy Management System

The membership functions in the previous subsection are designed according to expert knowledge can be added into the initial generation of NSGA-II for fine tuning. The solution obtained by expert membership functions can guide NSGA-II to search and

converge faster to the Pareto optimal front. The detailed implementation of NSGA-II for fuzzy membership functions tuning are shown in this section.

5.3.1 Optimizing of Fuzzy Membership Functions using NSGA-II

The proposed FEMS aims to minimize the operating cost and average peak load from (3.42) and (3.43) of the grid-connected microgrid respectively by tuning the input fuzzy membership functions using NSGA-II.

The proposed NSGA-II algorithm for tuning membership functions are implemented using M-script file in MATLAB, and the FLC and grid-connected microgrid are implemented in Simulink. All the parameters required by NSGA-II are determined through a heuristic approach and shown in Table 5.5.

Table 5.5 NSGA-II parameters

	P	G	λ	ψ	ρ_c	ρ_m
Parameters	100	100	40	2	0.9	0.05

where P are the total number of chromosomes, G is the total number of generations, λ is the number of selected chromosomes for crossover, ψ is the crossover parameter, ρ_c and ρ_m is the crossover and mutation probability respectively.

Three case studies are presented in this section as follows:

1. Case study I: Minimizing operating cost
2. Case study II: Minimizing average peak load (APL)
3. Case study III: Multi-objective optimization

Case study I and II are done to find the extreme points of tradeoff on the solution space with competing objective functions. Case study I and II investigates a single objective optimization where cost or average peak load are minimized respectively. In these cases, standard GA is implemented. Case study III is a multi-objective optimization where cost and APL are minimized together. In this case, NSGA-II is implemented.

For each case study, the FEMS is tuned offline with historical data from 1 January 2013, to 31 December 2013, and validated online with data from 1 January 2014 to 31

March 2014. All case studies investigate the effect of adding the expert system fuzzy membership functions into the initial generation of GA/NSGA-II. As such, each case study is repeated twice, first with expert system fuzzy membership functions in the initial population are labelled as $Predefined$ and the second without any expert fuzzy membership functions are labelled as *Random*.

An aggregated multi-objective GA is used as a comparison to NSGA-II. As a comparison to NSGA-II for case study III, the two fitness functions, f_1 and f_2 from (3.42) and (3.43) are normalized using (5.3) and sum into a single figure of merit using (5.4). Normalizing both objective before summing them up gives an equal importance to both objectives instead of using weighted sum where additional weights parameter must be determined [149].

$$X' = \frac{X - min(X)}{max(X) - min(X)} \tag{5.3}$$

$$f_{agg} = f_1 + f_2 \tag{5.4}$$

The results of aggregated multi-objective optimization is compared with NSGA-II. Furthermore, an expert tuned FEMS from Section 5.2 is used as a comparison with the proposed methodology in case study I and II. Case study I and II is to investigate the extreme points of each objective function on the solution space.

5.3.1.1 Case study I: Minimizing Operating Cost

The offline tuning and online validation results are shown in Table 5.6a and 5.6b respectively. In offline tuning, the operating cost is reduced by approximately 5.5% and 3.8% in predefined and random. The APL is reduced by 6.9% and 8.1% in predefined and random respectively. GA with predefined membership functions in the initial population produce a better solution than random membership functions in terms of operating cost in this case study. Not only did it provide a lower operating cost, it also has lower APL.

The population average fitness and fittest solution for each generation is shown in Fig. 5.7. GA with predefined expert knowledge membership functions can find a solution with a lower operating cost than a randomly initialized GA.

Table 5.6 Offline and online results for case study I

(a) Offline tuning of FEMS for minimizing operating cost

FEMS	Cost($)	APL(kW)	ΔPercentage (%)	
			Cost	APL
Expert FEMS	19246.5	12.5	-	-
GA Predefined	18188.1	11.6	-5.5	-6.9
GA Random	18507.9	11.5	-3.8	-8.1

(b) Online validation of FEMS for minimizing operating cost

FEMS	Cost($)	APL(kW)	ΔPercentage (%)	
			Cost	APL
Expert FEMS	4780.6	12.5	-	-
GA Predefined	4632.9	11.8	-3.1	-5.8
GA Random	4684.5	12.1	-2.0	-3.6

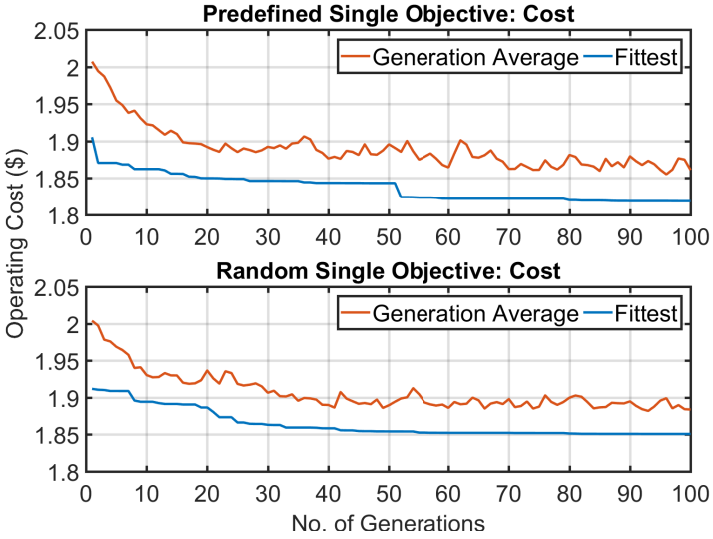

Fig. 5.7 Offline tuning result, single objective optimization: cost

5.3.1.2 Case study II: Minimizing Average Peak Load

From this subsection onwards, only the online validation results are shown. The objective of case study II is to reduce the APL of the microgrid. The result of the online validation is shown in Table 5.7. The APL is reduced by approximately 21.2% and 11.4% for predefined and random respectively.

GA with predefined membership functions in the initial population produce a better solution than random membership functions in this case study as well. Not only did it provide a lower APL, it also reduced the operating cost.

Table 5.7 Online validation of FEMS for minimizing APL

FEMS	Cost($)	APL(kW)	ΔPercentage (%)	
			Cost	APL
Expert FEMS	4780.6	12.5	-	-
GA Predefined	4796.8	9.9	-0.3	-21.2
GA Random	4822.4	11.1	-0.9	-11.4

Similar to case study I, GA with predefined expert membership functions can reach a lower APL faster than a randomly initialized GA as shown in Fig. 5.8.

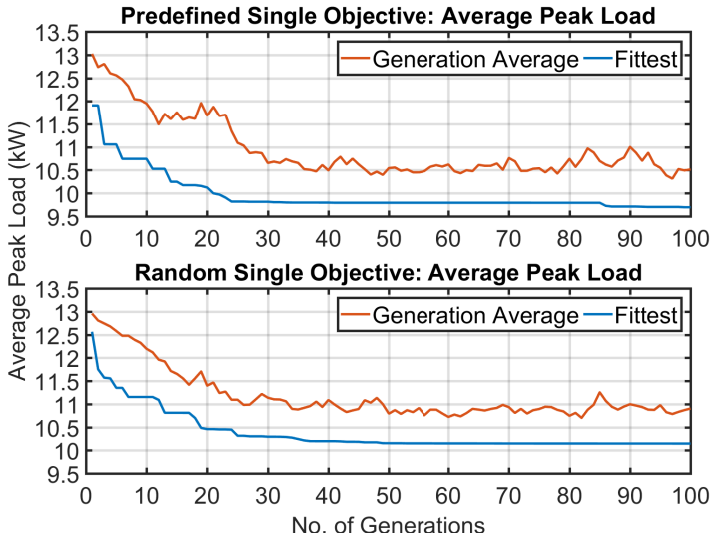

Fig. 5.8 Offline tuning result, single objective optimization: average peak load

In case study I, having the expert tuned membership functions in the initial GA population yields better results. For instances, even though minimizing operating cost is the objective function, it reduces the average peak load as well.

It is important to note that in online validation, for case study I: minimizing operating cost, the lowest operating cost is $4632.9 and the APL is 11.8kW. In case study II: minimizing APL, the lowest APL is 9.9kW and the operating cost is $4796.8. These two points are the extreme points in the solution space. By comparing the results in single objective optimization from Table 5.6b and 5.7, both objectives functions are in conflict. When the operating cost is minimized in case study I, the APL increases and vice-versa in case study II.

In standard GA optimization, only a single solution can be found in a single iteration. This gives a limited perspective on the trade-off relation between the two objective functions. When comparing case study I and II, case study I have a lower operating cost while case study II have a lower average peak load. This shows that they are competing objective functions and cannot be minimized simultaneously.

5.3.1.3 Case study III: Multi-Objective Optimization

Case study III compares three FEMS namely; expert system, aggregated multi-objective GA and NSGA-II. Similar to case study I and II, aggregated multi-objective GA and NSGA-II are further separated into predefined and random.

Fig. 5.10 shows the results for case study III. The aggregated GA fittest solution of each generation is plotted onto the scatter heat map as shown in Fig. 5.9a and Fig. 5.9b. Dark blue represents the first generation and, dark red represents the hundredth generation. The optimum region is on the bottom left of the heat map. From the first generation, the fittest solution of each generation improves and converges into the bottom left through the genetic operators in aggregated GA.

In FEMS optimized using NSGA-II, by comparing Fig.5.10a and Fig.5.10b, the NSGA-II predefined have a more diverse Pareto front compared to NSGA-II random. NSGA-II predefined also have more solutions on the Pareto front. The best compromise solution for NSGA-II are selected using (3.45) and (3.46).

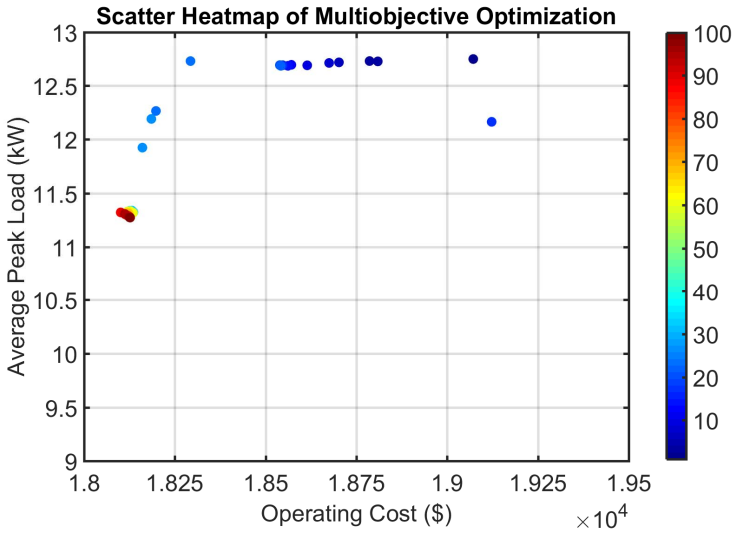

(a) Aggregated Predefined Multiobjective

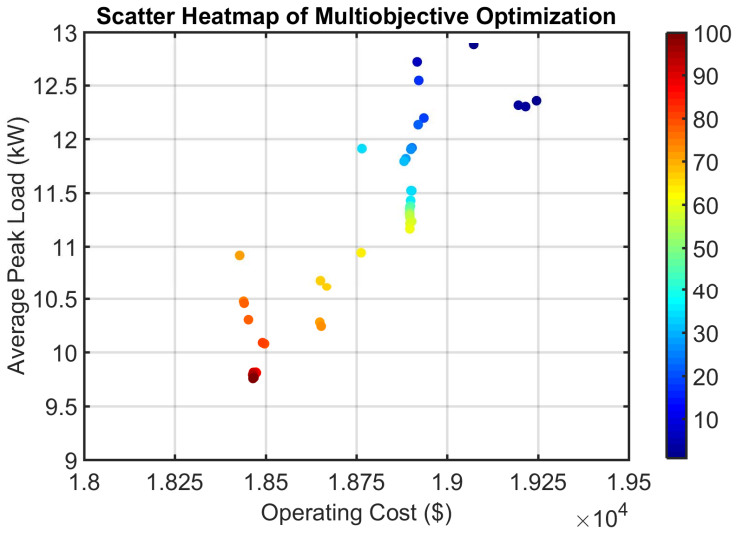

(b) Aggregated Random Multiobjective

Fig. 5.9 Solution space for aggregated GA

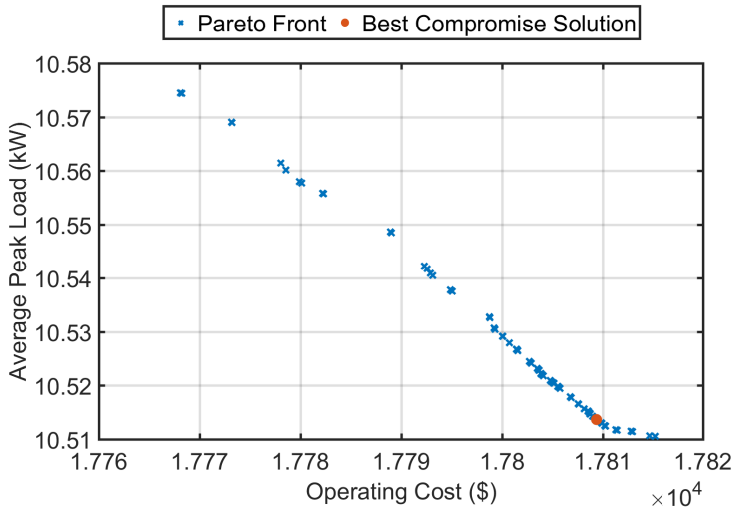

(a) NSGA-II predefined multiobjective

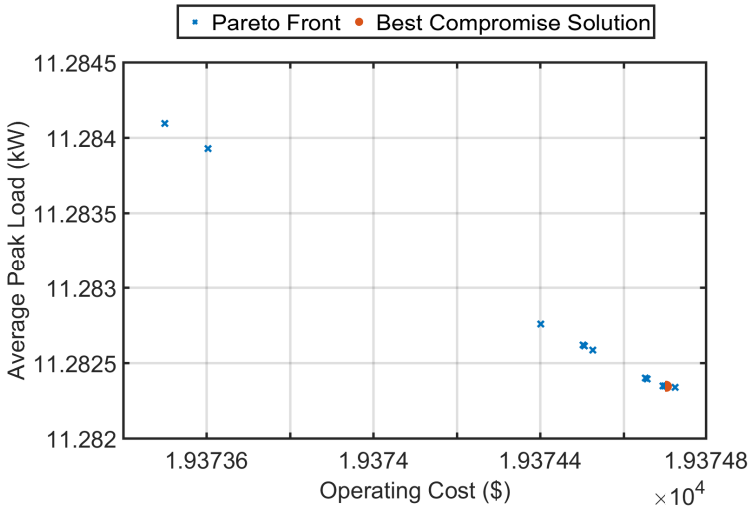

(b) NSGA-II random multiobjective

Fig. 5.10 Solution space for NSGA-II

The fittest and best compromise solution from case study III are presented in Table 5.8. Multiple solutions are found in the Pareto front using the proposed NSGA-II tuning of fuzzy membership functions. Whereas only a single solution is found using the previous methods.

Table 5.8 Online validation of FEMS for multi-objective optimization

FEMS	Cost ($)	APL (kW)	μ_1	μ_2	μ^k
Expert FEMS	4780.6	12.5	0.00	0.00	0.00
Aggregated Predefined	4666.2	12.5	1.00	0.00	0.22
Aggregated Random	4739.2	9.3	0.36	1.00	0.30
NSGA-II Predefined	4681.9	10.2	0.86	0.72	0.35
NSGA-II Random	4751.5	11.6	0.25	0.28	0.12

The solutions obtained by different FEMS are fuzzified using (3.45) and (3.46) to obtain the best compromise solution. Among these solutions, NSGA-II Predefined is the best compromise solution as it has the highest μ value. In the solution obtained by NSGA-II Predefined, the operating cost and APL are decreased 2.1% and 18.4% during online validation.

From Table 5.8, the solution obtained by Aggregated Predefined, Aggregated Random and NSGA-II Predefined are on the same Pareto front. However, aggregated multi-objective optimization can only obtain a single solution in a single run. To obtain the Pareto front requires multiple iterations. NSGA-II can obtain multiple solutions on the Pareto front in a single iteration.

The operating cost and average peak load of NSGA-II predefined is $4681.9 and 10.2kW respectively. By comparing with the best solution from case study I and II, all three solutions belong to the same Pareto front. However, the best compromise solution in case study III is also the best compromise solution between case study I to III from Fig. 5.11.

In multi-objective optimization, NSGA-II converges faster to the Pareto-optimal front when the initial population is initialized with expert membership functions. NSGA-II with predefined initial population has higher diversity. While NSGA-II can automatically generate all the membership functions for FEMS, empirical evidence from Case I and II have shown that the initial population with predefined expert MF can yield a more diversified Pareto front.

The fuzzy system can handle imprecise information, uncertainty and describe the behavior of a complex system without a precise mathematical model. While it is

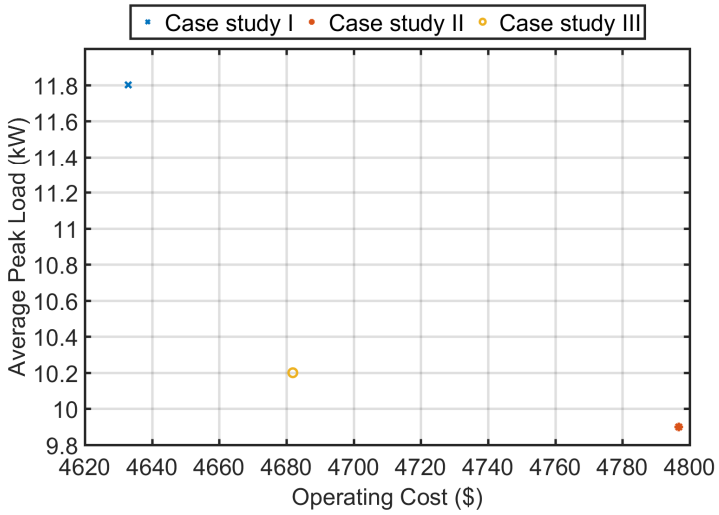

Fig. 5.11 Solutions of case study I-III

attractive for MOEA to automatically generate all the fuzzy parameters, i.e., fuzzy rules, membership function shape and membership functions, the trade-off between high accuracy and high interpretability must be considered prudently.

If all the fuzzy parameters are automatically generated, the search space would be vast and difficult to converge as each fuzzy parameter affect the other. The linguistic terms must be relevant to the placement of the membership functions. For instance, for fuzzy variable P_{ess}, linguistic term *negative big*, the membership function placement for this linguistic term would ideally be at the negative region and not the positive region. Hence for NSGA-II to generate all the fuzzy parameters would make the problem highly complex and takes a much longer computational time to get the Pareto solution. Furthermore, from Case study III, even though the membership functions are randomly generated in the initial population, NSGA-II have shown difficulty in finding diversity in the solution space.

Electricity is costly during peak demand, by discharging during high price period also reduces the peak demand. Reducing peak demand defer costly expansion of underutilized peaking power plant, transmission infrastructure, and distribution network. The average peak load is reduced by controlling the charging/discharging of the energy storage. In this manner, the consumption of the consumer can remain the same. The proposed methodology utilizes the real-time electricity pricing mechanism to enhance the operation of the current asset without affecting the consumption pattern of the consumer. It also does not require the intervention of the consumers to decide whether

to buy or sell from the main grid. Furthermore, the proposed methodology utilizes the available resources without any changes or expansion to the current infrastructure of the microgrid. The proposed FEMS can be applied to other ESS operation as it is designed with historical data and parameters of the ESS.

5.3.2 Experimental Validation on Energy Storage Test Bed

The proposed enhanced FEMS is experimentally validated in real-time using the energy storage test bed (ESTB) at Newcastle University, UK. An overview of the ESTB is shown in Fig. 5.12. The ESTB is connected to a 400V three phase network via two bi-directional AC/DC power converter rated at 360kVA, which are connected onto the Northern Power grid's distribution network.

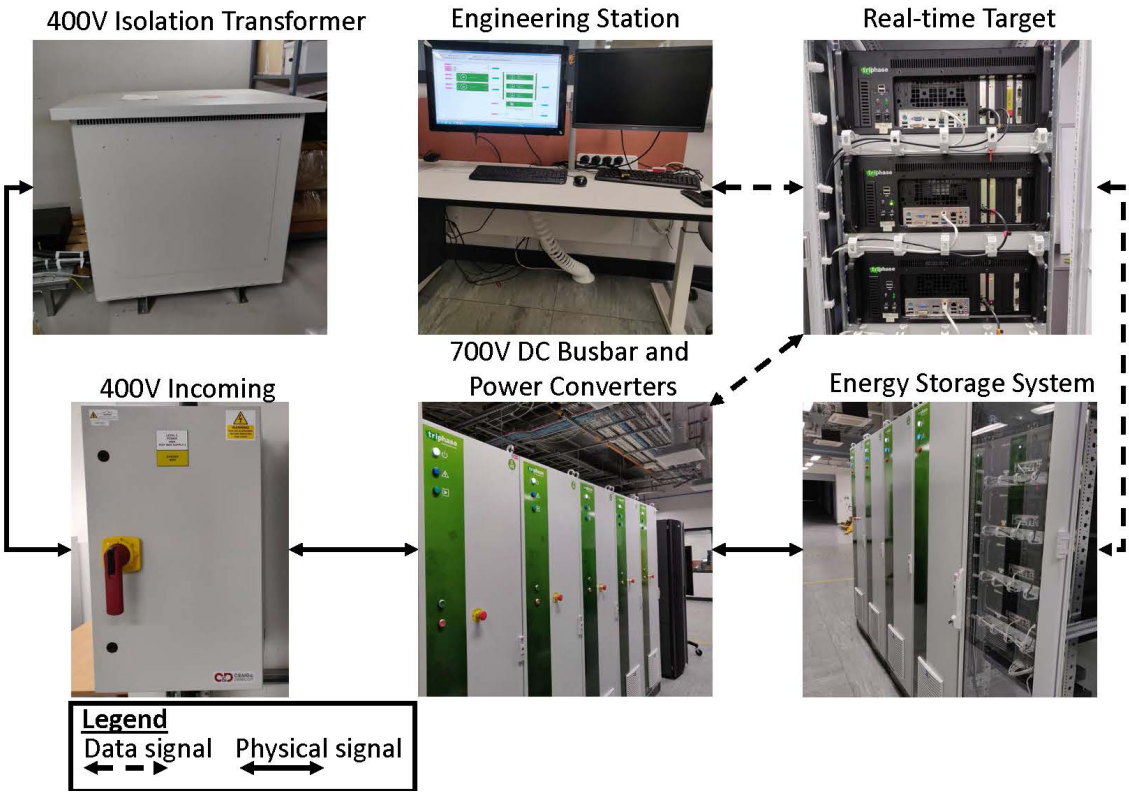

Fig. 5.12 Exerimental setup of energy storage test bed

5.3.2.1 400V Isolating Transformer

The ESTB is connected to the building network by a 400V transformer for isolation and protection purposes.

5.3.2.2 Engineering Station

The engineering station acts as a supervisory and control center for the ESTB. The proposed FEMS is implemented as a MATLAB Simulink model. The engineering station interfaces with the real-time target (RTT).

5.3.2.3 700V DC Busbar and Power Converters

The ESTB consists of two bi-directional AC/DC power converters rated at 360kVA and three bi-directional DC/DC power converters rated at 90kW. These power converters can accept voltage, current or power setpoints in real-time. These setpoints can be set as a constant value, time-varying or from historical data. The power converters are coupled to a 700V DC busbar.

5.3.2.4 Real-Time Target

The simulink model from the engineering station is compiled into C executed in the RTT. The RTT controls the voltage and current levels of the AC/DC converters, DC/DC converters and DC bus. This allow real-time control of the power converters and ESS.

5.3.2.5 Energy Storage System

A super-capacitor with ratings of 90 kW and 2 kWh are used in this setup. The operating voltage is between 300V to 650V. This ESS is connected to the DC/DC converter which is then coupled to the 700 DC bus.

This ESTB setup allows experimental validation of the different control methodologies such as the proposed methodology and voltage/frequency control in real-time.

The proposed FEMS is implemented in Simulink and subsequently sent to RTT where it runs in real-time. As the focus of this thesis is the operation of ESS, P_{load}, P_{pv} and P_{wind} are replaced with data signal instead of a physical signal.

5.3.2.6 Estimating Efficiency of Power Converters and Storage System

The efficiencies of the power converters and storage system are different when it operates at different power levels. As such, a constant efficiency does not accurately represent the nonlinear efficiencies of the power converters and storage system. An experiment is conducted to estimate the efficiencies for the power converters and storage system

at different power levels. The efficiency curve is implemented as a lookup table in Simulink for a better estimate of the SoC.

The SoC of the actual ESS is estimated from (5.5) [62, 150].

$$SoC_{\text{actual}} = \frac{V_{\text{OC}} - V_{\text{min}}}{V_{\text{max}} - V_{\text{min}}} \tag{5.5}$$

where V_{OC}, V_{max} and V_{min} are the open circuit, maximum and minimum operating voltages.

From (3.10), assuming that the actual SoC is equivalent to the model SoC.

$$SoC_{\text{actual}}(t) \approx SoC_{\text{model}}(t) \tag{5.6}$$

The η from (3.5) and (3.6) are further broken down into converters and storage efficiencies in (5.8). The charge and discharge efficiencies for power set-point p are $\eta_{\text{c}}(p)$ and $\eta_{\text{d}}(p)$ respectively.

$$\eta_{\text{c}}(p) = \eta_{\text{ converter in}}(p) \times \eta_{\text{ energy storage in}}(p) \tag{5.7}$$

$$\eta_{\text{d}}(p) = \eta_{\text{ converter out}}(p) \times \eta_{\text{ energy storage out}}(p) \tag{5.8}$$

where p is the different power set-points. The lookup table will interpolate between the power set-points and determine the efficiency.

Initially, the round-trip charge and discharge efficiencies for all power level, $\eta_{\text{c}}(p)$ and $\eta_{\text{d}}(p)$, are assumed to be 1. The energy storage is charged and discharged at a constant power set-point for 10s. The power set-points are increased from 1 kW to 15 kW for charging and -1 kW to -15 kW for discharging. The total energy stored and released for each power set-point are calculated with (5.9).

The DC/DC converter for the energy storage is set to charge and discharge at a different power setpoints for a fixed time interval of 10s. The total energy for power set-point p are calculated from (5.9).

$$\text{Total Energy}(p) = P_{\text{ess}}(t) \times t \tag{5.9}$$

where $P_{\text{ess}}(t)$ and t are the power setpoint and total time respectively.

Fig. 5.13 shows a comparison between the actual and model SoC with a constant efficiency of 1. The model consistently has a higher maximum and minimum SoC.

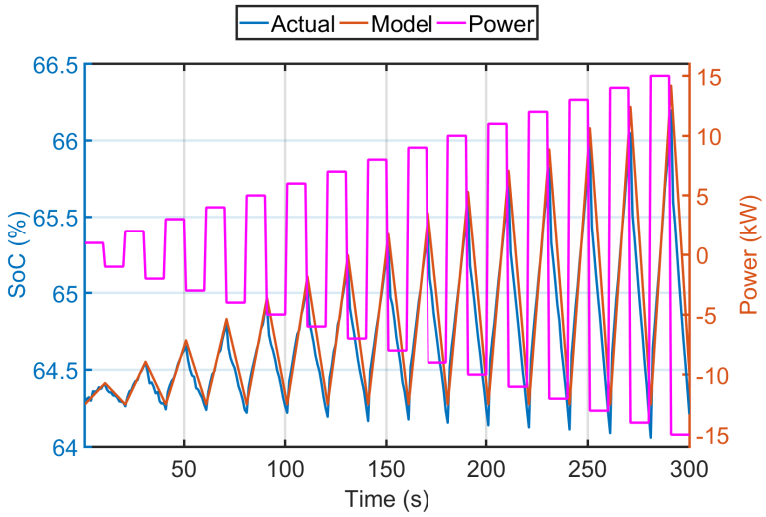

Fig. 5.13 Left axis, SoC of actual and model storage. Right axis, power set-point. Efficiencies of power converters and storage system are assumed to be 1.

The total energy stored and released of the actual energy storage for each power set-points can be obtained experimentally. These values are compared with the model. The estimated efficiencies are calculated using (5.10).

$$\eta(p) = \frac{\text{Model Energy Stored } (p)}{\text{Actual Energy Stored } (p)} \tag{5.10}$$

Table 5.9 shows the estimation of the power converters and storage efficiencies. This table is implemented into the Simulink model as a lookup table to extrapolate the efficiencies at different power levels.

Table 5.9 Estimation of power converters and ESS efficiencies

(a) Total energy stored

Power Setpoint (kW)	Actual Energy (kWh)	Model Energy (kWh)	η_c
1	0.0312	0.0278	0.89
2	0.0540	0.0556	1.03
3	0.0779	0.0833	1.07
4	0.1158	0.1111	0.96
5	0.1421	0.1389	0.98
6	0.1735	0.1667	0.96
7	0.1936	0.1944	1.00
8	0.2322	0.2222	0.96
9	0.2555	0.2500	0.98
10	0.2885	0.2778	0.96
11	0.3180	0.3056	0.96
12	0.3374	0.3333	0.99
13	0.3722	0.3611	0.97
14	0.3996	0.3889	0.97
15	0.4315	0.4167	0.97

(b) Total energy released

Power Setpoint (kW)	Actual Energy (kWh)	Model Energy (kWh)	η_d
1	0.0256	-0.0278	1.09
2	0.0577	-0.0556	0.96
3	0.0800	-0.0833	1.04
4	0.1192	-0.1111	0.93
5	0.1454	-0.1389	0.95
6	0.1723	-0.1667	0.97
7	0.1999	-0.1944	0.97
8	0.2307	-0.2222	0.96
9	0.2593	-0.2500	0.96
10	0.2949	-0.2778	0.94
11	0.3176	-0.3056	0.96
12	0.3420	-0.3333	0.97
13	0.3776	-0.3611	0.96
14	0.4010	-0.3889	0.97
15	0.4001	-0.4167	1.04

Mean absolute percentage error (MAPE) in (5.11) is used to quantify the agreement between the simulation model and experimental results.

$$M = \frac{1}{m}\sum_{t=1}^{m}\left|\frac{S_t - E_t}{S_t}\right| \tag{5.11}$$

where m, S_t and E_t are the total number of samples, simulation data and experimental data for time t respectively.

From Table 5.10, the MAPE of SoC and Pess are 1.87% and 1.66% respectively. This shows a good agreement between the model and experiment hence affirms the feasibility of the model and controller operation in real-time.

Table 5.10 MAPE of simulation and experiment

	MAPE (%)
SoC	1.87
Pess	1.66

Fig. 5.14 shows the difference between the actual storage system and the model SoC. The experimental result shows that the SoC MAPE of the lookup table approach is lower than a constant efficiency.

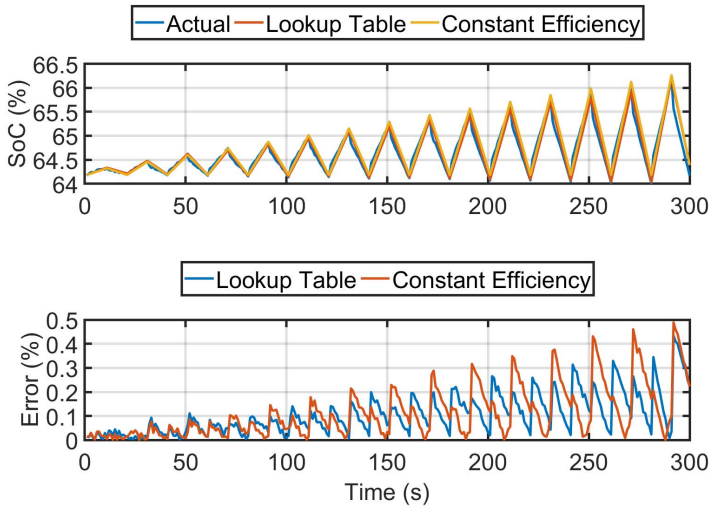

Fig. 5.14 Top, SoC of actual and model storage. Bottom, error between actual SoC and model SoC. Efficiencies of power converters and storage system are based on Table 5.9

The generalized energy storage model closely resemblance the SoC of an actual storage system. The efficiencies for different power levels are obtained experimentally. Empirically result shows that it better represents the actual storage instead of a constant efficiency for all power levels.

The difference in SoC between the model and actual storage system is reduce with an efficiency lookup table. The lookup considers the nonlinear characteristics of the power converters and storage system. The values for the lookup table are obtained experimentally using the SoC difference between the model and actual storage system.

The advantages of using a generalized energy storage model with lookup table are as follows:

- This model can be applied to different storage technology
- The lookup is obtained experimentally from the actual storage technology

There are many methods to model an energy storage system, generally they consider similar characteristic such as power and energy rating, and efficiency [59]. A generalized model with lookup table is a compromise between high complexity and high accuracy. As the aim of this thesis is the operation of a storage than modeling of storage, a generalized model with lookup table would be suffice. The generalized model can be applied to different types of storage technology during actual implementation. Whereas a complex model only applies to that specific storage technology.

5.3.2.7 Experimental Results

Fig. 5.15 compares the simulation power profile of ESS and SoC with the experiment. The SoC of the model can be accurately estimated using the generalized storage model from (3.10) and the actual ESS can follow the power setpoints from the proposed controller in real-time.

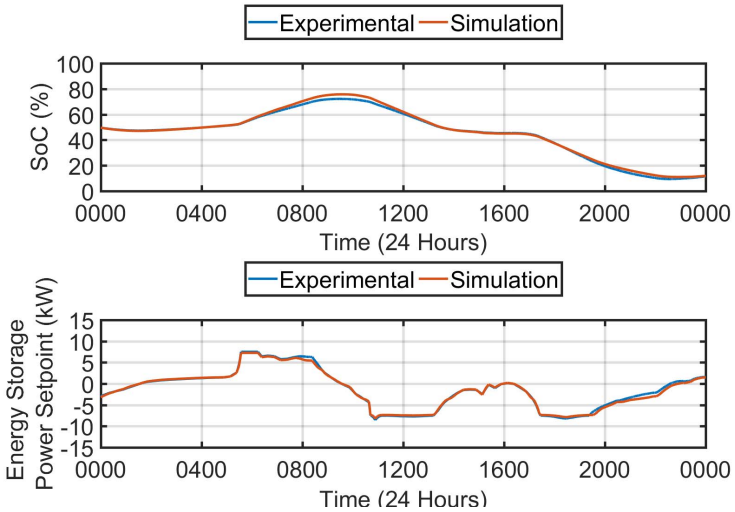

Fig. 5.15 Comparison between experimental and simulation results of the proposed FEMS

5.3.3 Summary of Enhanced FEMS

This section proposed a fuzzy based energy management system whose membership functions are tuned using NSGA-II. The objectives for NSGA-II are to minimize the operating cost and average peak load of the grid-connected microgrid with real-time pricing. The minimization of operating cost and average peak load is formulated into a multi-objective optimization problem with conflicting objective functions. Expert knowledge is integrated into the initial population of NSGA-II to obtain a diverse Pareto front in a single run. Three case studies were conducted in this section. Case study I and II present a single objective optimization problem, where only operating cost or average peak load is minimized using standard GA. Case study III presents a multi-objective optimization using NSGA-II and compared with an aggregated multi-objective GA. The results show that NSGA-II with expert knowledge in the initial population of GA is effective for handling multi-objective optimization with conflicting objective. NSGA-II is also able to obtain a diverse Pareto front. The proposed FEMS can be deploy to other microgrid with ESS for similar objectives as it is designed based on the historical data and not a specific storage technology. Furthermore, the proposed FEMS is experimentally validated and shows good agreement with the simulation.

5.4 Multi-Service of Single ESS: Reserve Service

This section presents the simulation results for an additional reserve service to the FEMS. It consists of a randomly generated service request of 15 kW (the storage maximum discharge rate for the energy storage) for 2 hours at different period of the availability window.

In this service, the minimum SoC of the ESS depends on the time to service (TTS). It has a dynamic minimum SoC which ensures that the ESS can provide a minimum of 15kW for two hours at the start of the service.

Apart from the uncertainties of RES, load and electricity market price, the uncertainty of the reserve request increases the complexity of the operation of ESS using mathematical optimization methods. It is also challenging to ensure that the ESS have enough energy at the start of the reserve window, a portion of energy is always reserve in [151].

The proposed method does not require any forecasting of the uncertain variables or a constant minimum SoC. It operates in real-time and have a dynamic minimum SoC. It ensures that the ESS always have enough energy to meet the reserve request at the start of the reserve window. Furthermore, the dynamic minimum SoC allows the ESS to be fully utilize during FEMS operation mode.

5.4.1 Simulation Results

The reserve service availability window is shown in Table 5.11. It is assumed that weekdays are working day and weekends are the non-working day. The service request can be activated at any time during the available window by the grid operator.

Table 5.11 Reserve service availability window

Working Day		Non-Working Day	
Start Time	End Time	Start Time	End Time
06:00	13:00	10:00	14:00
19:00	21:30	19:30	21:30

From Fig. 5.16, the ESS minimum SoC is always above 40% at the start of the reserve window. At the end of each reserve request, if the ESS minimum SoC is less than the minimum SoC, it will switch to the recovery operation mode which has a minimum SoC of 10%.

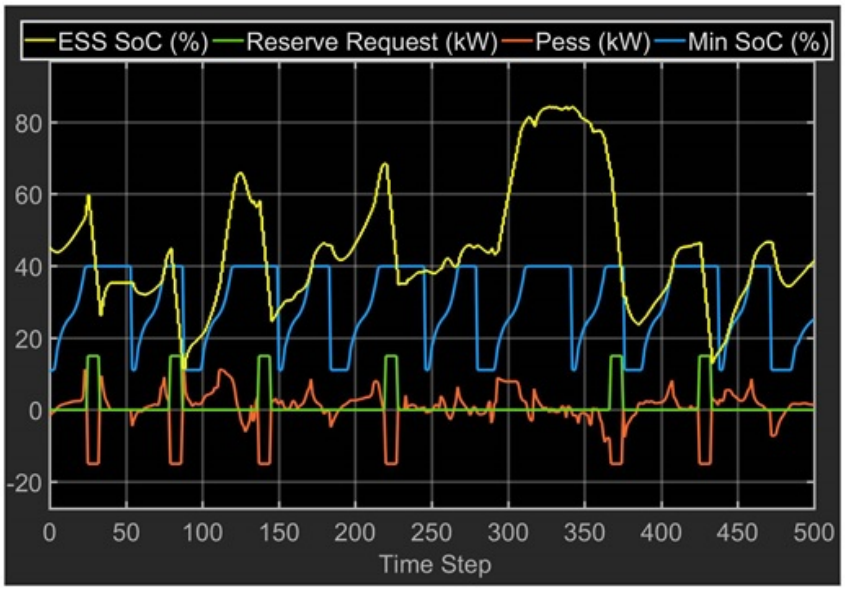

Fig. 5.16 Operation of energy storage with multiple services

The minimum SoC of the FLC will increase as it is approaching the reserve window from 10% to 40%. As such the energy storage will always have a minimum SoC of 30% to meet the reserve request of 15 kW for 2 hours. The reserve service request is met 96.4% of the time during the simulation period.

The reserve service of the ESS occurs during the peak period of the day hence it will greatly reduce the energy arbitrage opportunities as priority is given to fulfilling the reserve service. Furthermore, as the number of services for the ESS increases, it decreases the benefits of other services. For instance, when more reserve service is requested by the grid operator means less energy arbitrage and peak shaving for the consumer.

5.4.2 Summary of Multi-Service of Single ESS: Reserve Service

This section presented a multi-service operation of single ESS. It demonstrated the feasibility of having multiple services which benefits both storage owner and grid operator.

5.5 Summary

First, an expert designed FEMS is proposed in Section 5.2. The performance of the FEMS is compared with two benchmarking algorithm and empirical evidence shows that the proposed FEMS have a better solution on the Pareto front. Second, the membership functions of the FEMS is enhanced using NSGA-II in Section 5.3. The performance of the FEMS is further improved in this section. Finally, the feasibility of a multi-service operation of a single ESS is evaluated in Section 5.4.

Chapter 6

Conclusions and Future Works

6.1 Conclusions

Energy storage system (ESS) has the potential to provide services which supports the short- and long-term integration of stochastic renewable energy sources and grid operation. There is an urgent need to develop energy management systems that can efficiently utilize the potential of the ESS. In this direction, this thesis proposed and investigates numerous control strategies for multi-service of single ESS using computational intelligence techniques.

This thesis proposed a mathematical model for a grid-connected microgrid and ESS. The models are used to investigate the proposed methodologies for multi-service of a single ESS. These models can be modified to suit other microgrid configuration and storage technology. Furthermore, it allows rapid development, evaluation and comparison between different control strategies.

A forecasting-based methodology is proposed and investigated. The hyperparameters of the artificial neural networks (ANN) are tuned with the historical demand data. The mean absolute percentage error (MAPE) for extreme learning machine (ELM) is between 4.92% to 5.01% with a computation time of 7463s. The MAPE for deep belief network (DBN) is between 4.83% to 4.87% with a computational time of 10421s. Since the improvement is marginal compared to the increase in computation time, ELM is used as the forecasting method. After the forecast are obtained, the day-ahead operation of the ESS is formulated into a deterministic multi-objective optimization problem. The operation cost is used as the objective function and the peak demand is formulated as one of the inequality constraints. In this manner, the mixed integer linear programming (MILP) considers both services during the optimization process.

The operating cost is reduced from \$127.56 to \$89.58, with a peak demand of 32.78 kW when minimizing the operating cost. The true-optimum operating cost is \$41.21 with a peak demand of 36.54 kW for minimizing operating cost. When peak demand is added as an inequality constraint, the operating cost is slightly increased to \$90.60 and the peak demand is reduced to 24.67 kW. The true-optimum operating cost is \$45.84 with a peak demand of 7 kW for peak demand reduction. The drawback of this forecasting-based approach is the reliance on accurate day-ahead forecast. Furthermore, MILP can only obtain a single solution and not a set of Pareto solutions to investigate the trade-off relation between different objectives.

Multi-objective optimization using MILP requires additional changes to the problem formulation. This is achieved by modifying all but one of the objective functions into constraints or using a weighted sum approach. Among these approaches, Pareto optimal solutions cannot be obtained from MILP in a single run. Modifying all but one of the objective functions into constraints requires the user to determine the upper or lower limit of the constraints. A weighted sum approach requires testing different values of weight.

The uncertainties of the stochastic variables are considered using a fuzzy logic-based energy management system (FEMS). The FEMS is designed based on the historical data of the microgrid and does not rely on any forecast. The multi-services of a single ESS are considered in the designing of fuzzy rules. Empirical evidence from a comparison between FEMS and MILP shows that the FEMS is a dominant solution. The operating cost and standard deviation of P_{grid} are reduced from \$2205.54 to \$2141.23 and 7.84 to 5.42 respectively. The load factor is increased from 0.28 to 0.32 which signify a smoother power profile for P_{grid}. The FEMS is enhanced by using NSGA-II to tune its fuzzy membership functions. The operating cost and average peak load (APL) are reduced from \$4780.6 to \$4681.9 and 12.5 kW to 10.2 kW respectively. The best compromise solution is chosen from the Pareto optimal set and used in the experimental validation on the energy storage test bed (ESTB) in Newcastle University, UK. The difference between the ESS model and ESTB are validated using MAPE. It has a MAPE of 1.87% and 1.66% for state-of-charge estimation and P_{ess}. This shows a good agreement between the ESS model and ESTB.

An additional reserve service is added on top of the energy arbitrage and peak demand shaving service of the ESS. The minimum SoC of the ESS varies according to the time-to-service. Hence the controller ensures that there will be enough SoC at

the start of the service to provide a minimum of 15kW for two hours. The proposed controller is able to meet the RS 96.4% of the time.

While it is attractive to add more services to a single ESS it must be considered prudently. The multi-service of single ESS makes the mathematical formulation and quantifying the benefits challenging. Furthermore, it would drastically increase the life cycle of the ESS which is not considered during the planning phase.

The complexity and dimension of the problem drastically increase with the additional of more services. It is challenging to solve with mathematical optimization methods. Computational intelligence techniques such as fuzzy logic controller and multi-objective evolutionary algorithm are well-suited in this context where a good enough solution is sufficed.

6.2 Future Works

In this thesis, two approaches for multi-service of single ESS are proposed. In the first approach, a forecasting-based MILP scheduling is proposed. In the second approach, a FEMS enhanced with NSGA-II is proposed. While there has been significant progress, there are several areas requiring additional research.

- Storage capacity fading are not considered in this thesis, however it does not have a huge impact compared to the financial benefits it obtained from the energy arbitrage operation. Sizing of ESS for multi-service of single ESS. Short-term benefits with its provision of service and long-term cost associated with its effect on capacity degradation.

- For a higher accuracy forecast, the data can be clustered using clustering techniques such as k-nearest neighbor (k-NN). For instance, k-NN can be used to classify the load data into working day and nonworking day or photovoltaic power into seasonality. These data can be used to train different ANN models designed specifically to forecast the different data.

- In this research, it is assumed that the energy arbitrage operation of the ESS would not have a significant impact on the real-time electricity market price. This is applicable when the numbers of grid-connected microgrid is small. When there are a large number of grid-connected microgrid operating in this manner, it is important to develop an advance market mechanism to study this phenomenon.

- Following this direction, the alteration of the demand profile after multi-service of single ESS needs to be studied. The power flow, voltage and frequency deviation, transmission constraints of the power system under multiple grid-connected microgrids needs to be thoroughly investigate.

References

[1] E. Mojica-Nava, C. A. Macana, and N. Quijano, "Dynamic population games for optimal dispatch on hierarchical microgrid control," *IEEE Transactions on Systems, Man, and Cybernetics: Systems*, vol. 44, pp. 306–317, March 2014.

[2] R. H. Byrne, T. A. T. Nguyen, D. A. Copp, B. R. Chalamala, and I. Gyuk, "Energy management and optimization methods for grid energy storage systems," *IEEE Access*, vol. 6, pp. 13231–13260, 2018.

[3] G. Strbac, M. Aunedi, I. Konstantelos, R. Moreira, F. Teng, R. Moreno, D. Pudjianto, A. Laguna, and P. Papadopoulos, "Opportunities for energy storage: Assessing whole-system economic benefits of energy storage in future electricity systems," *IEEE Power and Energy Magazine*, vol. 15, pp. 32–41, Sept 2017.

[4] J. C. Vasquez, J. M. Guerrero, J. Miret, M. Castilla, and L. G. de Vicuna, "Hierarchical control of intelligent microgrids," *IEEE Industrial Electronics Magazine*, vol. 4, pp. 23–29, Dec 2010.

[5] A. Kwasinski, V. Krishnamurthy, J. Song, and R. Sharma, "Availability evaluation of micro-grids for resistant power supply during natural disasters," *IEEE Transactions on Smart Grid*, vol. 3, pp. 2007–2018, Dec 2012.

[6] B. Zhou and T. Littler, "Local storage meets local demand: a technical solution to future power distribution system," *IET Generation, Transmission Distribution*, vol. 10, no. 3, pp. 704–711, 2016.

[7] D. M. Greenwood, N. S. Wade, P. C. Taylor, P. Papadopoulos, and N. Heyward, "A probabilistic method combining electrical energy storage and real-time thermal ratings to defer network reinforcement," *IEEE Transactions on Sustainable Energy*, vol. 8, pp. 374–384, Jan 2017.

[8] P. Zou, Q. Chen, Q. Xia, G. He, and C. Kang, "Evaluating the contribution of energy storages to support large-scale renewable generation in joint energy and ancillary service markets," *IEEE Transactions on Sustainable Energy*, vol. 7, pp. 808–818, April 2016.

[9] T. Morstyn, B. Hredzak, and V. G. Agelidis, "Distributed cooperative control of microgrid storage," *IEEE Transactions on Power Systems*, vol. 30, pp. 2780–2789, Sept 2015.

[10] J. von Appen, T. Stetz, M. Braun, and A. Schmiegel, "Local voltage control strategies for pv storage systems in distribution grids," *IEEE Transactions on Smart Grid*, vol. 5, pp. 1002–1009, March 2014.

[11] H. Lund, G. Salgi, B. Elmegaard, and A. N. Andersen, "Optimal operation strategies of compressed air energy storage (caes) on electricity spot markets with fluctuating prices," *Applied Thermal Engineering*, vol. 29, no. 5, pp. 799 – 806, 2009.

[12] R. Sioshansi, P. Denholm, T. Jenkin, and J. Weiss, "Estimating the value of electricity storage in pjm: Arbitrage and some welfare effects," *Energy Economics*, vol. 31, no. 2, pp. 269 – 277, 2009.

[13] K. Meng, Z. Y. Dong, Z. Xu, Y. Zheng, and D. J. Hill, "Coordinated dispatch of virtual energy storage systems in smart distribution networks for loading management," *IEEE Transactions on Systems, Man, and Cybernetics: Systems*, vol. PP, no. 99, pp. 1–11, 2017.

[14] H. Khani and M. R. D. Zadeh, "Real-time optimal dispatch and economic viability of cryogenic energy storage exploiting arbitrage opportunities in an electricity market," *IEEE Transactions on Smart Grid*, vol. 6, pp. 391–401, Jan 2015.

[15] Y. Ru, J. Kleissl, and S. Martinez, "Storage size determination for grid-connected photovoltaic systems," *IEEE Transactions on Sustainable Energy*, vol. 4, pp. 68–81, Jan 2013.

[16] W. Hu, Z. Chen, and B. Bak-Jensen, "Optimal operation strategy of battery energy storage system to real-time electricity price in denmark," in *IEEE PES General Meeting*, pp. 1–7, July 2010.

[17] W. B. Powell and S. Meisel, "Tutorial on stochastic optimization in energy—part ii: An energy storage illustration," *IEEE Transactions on Power Systems*, vol. 31, no. 2, pp. 1468–1475, 2016.

[18] M. M. Baggu, A. Nagarajan, D. Cutler, D. Olis, T. O. Bialek, and M. Symko-Davies, "Coordinated optimization of multiservice dispatch for energy storage systems with degradation model for utility applications," *IEEE Transactions on Sustainable Energy*, pp. 1–1, 2018.

[19] Reliability Panel, The Australian Energy Market Comission, "Application of Frequency Operating Standards During Periods of Supply Scarcity," Tech. Rep. April, 2009.

[20] The Austrialian PV Assoc., "PV INTEGRATION ON AUSTRALIAN DISTRIBUTION," Tech. Rep. September, 2013.

[21] S. J. Ahn, J. W. Park, I. Y. Chung, S. I. Moon, S. H. Kang, and S. R. Nam, "Power-sharing method of multiple distributed generators considering control modes and configurations of a microgrid," *IEEE Transactions on Power Delivery*, vol. 25, pp. 2007–2016, July 2010.

[22] C. Zhao, U. Topcu, N. Li, and S. Low, "Design and stability of load-side primary frequency control in power systems," *IEEE Transactions on Automatic Control*, vol. 59, pp. 1177–1189, May 2014.

[23] T. Morstyn, B. Hredzak, and V. G. Agelidis, "Distributed cooperative control of microgrid storage," *IEEE Transactions on Power Systems*, vol. 30, pp. 2780–2789, Sept 2015.

[24] E. Liegmann and R. Majumder, "An efficient method of multiple storage control in microgrids," *IEEE Transactions on Power Systems*, vol. 30, pp. 3437–3444, Nov 2015.

[25] C. Zhai, H. Zhang, G. Xiao, and T. Pan, "Modeling and identification of worst-case cascading failures in power systems," *CoRR*, vol. abs/1703.05232, 2017.

[26] H. A. Mostafa, R. E. Shatshat, and M. M. A. Salama, "A review on energy management systems," in *2014 IEEE PES T D Conference and Exposition*, pp. 1–5, April 2014.

[27] T. T. Teo, T. Logenthiran, and W. L. Woo, "Forecasting of photovoltaic power using extreme learning machine," in *Smart Grid Technologies - Asia (ISGT ASIA), 2015 IEEE Innovative*, pp. 1–6, Nov 2015.

[28] T. Logenthiran, D. Srinivasan, and T. Z. Shun, "Demand side management in smart grid using heuristic optimization," *IEEE Transactions on Smart Grid*, vol. 3, pp. 1244–1252, Sept 2012.

[29] J. Xiao, P. Wang, and L. Setyawan, "Multilevel energy management system for hybridization of energy storages in dc microgrids," *IEEE Transactions on Smart Grid*, vol. 7, pp. 847–856, March 2016.

[30] T. Logenthiran, D. Srinivasan, A. M. Khambadkone, and H. N. Aung, "Multiagent system for real-time operation of a microgrid in real-time digital simulator," *IEEE Transactions on Smart Grid*, vol. 3, pp. 925–933, June 2012.

[31] A. C. Hua and B. Z. Syue, "Charge and discharge characteristics of lead-acid battery and lifepo4 battery," in *The 2010 International Power Electronics Conference - ECCE ASIA -*, pp. 1478–1483, June 2010.

[32] E. Banguero, A. Correcher, n. Pérez-Navarro, F. Morant, and A. Aristizabal, "A review on battery charging and discharging control strategies: Application to renewable energy systems," *Energies*, vol. 11, no. 4, 2018.

[33] B. Zakeri and S. Syri, "Electrical energy storage systems: A comparative life cycle cost analysis," *Renewable and Sustainable Energy Reviews*, vol. 42, pp. 569–596, 2015.

[34] J. Klaimi, R. Rahim-Amoud, L. Merghem-Boulahia, A. Jrad, and M. Esseghir, "An intelligent storage-based energy management approach for smart grids," in *2016 IEEE 12th International Conference on Wireless and Mobile Computing, Networking and Communications (WiMob)*, pp. 1–7, Oct 2016.

[35] S. Teleke, M. E. Baran, S. Bhattacharya, and A. Q. Huang, "Rule-based control of battery energy storage for dispatching intermittent renewable sources," *IEEE Transactions on Sustainable Energy*, vol. 1, pp. 117–124, Oct 2010.

[36] M. A. Abdullah, K. M. Muttaqi, D. Sutanto, and A. P. Agalgaonkar, "An effective power dispatch control strategy to improve generation schedulability and supply reliability of a wind farm using a battery energy storage system," *IEEE Transactions on Sustainable Energy*, vol. 6, pp. 1093–1102, July 2015.

[37] Y. Chang and T. H. Tay, "Efficiency and deregulation of the electricity market in singapore," *Energy Policy*, vol. 34, no. 16, pp. 2498 – 2508, 2006. Power market reform in Asian countries.

[38] T. Namerikawa, N. Okubo, R. Sato, Y. Okawa, and M. Ono, "Real-time pricing mechanism for electricity market with built-in incentive for participation," *IEEE Transactions on Smart Grid*, vol. 6, pp. 2714–2724, Nov 2015.

[39] K. Divya and J. Østergaard, "Battery energy storage technology for power systems—an overview," *Electric power systems research*, vol. 79, no. 4, pp. 511–520, 2009.

[40] R. Moreno, R. Moreira, and G. Strbac, "A milp model for optimising multi-service portfolios of distributed energy storage," *Applied Energy*, vol. 137, pp. 554–566, 2015.

[41] F. Zhang, Z. Hu, X. Xie, J. Zhang, and Y. Song, "Assessment of the effectiveness of energy storage resources in the frequency regulation of a single-area power system," *IEEE Transactions on Power Systems*, vol. 32, pp. 3373–3380, Sept 2017.

[42] J. W. Shim, G. Verbič, N. Zhang, and K. Hur, "Harmonious integration of faster-acting energy storage systems into frequency control reserves in power grid with high renewable generation," *IEEE Transactions on Power Systems*, vol. 33, pp. 6193–6205, Nov 2018.

[43] Y. Shen, D. Ke, Y. Sun, D. S. Kirschen, W. Qiao, and X. Deng, "Advanced auxiliary control of an energy storage device for transient voltage support of a doubly fed induction generator," *IEEE Transactions on Sustainable Energy*, vol. 7, pp. 63–76, Jan 2016.

[44] R. S. Weissbach, G. G. Karady, and R. G. Farmer, "A combined uninterruptible power supply and dynamic voltage compensator using a flywheel energy storage system," *IEEE Transactions on Power Delivery*, vol. 16, pp. 265–270, April 2001.

[45] V. Knap, S. K. Chaudhary, D. Stroe, M. Swierczynski, B. Craciun, and R. Teodorescu, "Sizing of an energy storage system for grid inertial response and primary frequency reserve," *IEEE Transactions on Power Systems*, vol. 31, pp. 3447–3456, Sept 2016.

[46] M. J. E. Alam, K. M. Muttaqi, and D. Sutanto, "Mitigation of rooftop solar pv impacts and evening peak support by managing available capacity of distributed energy storage systems," *IEEE Transactions on Power Systems*, vol. 28, pp. 3874–3884, Nov 2013.

[47] P. Palensky and D. Dietrich, "Demand side management: Demand response, intelligent energy systems, and smart loads," *IEEE Transactions on Industrial Informatics*, vol. 7, pp. 381–388, Aug 2011.

[48] H. Khani and H. E. Z. Farag, "Joint arbitrage and operating reserve scheduling of energy storage through optimal adaptive allocation of the state of charge," *IEEE Transactions on Sustainable Energy*, pp. 1–1, 2018.

[49] Y. Dvorkin, R. Fernández-Blanco, D. S. Kirschen, H. Pandžić, J. Watson, and C. A. Silva-Monroy, "Ensuring profitability of energy storage," *IEEE Transactions on Power Systems*, vol. 32, pp. 611–623, Jan 2017.

[50] I. Wilson, E. Barbour, T. Ketelaer, and W. Kuckshinrichs, "An analysis of storage revenues from the time-shifting of electrical energy in germany and great britain from 2010 to 2016," *Journal of Energy Storage*, vol. 17, pp. 446 – 456, 2018.

[51] B. J. Donnellan, D. J. Vowles, and W. L. Soong, "A review of energy storage and its application in power systems," in *2015 Australasian Universities Power Engineering Conference (AUPEC)*, pp. 1–6, Sept 2015.

[52] Z. Wang, A. Negash, and D. S. Kirschen, "Optimal scheduling of energy storage under forecast uncertainties," *IET Generation, Transmission Distribution*, vol. 11, no. 17, pp. 4220–4226, 2017.

[53] R. Moreira, R. Moreno, and G. Strbac, "Value of corrective network security for distributed energy storage applications," *IET Generation, Transmission Distribution*, vol. 10, no. 7, pp. 1758–1767, 2016.

[54] C. Suazo-Martínez, E. Pereira-Bonvallet, R. Palma-Behnke, and X. Zhang, "Impacts of energy storage on short term operation planning under centralized spot markets," *IEEE Transactions on Smart Grid*, vol. 5, pp. 1110–1118, March 2014.

[55] H. Hao, D. Wu, J. Lian, and T. Yang, "Optimal coordination of building loads and energy storage for power grid and end user services," *IEEE Transactions on Smart Grid*, vol. 9, pp. 4335–4345, Sept 2018.

[56] C. A. Hill, M. C. Such, D. Chen, J. Gonzalez, and W. M. Grady, "Battery energy storage for enabling integration of distributed solar power generation," *IEEE Transactions on smart grid*, vol. 3, no. 2, pp. 850–857, 2012.

[57] X. Lin, H. E. Perez, S. Mohan, J. B. Siegel, A. G. Stefanopoulou, Y. Ding, and M. P. Castanier, "A lumped-parameter electro-thermal model for cylindrical batteries," *Journal of Power Sources*, vol. 257, pp. 1 – 11, 2014.

[58] H. Ibrahim, A. Ilinca, and J. Perron, "Energy storage systems—characteristics and comparisons," *Renewable and Sustainable Energy Reviews*, vol. 12, no. 5, pp. 1221 – 1250, 2008.

[59] A. R. Sparacino, G. F. Reed, R. J. Kerestes, B. M. Grainger, and Z. T. Smith, "Survey of battery energy storage systems and modeling techniques," in *2012 IEEE Power and Energy Society General Meeting*, pp. 1–8, July 2012.

[60] L. Lam, P. Bauer, and E. Kelder, "A practical circuit-based model for li-ion battery cells in electric vehicle applications," in *2011 IEEE 33rd International Telecommunications Energy Conference (INTELEC)*, pp. 1–9, Oct 2011.

[61] Y. Parvini, J. B. Siegel, A. G. Stefanopoulou, and A. Vahidi, "Supercapacitor electrical and thermal modeling, identification, and validation for a wide range of temperature and power applications," *IEEE Transactions on Industrial Electronics*, vol. 63, pp. 1574–1585, March 2016.

[62] M. Ceraolo, G. Lutzemberger, and D. Poli, "State-of-charge evaluation of supercapacitors," *Journal of Energy Storage*, vol. 11, pp. 211 – 218, 2017.

[63] E. Frackowiak and F. Béguin, "Carbon materials for the electrochemical storage of energy in capacitors," *Carbon*, vol. 39, no. 6, pp. 937 – 950, 2001.

[64] V. Sedlakova, J. Sikula, J. Majzner, P. Sedlak, T. Kuparowitz, B. Buergler, and P. Vasina, "Supercapacitor equivalent electrical circuit model based on charges redistribution by diffusion," *Journal of Power Sources*, vol. 286, pp. 58 – 65, 2015.

[65] F. Rafik, H. Gualous, R. Gallay, A. Crausaz, and A. Berthon, "Frequency, thermal and voltage supercapacitor characterization and modeling," *Journal of Power Sources*, vol. 165, no. 2, pp. 928 – 934, 2007. IBA – HBC 2006.

[66] T. T. Teo, T. Logenthiran, W. L. Woo, and K. Abidi, "Forecasting of photovoltaic power using regularized ensemble extreme learning machine," in *2016 IEEE Region 10 Conference (TENCON)*, pp. 455–458, Nov 2016.

[67] J. E. C. Tee, T. T. Teo, T. Logenthiran, W. L. Woo, and K. Abidi, "Day-ahead forecasting of wholesale electricity pricing using extreme learning machine," in *TENCON 2017 - 2017 IEEE Region 10 Conference*, pp. 2973–2977, Nov 2017.

[68] Y. Q. Neo, T. T. Teo, W. L. Woo, T. Logenthiran, and A. Sharma, "Forecasting of photovoltaic power using deep belief network," in *TENCON 2017 - 2017 IEEE Region 10 Conference*, pp. 1189–1194, Nov 2017.

[69] V. De, T. T. Teo, W. L. Woo, and T. Logenthiran, "Photovoltaic power forecasting using lstm on limited dataset," in *2018 IEEE Innovative Smart Grid Technologies - Asia (ISGT Asia)*, pp. 710–715, May 2018.

[70] M. F. Anjos and M. V. Vieira, "Mathematical optimization approaches for facility layout problems: The state-of-the-art and future research directions," *European Journal of Operational Research*, vol. 261, no. 1, pp. 1–16, 2017.

[71] G. Bonvin, S. Demassey, C. Le Pape, N. Maïzi, V. Mazauric, and A. Samperio, "A convex mathematical program for pump scheduling in a class of branched water networks," *Applied Energy*, vol. 185, pp. 1702–1711, 2017.

[72] H. Li, S. Mi, Q. Li, X. Wen, D. Qiao, and G. Luo, "A scheduling optimization method for maintenance, repair and operations service resources of complex products," *Journal of Intelligent Manufacturing*, pp. 1–19, 2018.

[73] A. Ahmadi-Javid and P. Hooshangi-Tabrizi, "Integrating employee timetabling with scheduling of machines and transporters in a job-shop environment: A mathematical formulation and an anarchic society optimization algorithm," *Computers & Operations Research*, vol. 84, pp. 73–91, 2017.

[74] R. O. Ferguson and L. F. Sargent, *Linear programming*, vol. 19. McGraw-Hill, 1958.

[75] J. L. Higle, "Stochastic programming: optimization when uncertainty matters," in *Emerging Theory, Methods, and Applications*, pp. 30–53, Informs, 2005.

[76] L. Zedeh, "Fuzzy sets," *Information and control*, vol. 8, no. 3, pp. 338–353, 1965.

[77] A. Konak, D. W. Coit, and A. E. Smith, "Multi-objective optimization using genetic algorithms: A tutorial," *Reliability Engineering & System Safety*, vol. 91, no. 9, pp. 992–1007, 2006.

[78] J. D. Schaffer, "Multiple objective optimization with vector evaluated genetic algorithms," in *Proceedings of the 1st International Conference on Genetic Algorithms*, (Hillsdale, NJ, USA), pp. 93–100, L. Erlbaum Associates Inc., 1985.

[79] K. Deb, A. Pratap, S. Agarwal, and T. Meyarivan, "A fast and elitist multiobjective genetic algorithm: Nsga-ii," *IEEE Transactions on Evolutionary Computation*, vol. 6, pp. 182–197, Apr 2002.

[80] J. H. Holland, "Genetic algorithms," *Scientific american*, vol. 267, no. 1, pp. 66–73, 1992.

[81] K. Deep, K. P. Singh, M. L. Kansal, and C. Mohan, "A real coded genetic algorithm for solving integer and mixed integer optimization problems," *Applied Mathematics and Computation*, vol. 212, no. 2, pp. 505–518, 2009.

[82] J. Zhong, X. Hu, J. Zhang, and M. Gu, "Comparison of performance between different selection strategies on simple genetic algorithms," in *Computational Intelligence for Modelling, Control and Automation, 2005 and International Conference on Intelligent Agents, Web Technologies and Internet Commerce, International Conference on*, vol. 2, pp. 1115–1121, IEEE, 2005.

[83] G. Rudolph, "Evolutionary search under partially ordered fitness sets," *HT014601767*, 2001.

[84] E. Zitzler, K. Deb, and L. Thiele, "Comparison of multiobjective evolutionary algorithms: Empirical results," *Evolutionary computation*, vol. 8, no. 2, pp. 173–195, 2000.

[85] W. Stadler, "A survey of multicriteria optimization or the vector maximum problem, part i: 1776–1960," *Journal of Optimization Theory and Applications*, vol. 29, no. 1, pp. 1–52, 1979.

[86] K. Miettinen, *Nonlinear multiobjective optimization*, vol. 12. Springer Science & Business Media, 2012.

[87] K. Deb and J. Sundar, "Reference point based multi-objective optimization using evolutionary algorithms," in *Proceedings of the 8th annual conference on Genetic and evolutionary computation*, pp. 635–642, ACM, 2006.

[88] A. Zhou, B.-Y. Qu, H. Li, S.-Z. Zhao, P. N. Suganthan, and Q. Zhang, "Multiobjective evolutionary algorithms: A survey of the state of the art," *Swarm and Evolutionary Computation*, vol. 1, no. 1, pp. 32 – 49, 2011.

[89] G. Chiandussi, M. Codegone, S. Ferrero, and F. Varesio, "Comparison of multiobjective optimization methodologies for engineering applications," *Computers and Mathematics with Applications*, vol. 63, no. 5, pp. 912 – 942, 2012.

[90] J. Horn, N. Nafpliotis, and D. E. Goldberg, "A niched pareto genetic algorithm for multiobjective optimization," in *Proceedings of the First IEEE Conference on Evolutionary Computation. IEEE World Congress on Computational Intelligence*, pp. 82–87 vol.1, Jun 1994.

[91] E. Zitzler and L. Thiele, "An evolutionary algorithm for multiobjective optimization: The strength pareto approach," 1998.

[92] L. A. Pereira, S. Haffner, G. Nicol, and T. F. Dias, "Multiobjective optimization of five-phase induction machines based on nsga-ii," *IEEE Transactions on Industrial Electronics*, vol. 64, pp. 9844–9853, Dec 2017.

[93] P. Murugan, S. Kannan, and S. Baskar, "Application of nsga-ii algorithm to single-objective transmission constrained generation expansion planning," *IEEE Transactions on Power Systems*, vol. 24, pp. 1790–1797, Nov 2009.

[94] M. R. AlRashidi and M. E. El-Hawary, "A survey of particle swarm optimization applications in electric power systems," *IEEE transactions on evolutionary computation*, vol. 13, no. 4, pp. 913–918, 2009.

[95] M. A. Abido, "Multiobjective evolutionary algorithms for electric power dispatch problem," *IEEE Transactions on Evolutionary Computation*, vol. 10, pp. 315–329, June 2006.

[96] Y. Del Valle, G. K. Venayagamoorthy, S. Mohagheghi, J.-C. Hernandez, and R. G. Harley, "Particle swarm optimization: basic concepts, variants and applications in power systems," *IEEE Transactions on evolutionary computation*, vol. 12, no. 2, pp. 171–195, 2008.

[97] N. Sinha, R. Chakrabarti, and P. Chattopadhyay, "Evolutionary programming techniques for economic load dispatch," *IEEE Transactions on evolutionary computation*, vol. 7, no. 1, pp. 83–94, 2003.

[98] R. J. Schalkoff, *Artificial neural networks*, vol. 1.

[99] H. S. Hippert, C. E. Pedreira, and R. C. Souza, "Neural networks for short-term load forecasting: A review and evaluation," *IEEE Transactions on power systems*, vol. 16, no. 1, pp. 44–55, 2001.

[100] S. B. Kotsiantis, I. Zaharakis, and P. Pintelas, "Supervised machine learning: A review of classification techniques," *Emerging artificial intelligence applications in computer engineering*, vol. 160, pp. 3–24, 2007.

[101] Z. C. Lipton, J. Berkowitz, and C. Elkan, "A critical review of recurrent neural networks for sequence learning," *arXiv preprint arXiv:1506.00019*, 2015.

[102] M. W. Gardner and S. Dorling, "Artificial neural networks (the multilayer perceptron)—a review of applications in the atmospheric sciences," *Atmospheric environment*, vol. 32, no. 14-15, pp. 2627–2636, 1998.

[103] R. Setiono and L. C. K. Hui, "Use of a quasi-newton method in a feedforward neural network construction algorithm," *IEEE Transactions on Neural Networks*, vol. 6, no. 1, pp. 273–277, 1995.

[104] M. T. Hagan and M. B. Menhaj, "Training feedforward networks with the marquardt algorithm," *IEEE transactions on Neural Networks*, vol. 5, no. 6, pp. 989–993, 1994.

[105] A. Choromanska, M. Henaff, M. Mathieu, G. B. Arous, and Y. LeCun, "The loss surface of multilayer networks," *CoRR*, vol. abs/1412.0233, 2014.

[106] G.-B. Huang, Q.-Y. Zhu, and C.-K. Siew, "Extreme learning machine: theory and applications," *Neurocomputing*, vol. 70, no. 1-3, pp. 489–501, 2006.

[107] G. E. Hinton, S. Osindero, and Y.-W. Teh, "A fast learning algorithm for deep belief nets," *Neural computation*, vol. 18, no. 7, pp. 1527–1554, 2006.

[108] I. Guyon, "A scaling law for the validation-set training-set size ratio," *AT&T Bell Lab.*, vol. 1, 08 1996.

[109] T. Fushiki, "Estimation of prediction error by using k-fold cross-validation," *Statistics and Computing*, vol. 21, no. 2, pp. 137–146, 2011.

[110] S. B. Sulistyo, W. L. Woo, and S. S. Dlay, "Regularized neural networks fusion and genetic algorithm based on-field nitrogen status estimation of wheat plants," *IEEE Transactions on Industrial Informatics*, vol. 13, pp. 103–114, Feb 2017.

[111] G. Zhang, B. E. Patuwo, and M. Y. Hu, "Forecasting with artificial neural networks:: The state of the art," *International journal of forecasting*, vol. 14, no. 1, pp. 35–62, 1998.

[112] T. Namerikawa, N. Okubo, R. Sato, Y. Okawa, and M. Ono, "Real-time pricing mechanism for electricity market with built-in incentive for participation," *IEEE Transactions on Smart Grid*, vol. 6, pp. 2714–2724, Nov 2015.

[113] L. Bird and D. Lew, "Integrating wind and solar energy in the us bulk power system: Lessons from regional integration studies," tech. rep., National Renewable Energy Laboratory (NREL), Golden, CO., 2012.

[114] S. Wang, Y. Tang, J. Shi, K. Gong, Y. Liu, L. Ren, and J. Li, "Design and advanced control strategies of a hybrid energy storage system for the grid integration of wind power generations," *IET Renewable Power Generation*, vol. 9, no. 2, pp. 89–98, 2015.

[115] F. Zhang, K. Meng, Z. Xu, Z. Dong, L. Zhang, C. Wan, and J. Liang, "Battery ess planning for wind smoothing via variable-interval reference modulation and self-adaptive soc control strategy," *IEEE Transactions on Sustainable Energy*, vol. 8, pp. 695–707, April 2017.

[116] D. Arcos-Aviles, J. Pascual, L. Marroyo, P. Sanchis, and F. Guinjoan, "Fuzzy logic-based energy management system design for residential grid-connected microgrids," *IEEE Transactions on Smart Grid*, vol. PP, no. 99, pp. 1–1, 2017.

[117] T. T. Teo, T. Logenthiran, W. L. Woo, and K. Abidi, "Intelligent controller for energy storage system in grid-connected microgrid," *IEEE Transactions on Systems, Man, and Cybernetics: Systems*, pp. 1–9, 2018.

[118] H. Mohsenian-Rad, "Optimal bidding, scheduling, and deployment of battery systems in california day-ahead energy market," *IEEE Transactions on Power Systems*, vol. 31, pp. 442–453, Jan 2016.

[119] Y. Wang, X. Lin, and M. Pedram, "A near-optimal model-based control algorithm for households equipped with residential photovoltaic power generation and energy storage systems," *IEEE Transactions on Sustainable Energy*, vol. 7, pp. 77–86, Jan 2016.

[120] X. D. Sun, K. H. Koh, B. G. Yu, and M. Matsui, "Fuzzy-logic-based v/f control of an induction motor for a dc grid power-leveling system using flywheel energy storage equipment," *IEEE Transactions on Industrial Electronics*, vol. 56, pp. 3161–3168, Aug 2009.

[121] S. Zhang, Y. Mishra, and M. Shahidehpour, "Fuzzy-logic based frequency controller for wind farms augmented with energy storage systems," *IEEE Transactions on Power Systems*, vol. 31, pp. 1595–1603, March 2016.

[122] J. Liu, J. Wen, W. Yao, and Y. Long, "Solution to short-term frequency response of wind farms by using energy storage systems," *IET Renewable Power Generation*, vol. 10, no. 5, pp. 669–678, 2016.

[123] R. AlBadwawi, W. Issa, M. Abusara, and M. Tapas, "Supervisory control for power management of an islanded ac microgrid using frequency signalling-based fuzzy logic controller," *IEEE Transactions on Sustainable Energy*, pp. 1–1, 2018.

[124] T. T. Teo, T. Logenthiran, W. L. Woo, and K. Abidi, "Fuzzy logic control of energy storage system in microgrid operation," in *2016 IEEE Innovative Smart Grid Technologies - Asia (ISGT-Asia)*, pp. 65–70, Nov 2016.

[125] T. T. Teo, T. Logenthiran, W. L. Woo, and K. Abidi, "Near-optimal day-ahead scheduling of energy storage system in grid-connected microgrid," in *2018 IEEE Innovative Smart Grid Technologies - Asia (ISGT Asia)*, pp. 1257–1261, May 2018.

[126] M. R. Sandgani and S. Sirouspour, "Energy management in a network of grid-connected microgrids/nanogrids using compromise programming," *IEEE Transactions on Smart Grid*, vol. PP, no. 99, pp. 1–1, 2017.

[127] R. Zhang and J. Tao, "Ga based fuzzy energy management system for fc/sc powered hev considering h2 consumption and load variation," *IEEE Transactions on Fuzzy Systems*, vol. PP, no. 99, pp. 1–1, 2017.

[128] H. Kanchev, F. Colas, V. Lazarov, and B. Francois, "Emission reduction and economical optimization of an urban microgrid operation including dispatched pv-based active generators," *IEEE Transactions on Sustainable Energy*, vol. 5, pp. 1397–1405, Oct 2014.

[129] M. Fazzolari, R. Alcala, Y. Nojima, H. Ishibuchi, and F. Herrera, "A review of the application of multiobjective evolutionary fuzzy systems: Current status and further directions," *IEEE Transactions on Fuzzy Systems*, vol. 21, pp. 45–65, Feb 2013.

[130] A. Haghighi and A. Z. Asl, "Uncertainty analysis of water supply networks using the fuzzy set theory and nsga-ii," *Engineering Applications of Artificial Intelligence*, vol. 32, pp. 270 – 282, 2014.

[131] H. Ishibuchi and Y. Nojima, "Analysis of interpretability-accuracy tradeoff of fuzzy systems by multiobjective fuzzy genetics-based machine learning," *International Journal of Approximate Reasoning*, vol. 44, no. 1, pp. 4–31, 2007.

[132] O. Guenounou, A. Belmehdi, B. Dahhou, and N. Belkherchi, "Intelligent design of fuzzy logic controller using nsga-ii," in *2011 11th International Conference on Intelligent Systems Design and Applications*, pp. 172–177, Nov 2011.

[133] R. AlcalÁ, P. Ducange, F. Herrera, B. Lazzerini, and F. Marcelloni, "A multiobjective evolutionary approach to concurrently learn rule and data bases of linguistic fuzzy-rule-based systems," *IEEE Transactions on Fuzzy Systems*, vol. 17, pp. 1106–1122, Oct 2009.

[134] A. Merabet, K. T. Ahmed, H. Ibrahim, R. Beguenane, and A. M. Y. M. Ghias, "Energy management and control system for laboratory scale microgrid based wind-pv-battery," *IEEE Transactions on Sustainable Energy*, vol. 8, pp. 145–154, Jan 2017.

[135] R. Fourer, D. M. Gay, and B. W. Kernighan, "A modeling language for mathematical programming," *Management Science*, vol. 36, no. 5, pp. 519–554, 1990.

[136] A. W. L. Lim, T. T. Teo, M. Ramadan, T. Logenthiran, and V. T. Phan, "Optimum long-term planning for microgrid," in *TENCON 2017 - 2017 IEEE Region 10 Conference*, pp. 1457–1462, Nov 2017.

[137] I. Papic, "Simulation model for discharging a lead-acid battery energy storage system for load leveling," *IEEE transactions on energy conversion*, vol. 21, no. 2, pp. 608–615, 2006.

[138] B. L. Miller and D. E. Goldberg, "Genetic algorithms, tournament selection, and the effects of noise," *Complex systems*, vol. 9, no. 3, pp. 193–212, 1995.

[139] R. B. Agrawal, K. Deb, and R. Agrawal, "Simulated binary crossover for continuous search space," *Complex systems*, vol. 9, no. 2, pp. 115–148, 1995.

[140] E. M. Authority, "Half hourly system demand data (from 2 feb 2012 onwards)."

[141] P. Lusis, K. R. Khalilpour, L. Andrew, and A. Liebman, "Short-term residential load forecasting: Impact of calendar effects and forecast granularity," *Applied Energy*, vol. 205, pp. 654 – 669, 2017.

[142] M. A. Keyvanrad and M. M. Homayounpour, "A brief survey on deep belief networks and introducing a new object oriented MATLAB toolbox (deebnet)," *CoRR*, vol. abs/1408.3264, 2014.

[143] Y. Ru, J. Kleissl, and S. Martinez, "Storage size determination for grid-connected photovoltaic systems," *IEEE Transactions on Sustainable Energy*, vol. 4, pp. 68–81, Jan 2013.

[144] W. Hu, Z. Chen, and B. Bak-Jensen, "Optimal operation strategy of battery energy storage system to real-time electricity price in denmark," in *IEEE PES General Meeting*, pp. 1–7, July 2010.

[145] W. Tang and Y. J. A. Zhang, "Optimal battery energy storage system control in microgrid with renewable energy generation," in *2015 IEEE International Conference on Smart Grid Communications (SmartGridComm)*, pp. 846–851, Nov 2015.

[146] T. Logenthiran, D. Srinivasan, and T. Z. Shun, "Demand side management in smart grid using heuristic optimization," *IEEE Transactions on Smart Grid*, vol. 3, pp. 1244–1252, Sept 2012.

[147] C. Draxl, B. Hodge, A. Clifton, and J. McCaa, "Overview and meteorological validation of the wind integration national dataset toolkit," tech. rep., NREL/TP-5000-61740. Golden (CO): National Renewable Energy Laboratory (forthcoming), 2015.

[148] X. Zhang, Y. Tian, R. Cheng, and Y. Jin, "An efficient approach to nondominated sorting for evolutionary multiobjective optimization," *IEEE Transactions on Evolutionary Computation*, vol. 19, pp. 201–213, April 2015.

[149] R. Wang, Z. Zhou, H. Ishibuchi, T. Liao, and T. Zhang, "Localized weighted sum method for many-objective optimization," *IEEE Transactions on Evolutionary Computation*, vol. PP, no. 99, pp. 1–1, 2016.

[150] K. Mansiri, S. Sukchai, and C. Sirisamphanwong, "Fuzzy control algorithm for battery storage and demand side power management for economic operation of the smart grid system at naresuan university, thailand," *IEEE Access*, vol. 6, pp. 32440–32449, 2018.

[151] R. Hollinger, L. M. Diazgranados, F. Braam, T. Erge, G. Bopp, and B. Engel, "Distributed solar battery systems providing primary control reserve," *IET Renewable Power Generation*, vol. 10, no. 1, pp. 63–70, 2016.